EFFECTIVE UTILIZATION AND MANAGEMENT OF PV AND BATTERY BASED POWER SUPPLY SYSTEM FOR TELECOM LOAD

Thesis

Submitted in partial fulfillment of the requirements for the degree of

DOCTOR OF PHILOSOPHY

by

J SAIKRISHNA GOUD

DEPARTMENT OF ELECTRICAL AND ELECTRONICS ENGINEERING

NATIONAL INSTITUTE OF TECHNOLOGY KARNATAKA

SURATHKAL, MANGALORE -575025

OCTOBER, 2019

DECLARATION

by the Ph.D. Research Scholar

I hereby *declare* that the Research Thesis entitled Effective Utilization and Management of PV and Battery Based Power Supply System for Telecom Load which is being submitted to the National Institute of Technology Karnataka, Surathkal in partial fulfillment of the requirement for the award of the Degree of Doctor of Philosophy in Electrical and Electronics Engineering is a *bonafide report of the research work carried out by me*. The material contained in this Research Thesis has not been submitted to any University or Institution for the award of any degree.

.....

J Saikrishna Goud, 158019EE15F07
Department of Electrical and Electronics Engineering

Place: NITK-Surathkal
Date:

CERTIFICATE

This is to *certify* that the Research Thesis entitled **Effective Utilization and Management of PV and Battery Based Power Supply System for Telecom Load** submitted by J Saikrishna Goud (Register Number: 158019EE15F07) as the record of the research work carried out by him, is *accepted as the Research Thesis submission* in partial fulfillment of the requirements for the award of degree of Doctor of Philosophy.

Dr. R. Kalpana
(Research Guide)

Dr. Shubhanga K N
(Chairman-DRPC, EEE Dept.)

Acknowledgements

I would like to thank a number of people who contributed to this dissertation in many different ways:

Firstly, I would like to express my deepest gratitude to my supervisor, Dr. R Kalpana, Assistant Professor, Department of Electrical and Electronics Engineering, for her guidance, encouragement and showing trust in me all the time.

I would like to thank my research progress assessment committee (RPAC) members Dr. Debashisha Jena and Dr. V. Geetha, for their constructive feedback and guidance. Also, I would like to thank Dr. Shubhanga K N, Head of the Department of Electrical and Electronics Engineering, NITK, Surathkal. Thanks also go to Dr. Venkatesa Perumal and Dr. Vinatha U, former HODs for providing the necessary resources in the department to carry out my research. I also wish to thank the non-teaching staff of the EEE department, In particular, K.M. Naik for providing necessary support in conducting experimentation.

I am truly grateful to Saikumar, Raviteja, Srikanth Tunga and Venkat Vanjari for their support in carrying out my research work. I would like to express my heartful thanks to all my colleagues, I have gained a lot from therm through scholarly interactions.

I would like to express my deepest gratitude towards my parents and my sister for their love and patience which kept me going on this journey. Their faith and unconditional love towards me are the reason for whatever I have achieved in my life. I would like to dedicate this dissertation to my Late grandfather for his love, affection and inspiration.

J SAIKRISHNA GOUD

Abstract

One of the major sectors which have seen a rapid growth in the last decade is mobile telecommunications. It has not only become an important part in peoples lives but also playing a part in world business as the entire world is connected by telecommunication networks. The growing power demand and the dwindling fossil fuels resulted in the unreliable power supply, which is the critical challenge facing by telecommunication industries. Currently, telecom towers are using Diesel Generators (DG) as source of supply, which is rather expensive and emits environmental pollutants. This study analyses the solar photovoltaic (PV) system and battery based hybrid power supply system to reduce the usage of DG.

The effective utilization and management of the PV and Battery sources increases the efficiency and reliability of the system. Therefore, in this work, a literature review related to maximum power point tracking of PV array, Li-Ion battery aging mechanism and battery state of health (SoH) estimation techniques have been presented.

Non-uniform insolation conditions on PV array is the most common phenomenon and it affects the efficiency of the system. Therefore, in this study two global maximum power point tracking (GMPPT) algorithms have been developed. The first GMPPT technique is scanning based two stage hill climbing technique and the second GMPPT technique is artificial bee colony based soft computing technique. Both the techniques have been developed to track the global maximum power point (GMPP) with the fast convergence speed and with the highest tracking accuracy. Moreover, both the GMPPT techniques uses single current sensor for tracking the (GMPP) to reduce the overall cost of the system. The proposed GMPPT techniques are experimentally validated and its performance characteristics are compared with other GMPPT techniques proposed in literature.

Battery is the important power source in the PV and battery based hybrid power supply system. Therefore, reliable power supply to the telecom load depends on the health of the battery. Hence, the knowledge of battery aging mechanism is very vital and helps to configure the right time to replace the battery. In this study, mathematical model of a Li-Ion bat-

tery with aging parameters and two SoH estimation algorithms have been developed. The first SoH estimation technique measures the degradation in capacity of the battery over a period and thus estimates the life. The second method estimates the life of the battery by measuring the DC resistance. Both the techniques have been validated using MATLAB/Simulink platform and an experimental prototype.

The telecom load operates in a pulsed-power mode intermittently, also the power consumption depends on signal traffic. Maintaining the constant voltage at the DC load terminals during the pulsed power operation is the biggest challenge. Therefore, in this study, Type II compensator is developed to regulate the load voltage with fast response time. The stability analysis of system with Type II compensator is analyzed using the MATLAB/Simulink tool. Moreover, the developed voltage regulator system has been tested for various load and also input voltage varying conditions.

Contents

List of Figures

List of Tables

Nomenclature

ABC	Artificial bee colony
ACO	Ant colony optimization
ANN	Artificial neural network
BMS	Battery management system
BTS	Base transceiver station
CAPEX	Capital expenditure
DC	Direct current
DE	Differential evolutionary
DG	Diesel generator
DoD	Depth of discharge
EIS	Electrochemical impedance spectroscopy
EKF	Extended Kalman filter
EoL	End of life
ESR	Equivalent series resistance
FA	Fireflies algorithm
FLC	Fuzzy logic controller
F_{ocv}	Fractional open circuit voltage
F_{scc}	Fractional short circuit current
G	Insolation or Irradiation
GA	Genetic algorithm
GMPPT	Global maximum power point tracking
GP	Global peak
G_{STC}	Insolation at standard test conditions
GWO	Grey wolf optimization
HC	Hill climbing
I_d	Diode reverse saturation current
I_{dc_linl}	DC link current
INC	Incremental conductance
I_{ph}	Photo current
I_{pv}	Photovoltaic current
K	Boltzman's constant
LFP	Lithium iron phosphate

Li-Ion	Lithium Ion
MPP	Maximum power point
OPEX	Operational expenditure
P & O	Perturb and observe
PSC	Partial shading condition
PV	Photovoltaic
q	electron charge
RES	Renewable energy storage
SEI	Solid electrolytic interface
SMPS	Switch mode power supply
SoC	State of charge
SoH	State of health
SVM	Support vector machine
v_{dc_linl}	DC link voltage
V_{pv}	Photovoltaic voltage

Chapter 1

INTRODUCTION

Contents

1.1 GENERAL

Mobile telecommunication is one of the major sectors which has seen rapid growth in recent times, and it is also playing a critical role in world business as telecommunication (telecom) networks connect the entire world. Telecom loads are the essential loads which require the uninterrupted quality power; however, due to increase in power demand and diminishing fossil fuels, the power utility companies are unable to provide reliable and quality power. Moreover, developing nations like India has seen a rapid power demand in these years, but due to diminishing coal reserves and

poor infrastructure resources for power generation and distribution, the power utility companies are unable to provide quality power to the country. Moreover, poor quality of power substantially increases the operational expenditure of system. In the midst of these adversities, the telecom sector has seen a fast development in the last decade.

The power supply equipments required for the telecom network is housed by Base Transceiver Station (BTS). Generally BTS stations are classified into three groups based on their power consumption levels (Liu et al., 2013). A small rating BTS station consumes 400 to 1000W, a medium rating station consumes 1000 to 2000W and super macro (High power rating) station consumes more than 2000W of power. Typically, 80% of telecom towers have power rating around 3.5kW. Majority of these BTS are powered by electrical grid which is basically the conventional energy produced by fossil fuels. Many telecom towers are present in rural areas where this electrical grid power is unreliable or not available at all. It is observed that the main challenge faced by the telecom industry today is to supply continuous and quality power to BTS located in rural areas.

To provide a continuous power, telecom industries use standalone Diesel Generator (DG) as the main backup source of electricity. These DGs have high long term costs due to maintenance, fuel requirement and fuel transport. Cost of using DG as an alternative source is three times more than that of grid power (Prema et al., 2014). Further, DG can be loud and it emits pollutants like unburned HC, CO and NO_x that can have adverse health and environmental effects. DG emits 2.7kg of CO_2 with burning one liter of diesel (North, 2007).

On the other hand, renewable energy sources (RES) are becoming a major alternative to the use of fossil fuel for supplying continuous power to BTS stations. Solar energy is the one, which is abundant and reliable. In addition, reduction in the cost of the photovoltaic (PV) panel and rapid advancements in PV technology have made solar energy the most popular and efficient distributed energy source in recent times. Moreover, PV systems are best suitable for BTS load, since the peak demand of typical BTS load is only in few kWs.

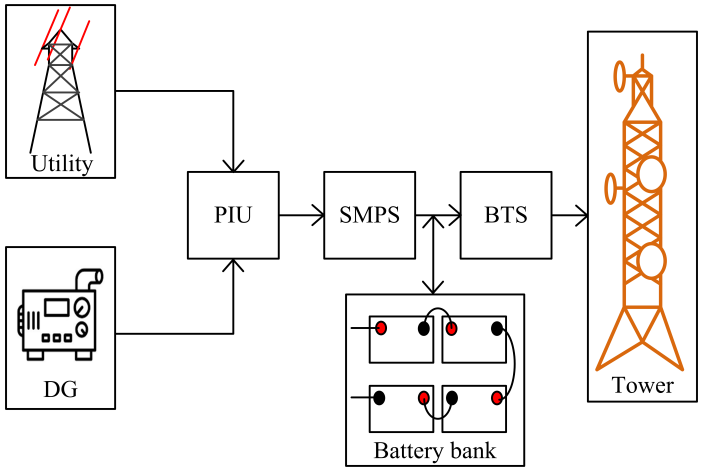

Figure 1.1: Block diagram of a conventional power supply system for telecom load

1.1.1 POWER SUPPLY CONFIGURATIONS FOR TELECOM LOAD

In conventional telecom stations where access to grid electricity is available, it uses DG and batteries as backup sources in case of power outages. During which, the battery acts as primary source of supply to meet entire telecom (i.e., base transceiver station (BTS)) load as energy cost per unit of battery is very less compared to the DG per unit cost. And when battery gets drained DG meets the demand of BTS. Fig. 1.1 shows the architecture of a conventional power supply scheme of BTS station where grid power supply is available. Power interface unit (PIU) in Fig. 1.1 switches between the power sources and SMPS converts the supply AC voltage to 48V DC for BTS loads. In most of the cases, DG runs with 20% to 30% of its rated load in conventional system and due to this the fuel consumption and carbon footprint is more. In rural areas, where access to the grid is unavailable, DG is the only source of supply. In this case, the operational expenditure is very high due to DG. Therefore, these limitations have led to pay more focus on standalone hybrid power supply systems.

Analysis of literature shows that the hybrid systems such as PV/Battery/DG, PV/DG and PV/Battery hybrid configurations reduces the use of diesel consumption and operational cost of the system for BTS stations where there is no access to grid supply. (Liu et al., 2013) have proposed a method where DG supplies power to both load as well as battery to improve the load on the DG to operate at optimal

operating point on fuel consumption characteristics. (Yamegueu et al., 2011) and (Ajan et al., 2003) have explained experimental analysis of PV/DG hybrid system, where PV and DG are rated to meet peak load of the system, during sunlight hours PV is scheduled to meet the load, in case PV is unavailable DG supplies the load. In this configuration CAPEX and OPEX is less, but smooth power flow is a big challenge since PV power output is uncertain. The conventional configuration PV/Battery/DG used for standalone mode is shown in Fig. 1.2.

An energy storage system (i.e. battery) is incorporated to the PV/DG configurations to ensure the reliability of a system (Kaldellis et al., 2011). (Kaldellis, 2010) have optimally sized the components of DG/PV/Battery system to ensure the reliability of the supply to BTS load. Also, the cost benefit analysis and sensitivity analysis of a complete system is done. In the context of hybrid power supply based street lighting, (Lagorse et al., 2009) have proposed PV/Battery/Fuel Cell. In this proposition the fuel cell replaces conventional DG which therefore reduces the green house emission.

In countries where solar insolation is ample and with the falling PV panel cost, optimally sized PV and battery alone can supply the reliable power to the BTS load (Energy, 2012). However, supplying a continuous power using standalone PV and Battery is still a challenging task. Optimal design methodology of PV and battery system for the continuous seamless power supply to the BTS load is given in the Appendix A.

This research work mainly focuses on effective utilization of PV and battery sources in a standalone PV-Battery power supply system to supply reliable power to the BTS load. Fig. 1.3 shows the block diagram of PV-Battery power supply system. Further, brief insights and working details of PV and battery are explained in the following sections.

1.2 PHOTOVOLTAIC SYSTEMS

PV cells are the fundamental building blocks for the large PV power system. The incident sunlight on PV cell generates the charge carriers and which produces the current (Amps). Typically, PV cells are very small and produces power in the range of $1-2W_p$, hence a group of such cells are connected in series and/or parallel to form a PV module, and which can produce power in the range of a few hundred watts.

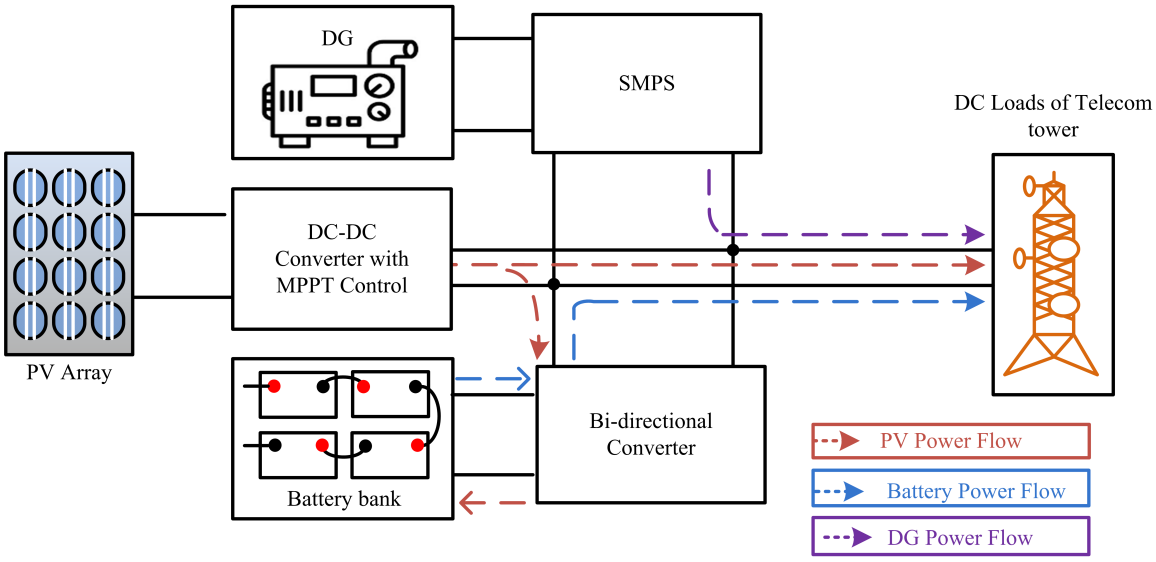

Figure 1.2: Block diagram of PV-Battery-DG power supply system for telecom load

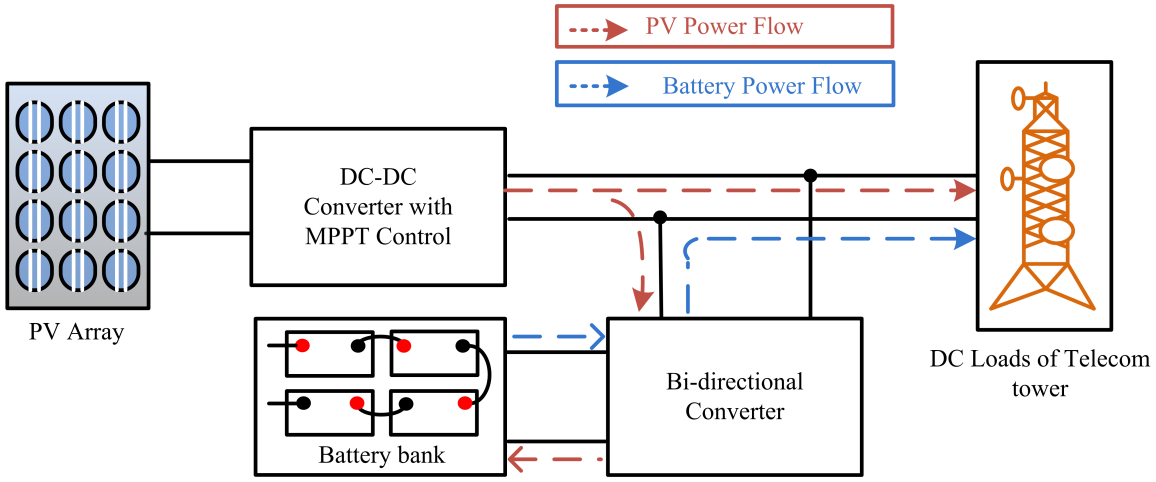

Figure 1.3: Block diagram of PV-Battery power supply system for telecom load

Further, to increase the power rating of the system PV modules are connected in series and/or parallel to form a PV array.

The power generated by PV module depends on solar insolation (irradiation) falling on its surface and ambient temperature of the PV cell. Therefore, to analyze the electrical characteristics of PV cell and PV array in various operating conditions, mathematical model of a PV cell will be discussed in next section.

1.2.1 MATHEMATICAL MODEL OF PHOTOVOLTAIC CELL

An electrical equivalent model of a PV cell is required to analyze the characteristics of a PV cell for solar insolation and temperature variations. However, there are different equivalent circuit models viz. single diode, two diode and dynamic model as shown in Fig. 1.4 (Kim et al., 2013) and (Villalva et al., 2009). Amongst these, single diode model is the most popular, simple and it is developed using the Schottky diode equation. The model of a PV cell considers the solar insolation and PV cell operating temperature as the inputs. The equation for the PV current is described as,

$$I_{PV} = I_{ph} - I_d - \frac{V_{pv} + I_{pv}R_s}{R_p} \tag{1.1}$$

where, I_{ph} is the photo current generated from the solar insolation, I_d is the diode reverse saturation current, R_s and R_p are resistance due to material contacts and leakage resistance respectively and V_{pv} and I_{pv} are voltage and currents of PV cell respectively. The equation for I_d is described as follows,

$$I_d = I_0 \left[exp\left(\frac{V_{pv} + I_{pv}R_s}{AV_t} \right) - 1 \right] \tag{1.2}$$

where, I_0 is the reverse saturation current of the diode, V_t is the thermal voltage of the diode and A is the ideality factor of the diode.

To simplify the computation ideality factor (A) is considered as 1. The photo current (I_{ph}) is expressed as follows,

$$I_{ph} = \left[I_{scSTC} \left(\frac{R_s + R_p}{R_p} \right) + K_i \Delta T \right] \frac{G}{G_{STC}} \tag{1.3}$$

where, I_{scSTC} is the short circuit current of PV cell at STC condition, $\Delta T = T_{cell} - T_{STC}$, G is the solar insolaion W/m^2 falling on PV cell, G_{STC} is the insolaion a STC and the constant K_i is the short circuit current coefficient in $mA/^\circ K$ provided

in the technical data sheet. STC conditions are $T_{STC} = 25°C, G_{STC} = 1000W/m^2$.

The diode saturation current with variation in temperature is given by,

$$I_0 = \frac{I_{scSTC} + K_i \Delta T}{exp\left(V_{ocSTC} + \frac{K_v \Delta T}{AV_t}\right) - 1} \tag{1.4}$$

where, K_v is the open circuit voltage coefficient in $mV/°K$ provided in the data sheet, V_{ocSTC} is the open circuit voltage of PV cell at STC and V_t is the thermal voltage of the diode and it is expressed as follows,

$$V_t = \frac{KT}{q} \tag{1.5}$$

where, K is Boltzman's constant ($1.238 \times 10^{-23} J/K$), T is the ambient temperature in Kelvin and q is the electron charge ($1.69 \times 10^{-19} C$).

Using equations (1.1)-(1.5) and number of series & parallel (i.e., n_s, n_p) cells, a complete PV module can be modeled. Final equation to model the PV module is expressed as follows,

$$I_{pv} = n_p I_{ph} - n_p I_0 \left[exp\left(\frac{n_p V_{pv} + n_s I_{pv} R_s}{n_p n_s A V_t}\right) - 1\right] - \frac{n_p V_{pv} + n_s I_{pv} R_s}{n_s n_p R_p \left(\frac{n_p}{n_s}\right)} \tag{1.6}$$

1.2.1.1 Electrical Characteristics of PV array

PV array exhibits different electrical characteristics (i.e., $I-V$ & $P-V$) under uniform and non-uniform insolation conditions on PV array. During uniform insolation conditions, PV array exhibits single maximum power point (MPP) in its $P-V$ curve, the position and amplitude of MPP will be influenced by solar insolation and ambient temperature of the array. $I-V$ & $P-V$ characteristics under different uniform conditions are shown in Figs. 1.5-1.6. From Fig. 1.5, it is clear that, maximum power produced by a PV cell is directly proportional to solar insolation. From Fig. 1.6, it is clear that, with the increase in PV cell ambient temperature maximum power produced by PV reduces.

In the practical applications many PV modules are connected in series and/or parallel to meet the load requirements as shown in Fig. 1.7. Hence, non-uniform insolation i.e., partial shading conditions (PSC) are unavoidable as some portion of

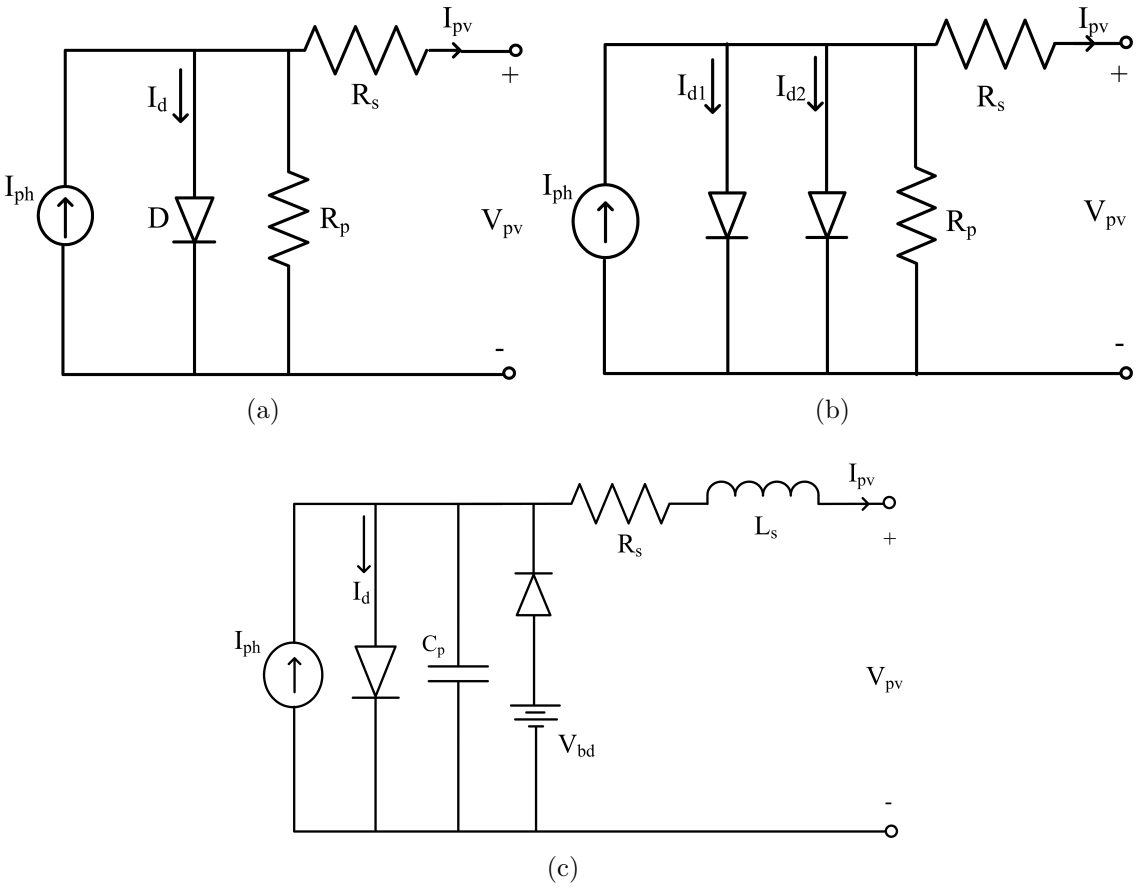

Figure 1.4: (a) One-diode model (b) Two-diode model (c) Dynamic model of a PV cell

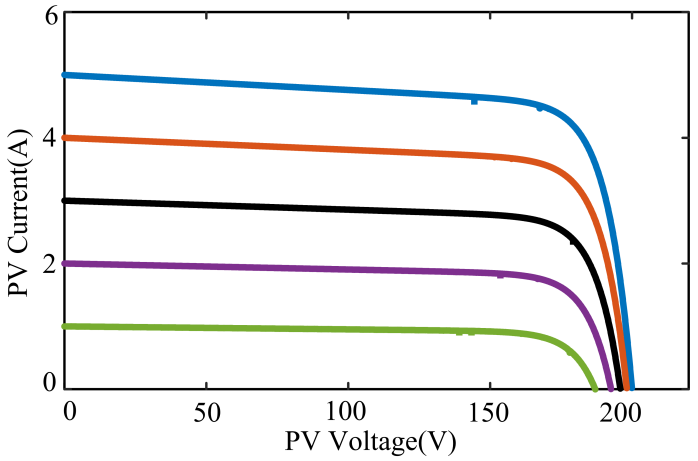

(a)

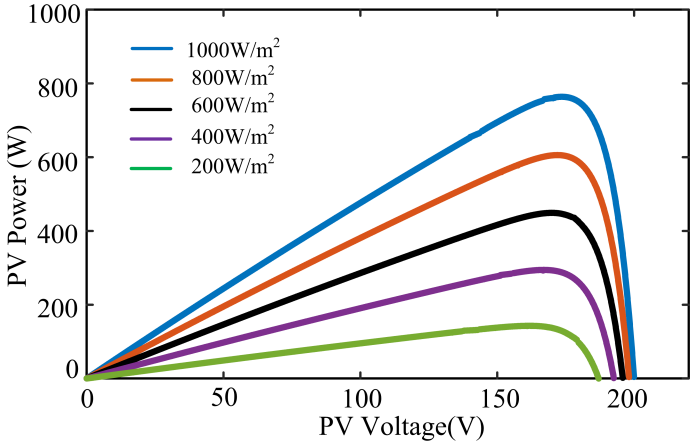

(b)

Figure 1.5: (a) $I-V$ (b) $P-V$ characteristics of a PV array for different uniform insolation conditions

the PV array may receive less solar insolation due to passing clouds over the modules or the shadowing effect of trees, etc.

During PSC, series connected PV arrays produce multiple local peaks and one global peak in their $P-V$ characteristics, also, multiple steps can be seen in the $I-V$ characteristics. It is due to the presence of bypass diodes across the PV module. The purpose of the bypass diode connections is to bypass the shaded module such that unshaded modules can provide uninterrupted power. To analyze the effect of PSC, four series connected modules have been modeled and its $P-V$ & $I-V$ characteristics is shown in Fig. 1.8.

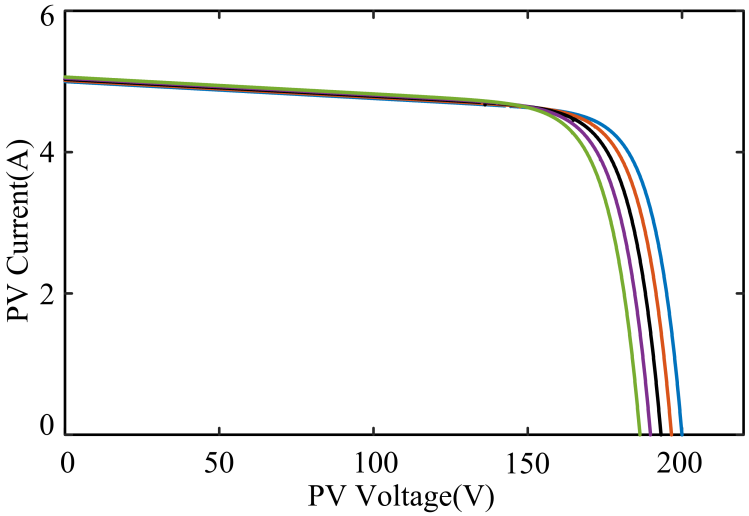

(a)

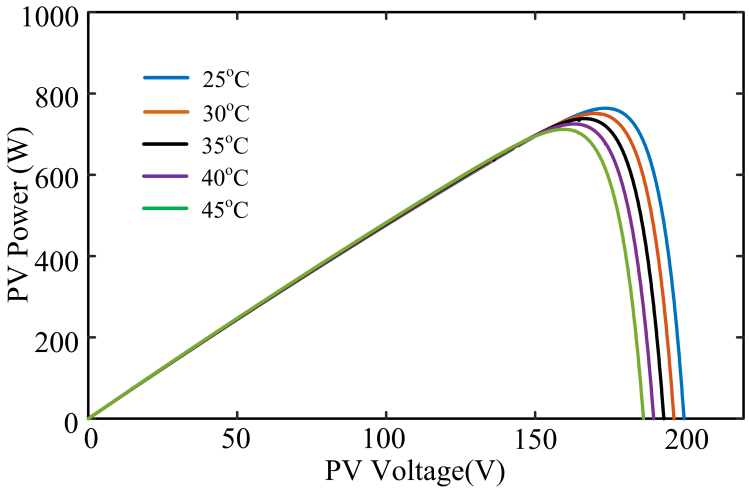

(b)

Figure 1.6: (a) $I-V$ (b) $P-V$ characteristics of a PV array at $1000W/m^2$ and at different temperature conditions

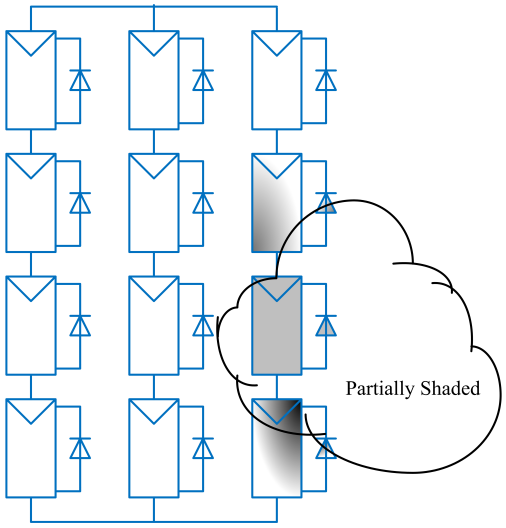

Figure 1.7: Partial shading on PV array

PSC is a common phenomenon in PV systems, and during which tracking the local peaks leads to huge power loss and it effects the efficiency of whole PV-Battery system. Moreover, continuous power supply to BTS load is not possible. Therefore, it is necessary to develop a global maximum power point tracking (GMPPT) algorithm for the effective utilization of PV.

1.3 ENERGY STORAGE SYSTEM

Rapid advancements in the Lithium ion (Li-Ion) technology resulted in high specific power and energy density. Therefore, Li-Ion batteries have become standard in applications like electric vehicles, distributed generation, consumer electronics, etc... Li-Ion batteries have higher cycle life than any other rechargeable batteries, charge retention of Li-Ion batteries is very good and the batteries can be cycled over a thousand times. However, these batteries are expensive and they are limiting factor for the service life of the complete product.

The term lithium-ion (Li-Ion) battery refers to a family of different chemistries such as Lithium Cobalt Oxide ($LiCoO_2$), Lithium Iron Phosphate ($LiFePO_4$ or LFP), Lithium Nickel Cobalt Aluminum Oxide ($LiNiCoAlO_2$ or NCA), Lithium Manganese Oxide ($LiMn_2O_4$ or LMO) and Lithium Nickel Manganese Cobalt Oxide ($LiNiMnCoO_2$ or NMC). A comparison chart of these Li-Ion chemistries have presented in Fig. 1.9. From the comparison chart, it is clear that LFP battery offers

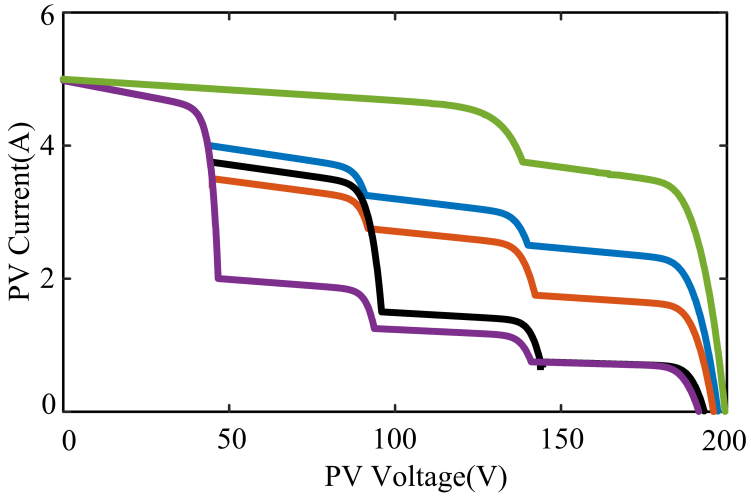

(a)

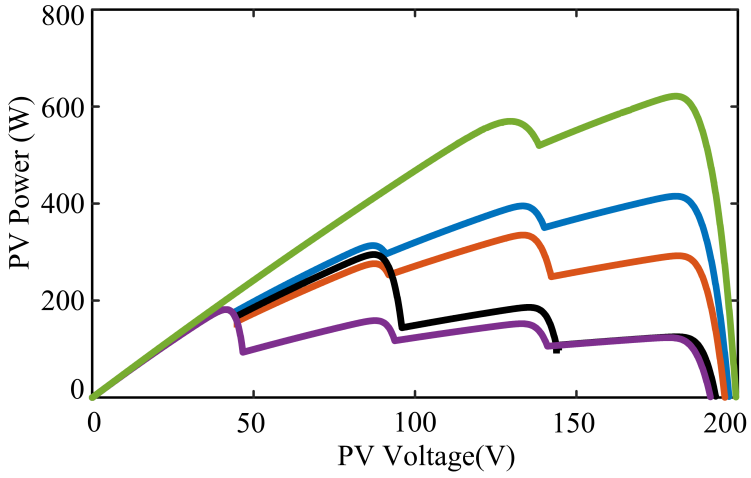

(b)

Figure 1.8: (a) $I-V$ (b) $P-V$ characteristics of PV array during non-uniform insolation conditions

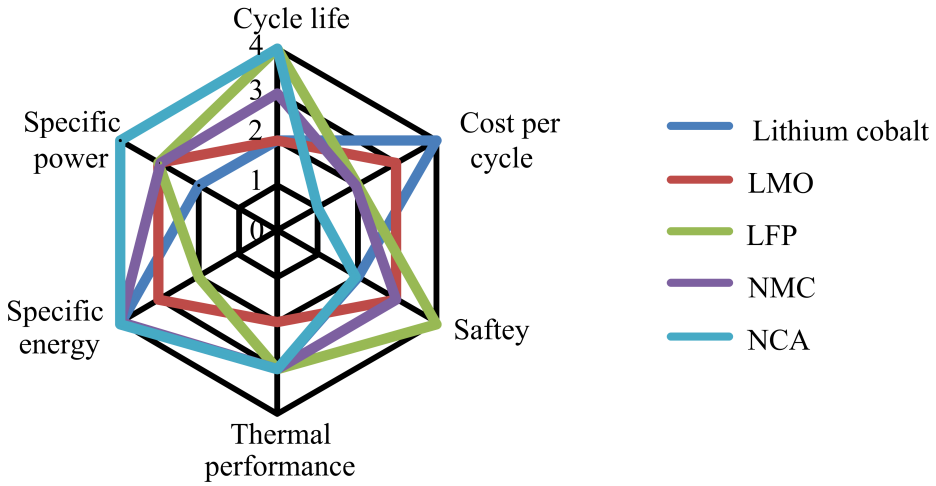

Figure 1.9: Comparison of different Li-Ion chemistries

good cycle life, low cost per cycle and good safety. Therefore, in the present study (i.e., PV-Battery power supply system) LFP battery is selected as energy storage system.

In most of the cases, before the product reaches to its end of life, batteries get damage due to improper operation and maintenance. Therefore, this increases the recurring cost of system as the battery has to be replaced multiple times. (Lam and Bauer, 2013) and (de Vries et al., 2015) have reported that charging/discharging the battery with high charge/discharge rate at elevated temperatures and overcharging and deep discharging the battery deteriorates the life (i.e., premature failure).

To prevent the premature failure of the battery, a battery management system (BMS) should be employed to monitor and control the battery operating conditions. However, most of the BMSs available today does not monitor the aging and health of the battery and they monitors only state of charge (SoC). Hence, it would be advantage to have knowledge on effect of different operating conditions on battery life and health condition of the battery. Moreover, knowing the health of the battery in advance, helps to improve the reliability of overall PV-Battery power supply system.

To know the health condition of the battery in advance, it is very important to have knowledge on battery runtime characteristics. Therefore, modeling of LFP battery will be discussed in the further sections.

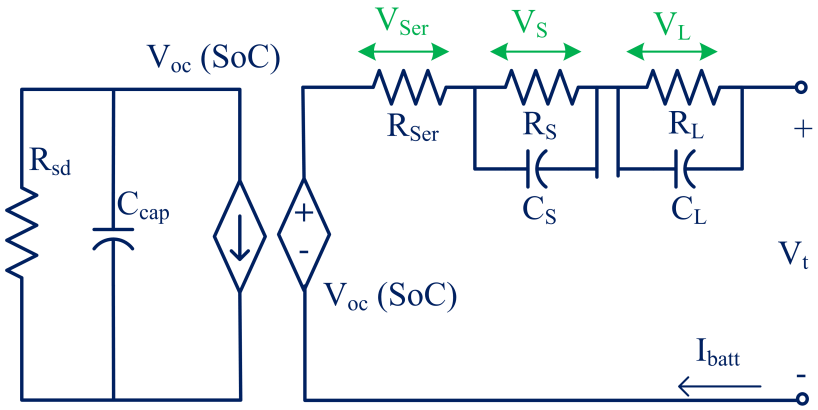

Figure 1.10: Electrical equivalent circuit of Li-Ion battery

1.3.1 MODELING OF LI-ION CELL

In literature, two types of battery models such as electrical equivalent circuit and electrochemical models have been proposed. In this study two RC network Thevenin electrical equivalent circuit model is adopted due to its less complexity (Lam et al., 2011). Fig. 1.10 shows the electrical model of a single cell Li-Ion battery. Wherein, V_{oc} is the open circuit voltage of battery and it depends on battery state of charge (SoC). SoC is the percentage of charge available in the battery with respect to rated capacity.

The two parallel RC networks represent the transient behavior, R_{Ser} is the internal resistance of the battery which contributes for the instantaneous voltage drop and R_{sd} contributes for the calendar life loss. Calendar loss is the degradation of battery life, when it is in idle condition. C_{cap} represents the rated capacity of the battery.

The battery parameters V_{oc}, R_{Ser}, R_S, R_L, C_S and C_L are the functions of SOC and expressed as (Lam et al., 2011),

$$V_{oc} = -0.5863 \times e^{-21.90 \times SoC} + 3.414 + 0.1102 \times SoC - \left(0.1718 \times e^{\frac{-0.008}{1-SoC}}\right) \quad (1.7)$$

$$R_{Ser} = 0.1298 \times SoC^4 - 0.2892 \times SoC^3 + 0.2273 \times SoC^2 - 0.07216 \times SoC + 0.0898 \quad (1.8)$$

$$R_S = -0.0108 \times e^{-11.03 \times SoC} + 0.01827 - 6.462 \times 10^{-3} \times SoC \quad (1.9)$$

$$C_S = 0.01697 \times SoC^3 - 1.007 \times 10^{-3} \times SoC^2 + 1.408 \times 10^{-3} \times SoC - 0.07216 \times SoC - 3.897 \times 10^{-2} \quad (1.10)$$

$$R_L = 0.295 \times e^{-20 \times SoC} + 0.04722 - 0.0242 \times SoC \quad (1.11)$$

$$C_L = 2.13 \times 10^6 \times SoC^6 - 6.007 \times 10^6 \times SoC^5 + 6.271 \times 10^6 \times SoC^4$$
$$-2.958 \times 10^6 \times SoC^3 + 5.998 \times 10^5 \times SoC^2 - 3.102 \times 10^4 \times SoC + 2.232 \times 10^3 \quad (1.12)$$

A 4Ah single cell LFP battery has been modeled using the above equations, the open circuit voltage characteristics, terminal voltage characteristics during discharging mode and run time characteristics during charging mode are shown in Fig. 1.11. In this section, only LFP cell modeling is discussed, the effect of different operating conditions (i.e., aging parameters) and their modeling will be discussed in detail in Chapter 4.

1.4 RESEARCH MOTIVATION

PV and Battery based power supply configuration for standalone telecom load reduces the operational cost by eliminating the use of diesel generator. However, non-uniform insolation conditions on PV array makes the system ineffective. To overcome this, an effective GMPPT algorithm is required for the efficient utilization of PV and to improve the overall system efficiency.

Li-Ion Batteries are used in PV/Battery power supply configuration for BTS load are less tolerant to the overcharge, deep discharge and charging/discharging at elevated temperatures. Therefore, monitoring and controlling the parameters such as battery voltage, SoC and charge/discharge currents enhance the battery life. Moreover, knowing the health of the battery and aging process helps the user to take the remedial action (i.e., operating the battery in safe conditions) to improve the reliability of overall system. Hence, it is necessary to develop a BMS which estimates the health of the battery and controls the battery parameters effectively. Therefore, literature review related to GMPPT techniques and Li-Ion battery life estimation techniques are discussed in next chapter.

1.5 PROBLEM STATEMENT

Tracking local maximum power point during partial shading condition makes system ineffective in PV, battery based hybrid power supply system. Moreover, overcharging and deep discharging the battery deteriorates the battery life, which affects the

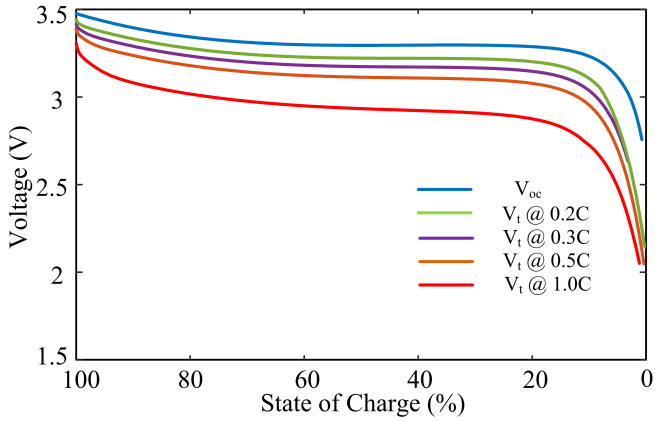

(a)

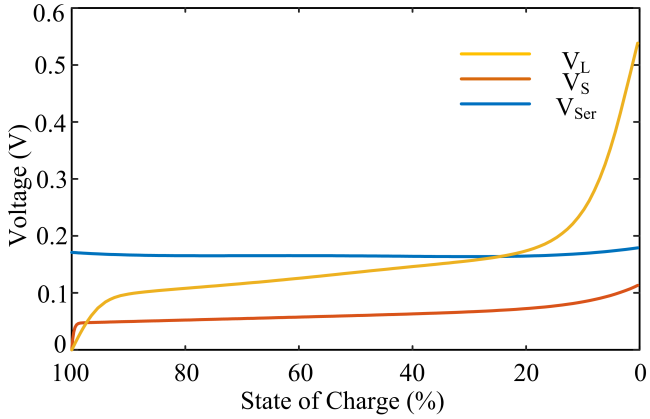

(b)

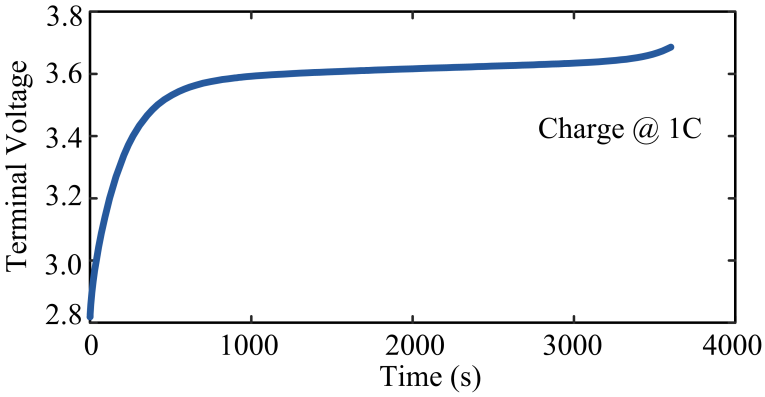

(c)

Figure 1.11: (a) Open circuit voltage and terminal voltage characteristics of LFP cell for various discharge rates (b) Voltage drop characteristics of battery modeling parameters for 1C discharge rate (c) runtime characteristics during charging mode

reliability of complete system. Therefore, it necessitates the development of control algorithm for the effective utilization and management of power sources in hybrid power supply system.

1.6 THESIS ORGANIZATION

The whole thesis is organized into six chapters as follows,

Chapter 1: A brief introduction to the BTS load, different power supply configurations for BTS load, limitations of conventional power supply configurations and introduction to the PV-Battery based power supply system are discussed in this chapter.

Chapter 2: State-of-the-art related to global maximum power point tracking (GMPPT) techniques, Li-Ion battery state of health (SoH) estimation techniques, identified research gaps and research objectives are discussed in this chapter.

Chapter 3: For the effective utilization of PV array during non-uniform insolation conditions, two different kinds of GMMPT techniques has been proposed in this chapter. The first method comes in the category of two-stage scanning based technique and the second method is a hybrid technique, which combines the artificial bee colony optimization and hill climbing algorithms. Tracking the GMPP with good tracking speed and efficiency are the major motives of this work. The proposed techniques have been validated using MATLAB/Simulink and also using a experimental prototype. The simulation and experimental performance of proposed GMPPT techniques are discussed in this chapter. Moreover, the proposed techniques have been compared with the other GMPPT techniques in literature.

Chapter 4: In PV-Battery power supply system batteries are the essential element and it decides the reliability of the overall system. Most of the times before the power supply system reaches to its end of life, batteries get damage due to improper operation and maintenance. Therefore, effect of operating conditions on battery life is discussed in this chapter.

Moreover, to estimate the life of the battery, two on-line state of health (SoH) estimation techniques are proposed in this chapter. The first technique measures the degradation in capacity of the battery over a period and thus estimates the life. The second method estimates the life of battery by measuring the DC resistance. Both the techniques have been validated using Matlab/Simulink platform and using a experimental prototype.

Chapter 5: For the safe operation of DC loads of BTS, it is required to maintain 48V constant DC supply at the load terminals. However, with the signal traffic load current varies and which effects the load voltage regulation. Therefore, in this chapter a voltage regulation technique is developed and tested in MATLAB/Simulink platform. Moreover, its performance characteristics are discussed in this chapter.

Chapter 6: This chapter concludes the contributions of the proposed research work and also discusses about scope for the possible future works.

Chapter 2

LITERATURE REVIEW

Contents

2.1 GENERAL

Since the present study deals with the PV and battery based hybrid power supply system, state-of-the-art related to maximum power point tracking techniques and battery management systems are discussed in this chapter.

2.2 MAXIMUM POWER POINT TRACKING TECHNIQUES

PV sources exhibit nonlinear electrical characteristics, thus their power-voltage ($P-V$) curves exhibit a single maximum power point (MPP) during uniform insolation. However, the maximum power point continuously moves its position based on solar insolation and PV module ambient temperature. Therefore, to extract the maximum power in all insolation conditions, a maximum power point tracking (MPPT) algorithm is necessary. Upon analyzing the literature, MPPT techniques can be broadly classified into two categories such as,

- Conventional MPPT (CMPPT)
- Global MPPT (GMPPT)

2.2.1 CMPPT TECHNIQUES

The conventional MPPT techniques include, fractional open circuit voltage (F_{ocv}), fractional short circuit current (F_{scc}), Perturb and Observe (P&O), Hill Climbing (HC) and Incremental conductance (INC).

2.2.1.1 Fractional Open Circuit Voltage and Fractional Short Circuit Current Techniques

(Schoeman and Wyk, 1982) have developed fractional open circuit voltage (F_{ocv}) technique on an approximation that, MPP voltage (V_{mpp}) occurs anywhere in the range of 65% to 90% of open circuit voltage (V_{oc}). Similarly to the F_{ocv}, (Masoum et al., 2002) have developed fractional short circuit current ((F_{scc})) technique, which is approximated on a relation that the PV current at MPP will be in the range of 80% to 90% of short circuit current (I_{sc}). For the periodic measurement of V_{oc} and I_{sc} of a PV array, whole circuit should be isolated from the PV array. This leads to momentary power loss. Accuracy of these techniques are less, since they are developed based on an approximation.

2.2.1.2 Perturb & Observe and Hill Climbing Techniques

Perturb & observe (P&O) technique measures the PV power in two successive time steps by giving a small voltage perturbation. Further, the direction of tracking is identified by observing the sign changes in PV power for every voltage perturbation. If the sign change of PV power is positive, then controller ensures that operating point is shifting towards the MPP. On the other hand, if the sign change is negative, controller changes the voltage perturbations in opposite direction. Therefore, once the MPP is tracked, operating point will have oscillations around the MPP. Hill climbing (HC) technique works similar to the P&O, but the only difference is perturbation in duty cycle is made instead of PV voltage (Veerachary et al., 2001). Fig.2.1 shows the flowchart of the P&O technique.

The tracking time of these techniques depends on step size in perturbation. If the step size is large, P&O will converge quickly. However, the oscillations around MPP will be high. On the other hand, convergence time will be poor, if the step size is less. To overcome this, an adaptive step size P & O technique is proposed by (Killi and Samanta, 2015). In adaptive P&O technique, perturbation step size changes with the $P-V$ curve slope.

2.2.1.3 Incremental Conductance Technique

Incremental conductance (INC) technique compares the instantaneous conductance I/V with the incremental conductance ($\Delta I/\Delta V$) to track the MPP. INC technique is developed on the fact that dP/dV is zero at the MPP, i.e.,

$$\frac{dP_{pv}}{dV_{pv}} = \frac{d(P_{pv}dI_{pv})}{dV_{pv}} = I_{pv} + V_{pv}\frac{dI_{pv}}{V_{pv}} = 0 \tag{2.1}$$

Equation (2.1) can be rearranged as,

$$\frac{I_{pv}}{V_{pv}} = -\frac{dI_{pv}}{dV_{pv}} = \frac{\Delta I_{pv}}{\Delta V_{pv}} \tag{2.2}$$

INC technique works on the basis of slope characteristics of $P-V$ curve during uniform insolation conditions. Typically, $P-V$ curve can be divided into three regions as explained using following relation;

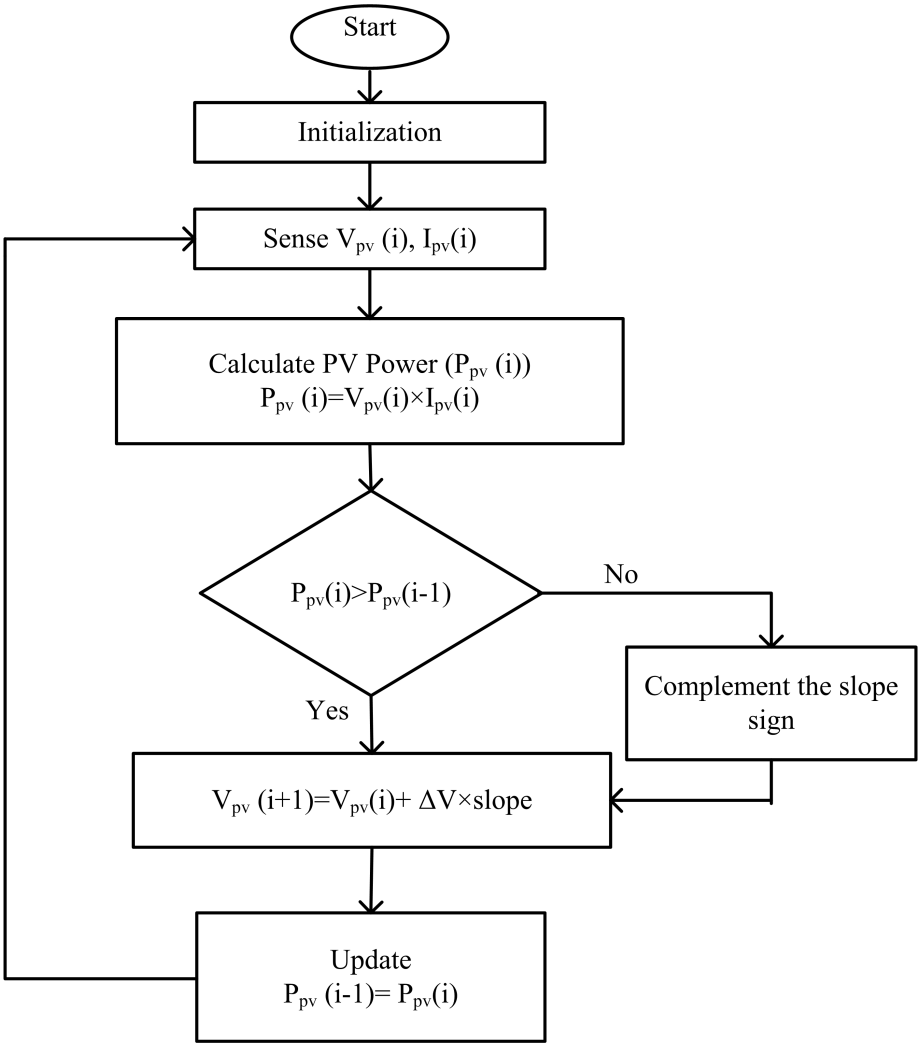

Figure 2.1: Flowchart for the Perturb and Observe MPPT Technique

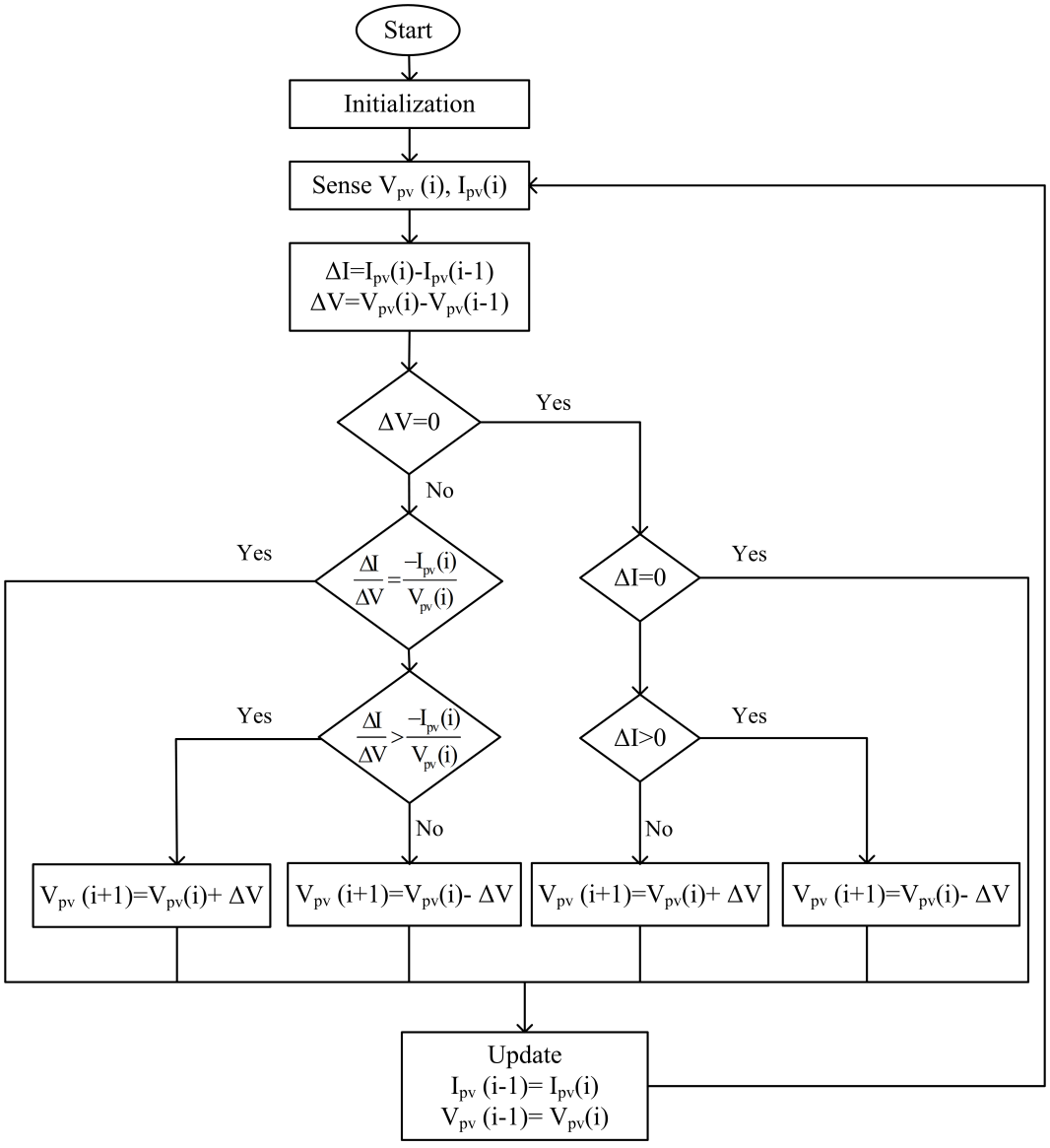

Figure 2.2: Flowchart for the INC Technique

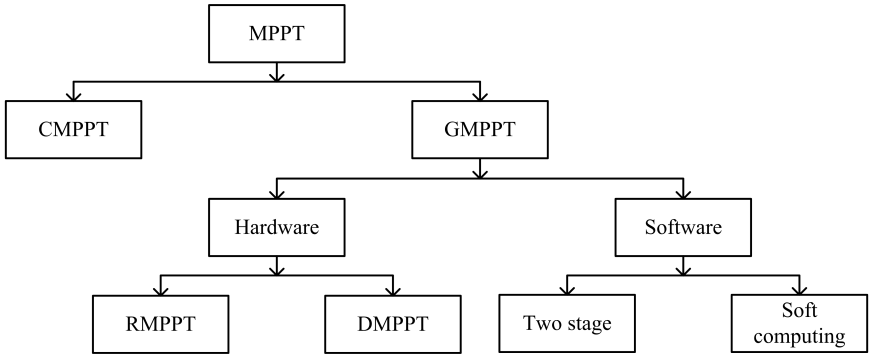

Figure 2.3: Classification of Various MPPT Techniques

$$\begin{cases} \frac{\Delta I_{pv}}{\Delta V_{pv}} = \frac{-I_{pv}}{V_{pv}}; at\ \ MPP \\ \frac{\Delta I_{pv}}{\Delta V_{pv}} > \frac{-I_{pv}}{V_{pv}}; right\ \ of\ \ MPP \\ \frac{\Delta I_{pv}}{\Delta V_{pv}} < \frac{-I_{pv}}{V_{pv}}; left\ \ of\ \ MPP \end{cases}$$

(Kuo et al., 2001) have implemented INC technique for a two-stage grid connected PV system. The tracking efficiency and oscillations around the MPP of this technique is same as P&O, but the INC works better under rapidly changing insolation conditions. Similar to the adaptive P&O, (Enrique et al., 2010) have developed an adaptive INC technique to track the MPP with faster convergence speed.

2.2.2 GMPPT TECHNIQUES

In practical environmental conditions, due to the fast variation in insolation, passage of clouds, shadow of buildings and dust on the PV cell surface results in non-uniform insolation on PV array. Thus, multiple peaks (local maxima and global maxima) occur in the power vs. voltage ($P-V$) characteristics. In this condition, CMPPT techniques fail to track the global maxima. To increase the efficiency of whole PV power system and for the effective utilization of PV array during non-uniform insolation conditions, it is required to operate the PV array at its global maxima (GMPP). In this section, operating principles of different GMPPT techniques will be discussed, and also their critical advantages and disadvantages will be discussed. The GMPPT techniques can be classified into two categories such as 1) Hardware 2) software based techniques. Classification of various MPPT techniques are shown in Fig.2.3.

Hardware based techniques are further classified into two categories such as 1)

RMPPT and 2) DMPPT. RMPPT techniques dynamically reconfigure the electrical connection scheme of PV array to mitigate the multiple peaks in the Power vs. Voltage characteristics of PV array. Total cross-tie, bridge-link and honey-comb are the basic connection schemes of PV array, these techniques requires greater number of switches to form a switching matrix to change the connection pattern (La Manna et al., 2014). Moreover, complexity of control algorithm used and total cost of the system is more. On the other hand, DMPPT techniques divide the PV array into subgroups and use the conventional MPPT technique for each subgroup (Pilawa-Podgurski and Perreault, 2013). This type of techniques best suits for small power rated systems and it requires separate power electronic interface circuits for each subgroup of a PV array. Therefore, it increases the overall cost of the system.

Software based algorithms track the GMPP by developing the control algorithm for the power electronic interface between PV array and load. The software based GMPPT algorithms are further classified into two groups such as two-stage algorithms and soft computing based optimization algorithms. These software based GMPPT technique includes two modes of operation such as,

1. Detecting the event of non-uniform insolation on PV array
2. Tracking the GMPP

Most of the GMPPT techniques in the literature, detects the event of partial shading on PV array by measuring either PV voltage or PV power in two consecutive time intervals and compares it with the threshold value as described in equations (2.3)-(2.4).

$$P_{pv}(K) - P_{pv}(K-1) > P_{threshold} \tag{2.3}$$

$$V_{pv}(K) - V_{pv}(K-1) > V_{threshold} \tag{2.4}$$

2.2.2.1 Two-Stage GMPPT Techniques

Two-stage GMPPT techniques, generally uses some searching process to identify the GMPP locality in stage 1. Further, in stage 2, conventional MPPT techniques are used to track and retain the GMPP. (Kobayashi et al., 2003) have presented a GMPPT technique, which tracks the GMPP by measuring the V_{oc} and I_{sc} of the PV array. This technique requires the additional circuitry to measure V_{oc} and I_{sc} periodically.

In another attempt, (Kobayashi et al., 2005) have presented a load line based two-stage GMPPT algorithm, this method shifts the operating point of the PV array to the vicinity of global peak by estimating the R_{mpp} value in stage 1 using the following equation (2.5);

$$R_{mpp} = K\frac{V_{mpp}}{I_{mpp}} \tag{2.5}$$

Where, K is the correction factor, V_{mpp} and I_{mpp} are approximated as 80% V_{oc} and I_{sc} respectively.

In stage 2, the conventional MPPT (i.e. INC) technique is used to track the GMPP. However, this method fails to track GMPP in some partial shading patterns, specifically when global peak exists in the right most corner in the $P-V$ characteristics. A short circuit pulse based GMPPT technique is proposed by (Noguchi et al., 2002). This method fails to track the GMPP in few shading conditions and it requires extra switch to measure short circuit for every few minutes.

(Ji et al., 2011) have presented a linear equation to find the vicinity of GMPP. Therefore, in stage 1, using this equation operating is shifted to GMPP neighborhood and in stage 2, conventional INC method is used to track and retain the GMPP.

(Koutroulis and Blaabjerg, 2012) have proposed a $P-V$ curve scanning based two-stage GMPPT technique. In this technique, the complete $P-V$ curve is scanned from maximum voltage to minimum voltage in stage one. During the scanning, at each sampling interval, PV voltage and current is measured and stored in memory to find the GMPP existing area. Further, in stage 2, conventional INC technique is used to track and retain the GMPP.

A duty cycle sweep based $P-V$ curve scanning two-stage GMPPT technique proposed in (Lei et al., 2011). In this technique, duty cycle of the power electronic interface between the PV array and load is varied from the range of 0 to 90%. Similar to the method in (Koutroulis and Blaabjerg, 2012), at every duty cycle, PV voltage and current is recorded to locate the GMPP. Further, conventional P&O technique is used to rack the GMPP in stage 2. Therefore, this technique requires the scanning of almost 80% of $P-V$ curve, which worsen the tracking performance.

In (Bifaretti et al., 2012) have proposed a switched capacitor boost circuit for tracing the $I-V$ characteristics to identify the GMPP in stage 1. Further, a conventional P&O technique is used in stage 2. The increased component count is the major

limitation of this technique. These periodical $P-V$ or $I-V$ curve scanning techniques have low implementation complexity, but they cannot converge to the GMPP in all insolation conditions.

A $P-V$ curve scanning based two-stage GMPPT algorithm is presented in (Patel and Agarwal, 2008) based on two assumptions such as LMPPs in a $P-V$ curve occur at multiples of 80% of PV module V_{oc} and power level of each LMPP increases as travelling towards GMPP and decreases after the GMPP. The GMPPT algorithm in (Patel and Agarwal, 2008) scans the $P-V$ curve at multiples of 80% of $V_{oc-module}$ and finds the neighbourhood of GMPP in stage 1 and the INC algorithm is implemented in stage 2 to retain the GMPP. This algorithm works well in all PSCs, however, it has slow tracking speed.

A two-stage GMPPT method in (Chen et al., 2014) detects the occurrence of PSC and calculates the number of LMPPs in a $P-V$ curve by measuring and comparing the voltage level of each PV module in an array. Upon detecting the event of PSC, a controller measures and compares the power level of each LMPP at 80% of $V_{oc-module}$ to identify the location of the GMPP. This method effectively identifies the event of PSCs, but requires a voltage sensor for each bypass diode in a PV string.

(Ghasemi et al., 2016) have proposed GMPPT technique in which a ramp duty cycle is given to power electronic interface between load and PV source. Continuous sampling of $P-V$ curve has been done in stage 1 to find the GMPP neighbourhood. In stage 2, P&O method is used to track and retain the GMPP. The sampling rate, rate of ramp duty cycles and the size of input capacitor used in interface circuit determine the tracking speed of the system. However, for the higher rate of ramp duty cycles chances of missing the GMPP is more.

(Escobar et al., 2012) have proposed a variable voltage controlled $P-V$ curve scanning technique. This technique uses the HC method and a dP/dV sign change to determine the power level of each LMPP and then finds the GMPP. This method tracks the GMPP accurately but tracking time increases with increase in the PV string voltage.

(Wang et al., 2016) have proposed two GMPPT techniques, the first of which works similarly to the method in (Escobar et al., 2012) with a reduced voltage search space. However, this method has a slow tracking speed, as a major portion of the $P-V$ curve has to be scanned. In the second method, a rapid GMPPT technique is presented to improve the tracking speed. This method measures the bypass diode

currents of each PV module and approximates the power level of each LMPP to identify the GMPP. The implementation cost is the major drawback of this method. A new MPPT approach that works under PSC is introduced by (Ji et al., 2011). In this technique, the voltage values of every LMPP must be previously stored in the controller memory. Therefore, this technique becomes system-dependent.

A Fibonacci sequence based $P-V$ curve scanning method is proposed by (Ahmed and Miyatake, 2008). This method works similar to conventional P&O, but the only difference with respect to the conventional algorithms is Fibonacci sequence determines the step size of perturbations. This method enhances the tracking speed. However, this method fails to locate GMPP during some partial shading conditions.

A modified hill climbing (HC) method in (Ramyar et al., 2017) measures the PV array current at multiples of 80% $V_{oc-module}$ to calculate the number of steps and their length in a current-voltage ($I-V$) curve to analyze the type of $P-V$ curve pattern. Further, using the HC method, all the identified LMPPs are tracked and their power levels are compared to identify the GMPP. This method tracks the GMPP accurately but scans a major portion of the $P-V$ curve.

In (Nguyen and Low, 2010), dividing rectangles (DIRECT) algorithm based $P-V$ curve scanning is proposed in stage 1, a P&O technique is used in stage 2 to retain the GMPP. Computational complexity and slow tracking speed are the major disadvantages of this method. (Boztepe et al., 2014) have proposed restricted voltage window search based GMPPT by selecting upper and lower limits to the search space for the fast tracking of GMPP. However, this method fails to track GMPP if two local peaks have the same power levels. The GMPPT method in (Furtado et al., 2018) also restricts the scanning range of $P-V$ curve using the maximum power trapezium area concept. Further, in stage 2, conventional INC technique is used to track the GMPP.

A power estimation based hybrid two-stage GMPPT algorithm is proposed by (Manickam et al., 2016). This method combines the conventional P&O algorithm and soft computing based PSO algorithm to track MPP during uniform insolation conditions. In stage one, P&O technique is used to track the first LMPP and to estimate the GMPP existing area. In stage two, PSO algorithm with reduced search space is initiated to locate the GMPP. This method has slow tracking speed since PSO is employed during PSC. A brief comparison of two-stage GMPPT techniques is listed in Table 2.1.

Table 2.1: Brief Working Principles of Different Two-stage GMPPT Techniques

#	Reference	Remarks
1	(Noguchi et al., 2002)	Identifies the GMPP by measuring the I_{sc}, requires additional circuit for measuring I_{sc}
2	(Ji et al., 2011)	A linear equation is developed to identify the GMPP vicinity, however chances of missing the GMPP is more in some of PSCs
3	(Koutroulis and Blaabjerg, 2012, Lei et al., 2011)	Converges in all PSCs. But, tracking speed is less, since it requires the scanning of almost 80% of $P-V$ curve
4	(Bifaretti et al., 2012)	Component count is more, since a switched capacitor $I-V$ tracer circuit is employed to locate the GMPP
5	(Patel and Agarwal, 2008)	Tracking speed is improved by scanning only neighborhood of each LMPP
6	(Ghasemi et al., 2016)	A ramp duty cycle is given to trace the $P-V$ characteristics across the input capacitor of interface circuit. No guarantee of convergence in some PSCs
7	(Escobar et al., 2012)	Variable voltage control scanning technique skips the some portion of $P-V$ curve to improve the tracking speed. Converges in all PSCs with good tracking speed
8	(Wang et al., 2016)	A separate current sensor is included for each series connected bypass diode to locate GMPP. Tracking speed is good but the cost of the system increased
9	(Ahmed and Miyatake, 2008)	Scans the $P-V$ curve using Fibonacci sequence to locate the GMPP, however chances of missing the GMPP is more in some PSCs
10	(Ramyar et al., 2017)	DIRECT algorithm is used for reduced scan of $P-V$ curve. Complex in computation and tracking speed is low

2.2.2.2 Soft Computing based GMPPT Techniques

As the $P-V$ characteristics during non-uniform insolation exhibits multimodal characteristics, soft computing based GMPPT techniques are very effective to track the GMPP. These techniques use the evolutionary and nature inspired principles to solve the global maxima problems. Firstly, evolutionary algorithms such as artificial neural networks (ANN) and fuzzy logic controllers (FLC) have been tested for MPPT applications. In the recent years, research is mainly focused on nature inspired optimization techniques to solve the MPPT problems.

ANNs are popularly used for solving the solutions for non-linear systems. Typically, in MPPT applications, three layer networks (i.e. input, hidden and output layer) have been used. The input layer of the network consists of information related to solar insolation or PV voltage/current and the output layer consists of duty cycle or reference voltage for the MPP. The input signals are processed using the hidden layer and then it will be transported to the output layer. The number of neurons used can be selected randomly or an empirical formula can be used. Using the radial basis function (Karatepe et al., 2009) have developed ANN technique for tracking GMPP. In another attempt, (El-Helw et al., 2017) have combined the ANN with P&O to enhance the tracking characteristics.

Similar to the ANN, FLC also works in three stages (i.e. fuzzifier, rule base and defuzzifier), but it has advantage of convenient user interface and ease of implementation. In literature, mostly FLC is combined with the other technique like ANN, genetic algorithm (GA) in MPPT applications (Tarek et al., 2013), (Bounechba et al., 2014). Despite of having advantages like tracking GMPP in all PSCs, ANN requires the separate sensors for measuring the solar insolation and PV module temperature, whereas, FLC requires the prior knowledge of system.

To overcome the shortcomings of ANN and FLC, metaheuristic nature inspired algorithm have been tested for the MPPT application. Particle swam optimization (PSO) is the first successful and most popular technique among these nature inspired algorithms. PSO is a population based optimization technique developed based on the bird flocking. In PSO, each particle moves to the global best value based on the success of neighbour particles and the success of its own.

The operation of PSO is shown in Fig. 2.4, where X_i^j is the i^{th} particles current position (i.e., in j^{th} iteration), V_j is the velocity in current position, V_{j+1} is the velocity of i^{th} particle in next iteration (i.e., $(j+1)^{th}$ iteration) and X_i^{j+1} is the

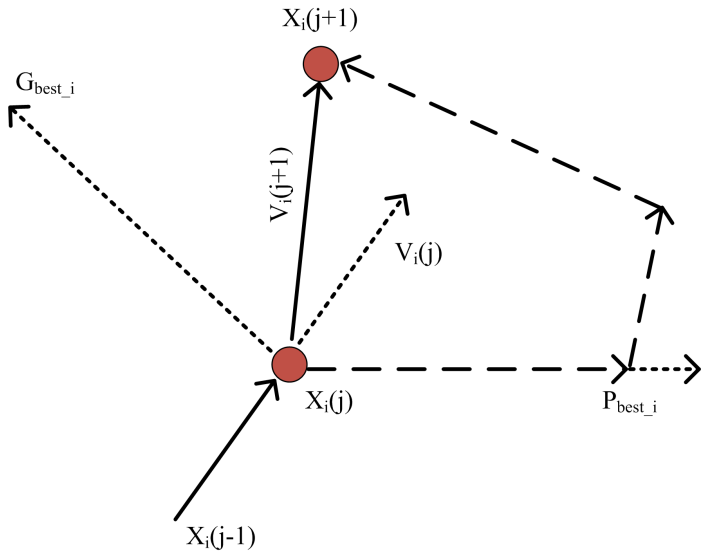

Figure 2.4: Vector representation of PSO Technique

position achieved in the next iteration. Each particle in the search space moves to the global best position using the following equation (2.6),

$$X_i(j+1) = X_i(j) + V_i(j+1) \tag{2.6}$$

The velocity of each particle is updated using equation (2.7),

$$V_i(j+1) = WV_i(j) + C_1 r_1 (P_{best_i} - X_i^j) + C_2 r_2 (G_{best_i} - X_i^j) \tag{2.7}$$

where, C_1, C_2 are acceleration coefficients, r_1 and r_2 are the random numbers $\in [0 \;\; 1]$ and W is the inertia weights, P_{best_i} and G_{best_i} are the personal and global best positions of the particles respectively.

(Miyatake et al., 2007) & (Liu et al., 2012) have implemented PSO technique to track the GMPP in partially shaded PV systems for constant voltage DC bus applications. However, population initialization is tedious process in this technique. (Ishaque et al., 2011) & (Ishaque and Salam, 2013) have proposed deterministic PSO, which avoids the rand function in the velocity equation (2.7) of conventional PSO. This technique uses minimum number of particles to track the GMPP. (Shi et al., 2015) have proposed dormant PSO, which operates in two-stages (i.e., active and inactive stages) to improve the tracking speed. (Li et al., 2019) have proposed overall distribution particle swarm optimization (OD-PSO) technique. Wherein, OD technique is

used to identify the GMPP vicinity and to reduce the search space for PSO to track the GMPP. This technique improves the tracking speed.

In addition to these methods, (Seyedmahmoudian et al., 2015) have combined differential evolutionary (DE) algorithm with PSO for MPPT application. To overcome the limitations in PSO. (Tey et al., 2018) have developed improved differential evolutionary (IDE) technique, unlike PSO, this technique requires the initialization of only two parameters, and thereby it reduces the tracking time. Further, to reduce the convergence time, (Kumar et al., 2017b) have fused Jaya optimization technique with DE. Wherein, Jaya technique pushes away the worst positions in search space and DE pulls the population towards the global maxima.

Artificial bee colony (ABC) is the metaheuristic optimization technique developed based on foraging behavior of bee colonies. (soufyane Benyoucef et al., 2015) & (Sundareswaran et al., 2015) have suitably modified conventional ABC algorithm for GMPPT application. (Sundareswaran et al., 2015) have compared the performance characteristics of ABC and PSO techniques for GMPPT application and found that ABC has better performance and guarantees convergence in all PSCs. For the better tracking characteristics and to track the GMPP in PSCs, (Fathy, 2015) have modified the inertia weights of nectar positions in conventional ABC algorithm. Selection of number of bees play a major role in this technique, if the number is less, the algorithm might end up tracking a LMPP.

(Yang and He, 2013) have developed Fireflies optimization technique based on the movement of fireflies with the intensity of light. (Sundareswaran et al., 2014b) have implemented FA technique for partially shaded PV system and its performance characteristics have been compared with PSO and P&O technique. Further, it is reported that MPP tracking characteristics using FA is superior to the PSO and P&O. However, FA technique still has a limitation of long computational time in each iteration. Therefore, to counter react to this problem, (Teshome et al., 2017) have modified FA technique with reduced number iterations.

(Sundareswaran et al., 2014a) have developed random search method (RSM) to track the GMPP. RSM is a unique approach, which initializes the population randomly in search area and starts the search process for global maxima. Authors have tested RSM for different PSCs and the results show that RSM converges in all PSCs with good tracking speed.

(Meng and Pan, 2016) have developed a unique evolutionary algorithm (i.e. Mon-

key king evolutionary (MKE)) based on a Chinese mythological novel. In this technique, a monkey king transforms into various small monkeys and searches for the global best position. (Kumar et al., 2017a) have implemented the MKE technique for $250W_p$ PV system. Similar to the MKE, based on the different states of human mental conditions (i.e., self-motivation, inspiration, excitement and over-excitement), a human psychology optimization (HPO) technique is proposed. (Kumar et al., 2017c) have validated HPO technique for $250W_p$ PV system. Moreover, HPO uses only single current sensor to track the GMPP.

(Mohanty et al., 2016) have used grey wolves optimization (GWO) technique to track the GMPP during PSC; GWO works based on the hunting procedure and leadership hierarchy of grey wolves. Although, GWO has the good tracking efficiency, the tracking speed needs to be further improved. Similar to the other nature inspired evolutionary algorithms, Ant colony optimization (ACO) (Jiang et al., 2013) and flower pollination (FP) (Ram and Rajasekar, 2017) techniques are tested for MPPT applications and from the results it is clear that these techniques converges in all shading conditions. A brief comparison of some of the soft computing based GMPPT techniques are listed in Table 2.2.

2.3 LI-ION BATTERY STATE OF HEALTH ESTIMATION TECHNIQUES

Li-Ion batteries have become popular choice over other rechargeable batteries due to several advantages such as high specific energy, high terminal voltage and long life cycle. However, these batteries have high cost and failure of which results in explosion, power supply interruption and huge replacement cost. To prevent this, a battery management system (BMS) should be employed to monitor and control the battery operating conditions. However, most of the BMSs available today do not monitor the health of the battery and they monitors only state of charge (SoC), charging voltage, charge/discharge rates and battery operating temperature. Therefore, this section mainly focuses on Li-Ion battery state of health (SoH) estimation techniques that are available in literature.

The performance and aging of the battery will be influenced by various stress factors such as overcharge, depth of discharge (DoD), operating temperature and

Table 2.2: Brief Working Principles of Different Soft Computing GMPPT Techniques

#	Reference	Remarks
1	(El-Helw et al., 2017)	Combined ANN with P&O. Requires the measurement of solar insolation and PV module temperature
2	(Tarek et al., 2013)	Fuzzy logic is combined with ANN. Complex in computation and Requires the measurement of solar insolation and PV module temperature
3	(Miyatake et al., 2007, Liu et al., 2012)	Employed PSO for global maxima searching. Initialization of population is tedious
4	(Ishaque et al., 2011, Ishaque and Salam, 2013)	Employed deterministic PSO, which eliminates random numbers from velocity equation to improve tracking speed.
5	(Manickam et al., 2016)	Tracking speed is improved. Search space for PSO is reduced by combining with and P&O
6	(Sundareswaran et al., 2015)	Compared performance of ABC and PSO. ABC is having better tracking efficiency and speed
7	(Yang and He, 2013)	FA performs better than PSO and P&O, but computational time is more
8	(Sundareswaran et al., 2014a)	Random search technique is used, number of iterations determines the tracking speed and accuracy
9	(Kumar et al., 2017b)	Jaya optimization and DE techniques are combined. During the searching Jaya technique eliminates the worst solution to improve the tracking speed
10	(Kumar et al., 2017c)	GMPP is tracked using different mental states of human mind. single sensor is used for GMPP tracking

charge/discharge rates. However, understanding the aging mechanism of battery is complex, as the aging of battery do not depend on single stress factor but number of factors and their interactions causes the battery aging. As the battery ages, a solid electrolyte interface (SEI) layer forms between the electrodes of the battery and

it causes the increase in impedance of the battery and reduction in usable capacity. Moreover, with the battery age loss of lithium takes place in th electrolyte (Vetter et al., 2005).

Knowing the effect of these stress factors and knowing the health of the battery in advance helps to enhance the cycle life of the battery and thus it prevents the premature failure of the battery. SoH is the index that describes the health of the battery and its performance compared with the new battery. However, it is not simple to measure the SoH as it is not a direct measurement. In literature, two types of SoH estimation methods are available such as,

- Destructive methods
- Non-destructive methods.

2.3.1 DESTRUCTIVE METHODS

Scanning transmission electron spectroscopy (STEM) (Zhou and Wang, 2007), X-ray diffraction (Maher and Yazami, 2014) and Raman spectroscopy (Markervich et al., 2005) are the destructive analysis SoH estimation methods. These techniques require the disconnection of battery from existing setup and the possibility of battery damage during the SoH estimation is more. Moreover, these techniques are not suitable for the industry applications (Berecibar et al., 2016a).

2.3.2 NON-DESTRUCTIVE METHODS

Generally, these non-destructive analysis techniques are further classified into two groups viz., experimental methods and adaptive battery model methods. The classification of SoH estimation techniques are shown in Fig.2.5.

2.3.2.1 Experiment based SoH Estimation Techniques

The aging of the battery brings about two major changes such as increase in impedance/DC resistance of the battery and reduction in its charge with holding capacity. Experiment based techniques continuously monitors the change in these parameters to estimate the SoH.

Due to the fact that battery impedance increases with the age, (Kozlowski, 2003) and (Bueschel et al., 2011) have performed electrolytic impedance spectroscopy (EIS)

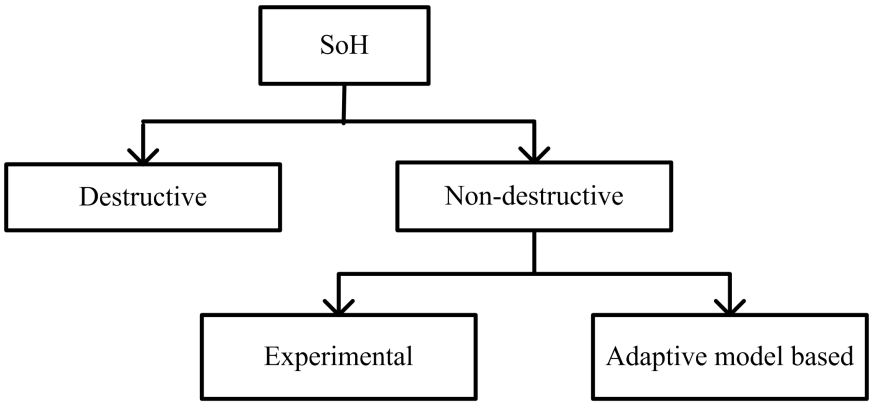

Figure 2.5: Classification chart of various SoH estimation techniques

analysis to measure the change in the impedance of the battery during its course of usage. Department of energy U.S. (Christophersen et al., 2002) & (Abraham et al., 2007) have analyzed the aging process of different chemistries of Li-Ion cells using the EIS test. EIS is the most popular non-destructive analysis method, which measures the response of electrochemical cell to an applied potential. This method requires the supply of small amplitude of AC voltages at different frequencies. EIS is an offline method which requires the disconnecting of battery from the existing system and supply of AC voltage signals. Moreover, on board implementation is very complex and costly. To overcome the problem of high cost and complexity, authors in (Escobar et al., 2012) and (Bohlen, 2008) have used passive EIS test. This technique avoids the supply of small amplitude AC signals for frequency analysis.

EIS test is not only used for SoH estimation using impedance growth values, most of the electrical equivalent circuits of rechargeable batteries have been modeled using EIS test results. These electrical models of battery later used in adaptive model based SoH estimation techniques.

Equation to calculate SoH using impedance measurement is as follows,

$$SoH = \frac{Z_{EoL} - Z_i}{Z_{EoL} - Z_{New}} \times 100 \qquad [\%] \tag{2.8}$$

where, Z_i is impedance of the battery at the i^{th} cycle, Z_{New} is impedance of the new battery and Z_{EoL} is the impedance of the battery at the end of life.

Estimating the SoH by measuring the DC resistance of the battery is a simple technique. Wherein, battery resistance is measured in every charge/discharge cycle

to estimate the SoH. Equation to estimate SoH using DC resistance is as follows;

$$SoH = \frac{R_{EoL} - R_i}{R_{EoL} - R_{New}} \times 100 \qquad [\%] \tag{2.9}$$

where, R_i is impedance of the battery at the i^{th} cycle, R_{New} is impedance of the new battery and R_{EoL} is the impedance of the battery at the end of life. Typically, R_{EoL} will be around 1.6 times of R_{New}.

Therefore, To measure the DC resistance, variation in battery voltage is observed for a short period of current pulse as given in equation (2.10). (Zhang et al., 1970) have used 1C discharge pulse to measure the resistance. Authors in (Wei et al., 2009) have also used measuring DC resistance growth to estimate the SoH of Li-ion battery used in electric vehicle application. In another attempt, authors in (Remmlinger et al., 2011) have used 3 different pulse currents of different time periods to measure the DC resistance accurately.

$$R = \frac{\Delta I}{\Delta V} \tag{2.10}$$

(Lam and Bauer, 2013) and (de Vries et al., 2015) have reported that with the battery age, usable capacity (i.e., rated capacity) of the battery degrades. There are two different capacity losses takes place as the battery gets aged. One capacity loss is due to keeping the battery in idle condition over a longer period of time, this type of loss is called as calendar loss. The second capacity loss results from several factors such as operating temperatures, over charge, deep discharge, high charge/ discharge rates, etc., this loss is also called as cycle loss. To estimate the SoH of a battery, change in usable capacity is compared with the capacity of the battery when it was new. SoH estimation using capacity fade can be calculated using equation (2.11),

$$SoH = \frac{Q_i}{Q_0} \times 100 \qquad [\%] \tag{2.11}$$

where, Q_i is the capacity of the battery at i^{th} cycle and Q_0 is the rated capacity or usable capacity of the battery when it was new.

Coulomb counting (i.e. current integration) is the most popular technique to measure the capacity Q_i of the battery. Authors in (Ng et al., 2009) have adopted coulomb counting technique for SoH estimation. In this technique, capacity of the battery is measured in every discharge cycle of the battery. For measuring the Q_i, this

method requires constant discharge current till the battery reaches to discharge cutoff voltage (i.e. 100% depth of discharge). Whereas, in practical applications discharge current varies over a time and also the depth of discharge (DoD) will not be 100% every time.

Coulomb counting technique requires the huge memory to store the accumulative capacity over a time. Moreover, a small error in current integration accumulates over a time and leads to inaccurate SoH estimation. In literature, coulomb counting technique is mostly used for SoC estimation.

In (Berecibar et al., 2016b), a unique SoH estimation of LFP cells have been proposed. This method uses differential voltage (DV) curves for SoH estimation, it is due to DV curves have ability to represent the degradation mechanism. This technique idenifies the changes in the shape of differential voltage plateaus in capacity vs. voltage curve. This technique has been experimentally validated on 18 different LFP cells. Moreover, this technique does not require 100% discharge like coulomb counting method.

Data fitting is the another type of experimental based SoH estimation technique, which uses the large set of resistance/impedance growth or capacity degradation and a characteristics map is formed from the data. Further, by comparing the real time battery parameters in every charge/discharge cycles with the characteristic map SoH can be obtained (Sarikurt et al., 2014) and (Goebel et al., 2008).

Authors in (Feng et al., 2013) have used probabilistic method to estimate the capacity of the battery using the experimental data (i.e, capacity, impedance). This technique works similar o the classical probability theory (i.e., probability of number of times same voltage is measured by considering Ah-V characteristics of new and aged battery). In (Saha et al., 2007) probabilistic method is combined with the electrical model of battery to estimate the SoH. Similar to the probabilistic methods, (Saha et al., 2009) have used Bayesian statistics method combined with the electrical model of the battery.

Data fitting, probabilistic and statistical methods require the huge set of experimental data of cells tested at different temperatures, different charge/discharge rates and different depth of discharge conditions. Collecting the huge set of data at different operating conditions is practically tedious.

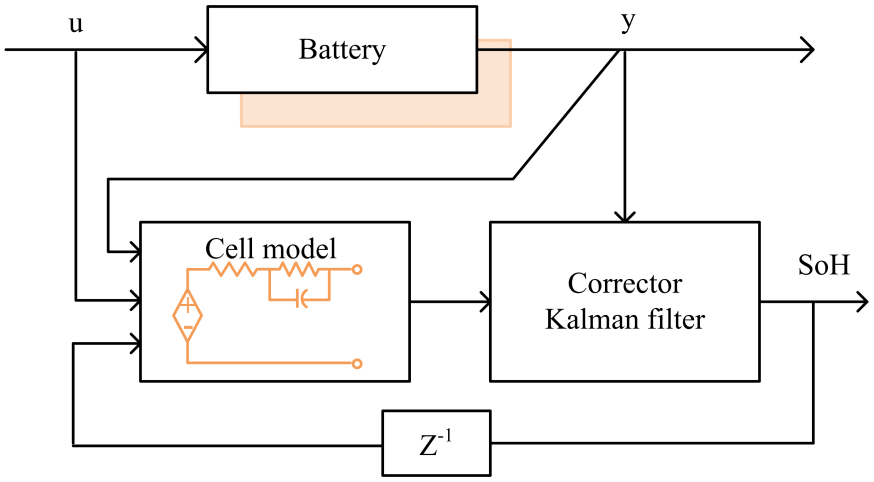

Figure 2.6: Block diagram of SoH estimation using KF Technique

2.3.2.2 Adaptive Battery Model Methods

Battery parameters estimation methods using the equivalent circuit model have been developed to determine health condition of the battery. There are different adaptive methods to estimate SoH, all these methods use electrical equivalent model which is build on battery aging parameters.

Kalman filter (KF) is very popular and old approach for estimating the state of a dynamic system. Typically, KF technique is a set of mathematical equations that consists of predictor and corrector type estimator. KF technique works in two-stages, in stage one, predictor estimates the current output variable. Further, in stage two, the estimated variable will get updated to achieve high estimation accuracy. The major advantage of KF technique is that, it provides dynamic error boundary for estimated values.

In (Remmlinger et al., 2013), an on line KF technique is developed, which uses battery internal resistance growth model to estimate the SoH. The battery model used in this technique considers only effect of temperature on battery age. However, in the practical applications along with the temperature, DoD, charge/discharge rates also shows considerable impact on battery aging. The block diagram of SoH estimation using KF technique is shown in Fig. 2.6 and the flowchart of the KF operation is shown in Fig. 2.7.

KF technique works better for linear systems, however battery exhibits non-linear characteristics. Hence, to overcome this limitation, KF technique is appropriately

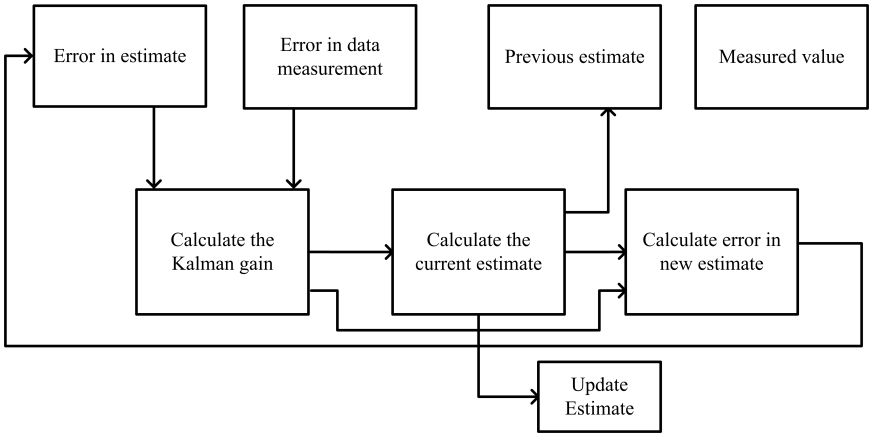

Figure 2.7: Flowchart of KF Technique

modified to form extended kalman filter (EKF). EKF technique uses Taylor series expansion to linearizes the model around an operating point. In (Plett, 2004) have used EKF technique to estimate SoH, similarly authors in (Hu et al., 2012) have developed multi scale frame work EKF technique, which estimates battery SoC and capacity degradation. Unscented kalman filter (UKF) is also a modified version of KF technique, which reduces the computation time (Zhang et al., 2009). All the kalman filtering techniques involve huge matrix operation, and requires accurate model of battery aging mechanism. Therefore, the computational and implementation complexity of these techniques are high.

For the better accuracy in estimation, (Schwunk et al., 2013) have used particle filter (PF) technique, which works similar to the EKF technique, but PF technique have advantages in parameter and state estimations of non-Gaussian or nonlinear time-varying system. Particle filter shows more accuracy than EKF method in highly nonlinear systems. However complexity in computation and time consumption are the limitations of the particle method. Similar to the KF and PF techniques, (Kim, 2010) have developed sliding mode observer technique, which works along with the battery aging model.

(Chen et al., 2013) have reported that battery diffusion capacitance has a correlation with the SoH. Therefore, Genetic algorithm (GA) technique is adopted in this study to identify the battery diffusion capacitance. Further, a equation is developed to estimate the SoH using the identified diffusion capacitance value.

(Andre et al., 2013) have proposed Artificial Neural Networks (ANN) method to estimate life of Li-ion battery. ANN uses battery model based parameter identification

to estimate the life. Moreover, authors have compared the performance of ANN with EKF technique. From the comparison results it is clear that, the implementation complexity of ANN is less compared to EKF. However, computational effort and memory requirement of ANN is less compared to EKF. Comparison of some of the popularly used SoH techniques are listed in Table. 2.3.

Table 2.3: Brief Working Principles of Different SoH Estimation Techniques

#	Reference	Method	Remarks
1	(Remmlinger et al., 2011)	DC Resistance Method	Current pulses are used to measure resistance. Low efficiency since effect if impedance variations ignored
2	(Ng et al., 2009)	Coulomb counting	Requires 100% DoD with constant discharge rate, error in current measurement effects the estimation efficiency
3	(Berecibar et al., 2016b)	DV curve comparison	Compares the changes in differential voltage curve
4	(Feng et al., 2013, Saha et al., 2007)	Probabilistic	Works on the principle of probability theorem, it requires huge set of battery aging data
5	(Remmlinger et al., 2013)	Kalman filter	Requires the accurate battery model, for non-linear systems estimation accuracy is poor
6	(Plett, 2004, Hu et al., 2012)	Extended Kalman filter	Improved version of KF technique, requires battery model, highly complex in computation
7	(Andre et al., 2013)	ANN	Requires huge battery test data for training, low computational complexity than EKF and it requires accurate battery aging model

2.4 SUMMARY

From the analysis of literature related to MPPT techniques it is observed that, the conventional MPPT techniques like F_{ocv} and F_{scc} have low tracking accuracy, and the other methods such as P&O, INC tracks the MPP with acceptable tracking efficiency during uniform insolation on whole PV array, but these methods get trapped in

the local peaks during non-uniform insolation conditions. Most of the two-stage GMPPT techniques have good tracking speed, but fails to track the GMPP in some of the PSCs. Moreover, these techniques have high steady state oscillations. Artificial intelligence and nature inspired evolutionary algorithms accurately tracks the GMPP in PSCs. Moreover, steady state oscillations are very less compared to two-stage GMPPT techniques. However, the computational complexity and low tracking speed are the major limitations.

Upon analyzing the literature related to battery SoH estimation it is observed that, destructive analysis based SoH estimation methods are not suitable for practical applications. On the other hand, most of the non-destructive analysis based SoH techniques are offline and they require accurate model of battery with aging parameters. Moreover, these techniques require huge set of EIS test reports for battery parameter modeling. Some of the on-line non-destructive SoH techniques require the battery to be discharged completely from fully charged state with a constant discharge rate, however in practical systems 100% discharge of the battery is undesirable.

2.5 IDENTIFIED RESEARCH AREAS

Non-uniform insolation conditions on PV array makes the PV-Battery system ineffective. The proposed GMPPT techniques in literature uses minimum of two sensors to track the GMPP and moreover they have poor tracking time and fails to track the GMPP during some of the PSCs. Therefore, it is worth to extend the research in developing the GMPPT technique with reduced number of sensors and with fast convergence speed.

Upon analyzing the literature, it is observed that, BMS plays a major role in any battery based systems. However, most of the BMSs available today in the literature does not monitor the health of the battery. Very few health estimation techniques have been discussed in the literature and mostly they are off-line techniques and they require accurate modeling of battery being tested. Therefore, it is worth to investigate the on-line techniques which works good in all practical load changing conditions.

From the telecom load characteristics, it is observed that, DC loads works at a constant voltage of 48V. However,load current varies with the signal traffic strength. Therefore, it is required to develop a voltage regulation method for the effective operation of the complete system.

2.6 RESEARCH OBJECTIVES

The proposed works aims to analyze, design, modeling and hardware implementation of PV and battery based hybrid power supply system for powering DC Loads of standalone telecom tower. After thorough literature survey of PV and energy storage systems the following areas have been identified for the proposed research work. The complete schematic of PV-Battery based power supply system with the proposed research objectives is shown in Fig. 2.8.

1. Development and experimental verification of global maximum power point tracking technique (GMPPT) in a PV and Battery powered BTS load application with the following characteristics.
    - Ability to detect the event of non-uniform insolation on PV array and to track the GMPP with reduced number of sensors.
    - Ability to track GMPP in all partial shading conditions with good tracking efficiency and with faster convergence time
2. Development of an on-line battery management system (BMS) for the Li-Ion battery used in PV-battery based power supply system with the following characteristics.
    - Development of BMS which monitors the battery parameters such as charging voltage, charging current and state of charge (SoC) during the battery is in charging mode (i.e. charging from PV source). Also, the BMS should able to estimate an accurate state of health (SoH) of a battery during discharging mode.
    - Experimental validation of proposed BMS using the laboratory prototype developed.
3. Development of a voltage regulation method to maintain a constant output voltage for the varying load conditions of DC-DC converter used for DC loads of BTS.

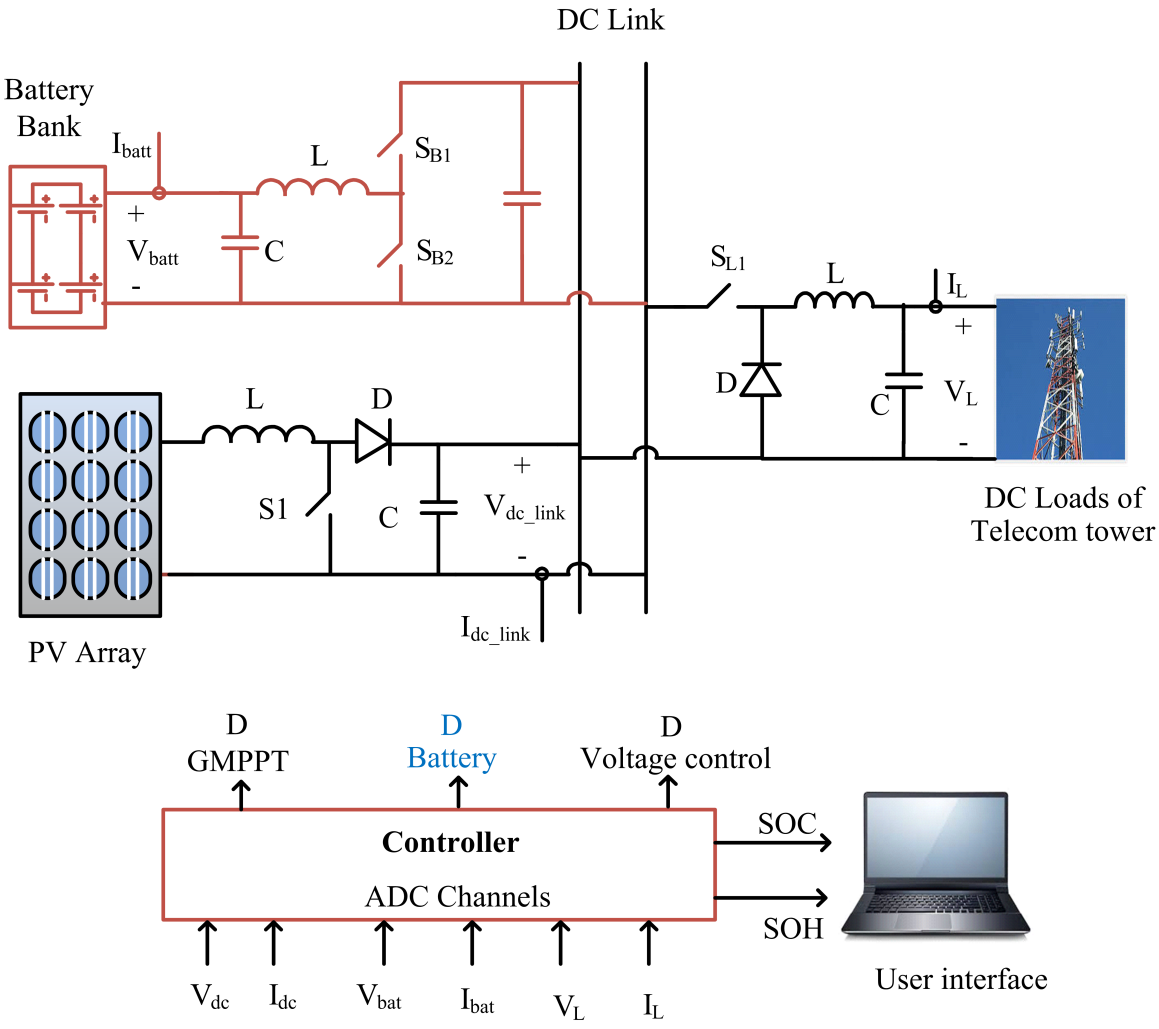

Figure 2.8: Schematic of PV-Battery power supply system

Chapter 3

EFFECTIVE UTILIZATION OF PHOTOVOLTAIC ARRAY USING GMPPT TECHNIQUES

Contents

3.1 GENERAL

In this chapter, for the effective utilization of PV array by tracking the GMPP in PSCs with the reduced tracking speed and with the high tracking accuracy, two GMPPT techniques have been proposed. The first method comes in the category of

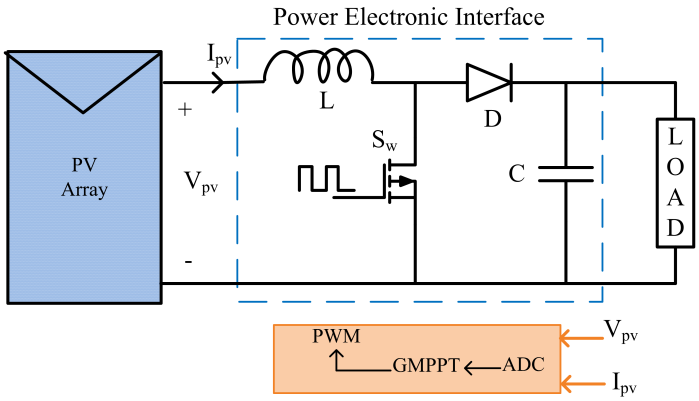

Figure 3.1: Block diagram of GMPP Tracking system

two-stage scanning based techniques and the second method is the combination of soft computing GMPPT technique and conventional HC technique.

3.2 TWO-STAGE SCANNING BASED GMPPT TECHNIQUE

The proposed two-stage GMPPT technique detects the incident of PSC and identifies the type of the $P-V$ curve to find the locality of GMPP in stage 1. In stage 2, a conventional hill climbing (HC) algorithm is used to track and conserve the GMPP during PSC. The detection of incident of PSC on PV array is explained as follows,

Generally, most of the two-stage GMPPT algorithms measure the PV power ($i.e, P_{pv} = V_{pv} \times I_{pv}$) in two successive perturbations to recognize the incident of PSC and to track the GMPP. However, in applications like PV-Battery power supply system (ref. Fig. 2.8 in chapter 2) requires two additional sensors (voltage and current) at the DC link terminals. Therefore, the overall count and cost of the sensors are increased in the system. Moreover, this increases the computational burden and memory requirement.

To reduce the component count, the proposed technique measures the variations in power electronic interface output current in two consecutive perturbations to identify the incident of PSC and to track the GMPP. Hence, one current sensor (refer Fig.3.1) is adequate to sense the incident of PSC and to track GMPP. The idea behind the selection of the single current sensor at the output terminal of power electronic interface is as follows,

During the steady state power balanced condition,

$$P_{pv} = V_{pv} Ipv = \frac{V_{load} I_{load}}{\eta} \tag{3.1}$$

Since, the boost DC-DC converter is used as power electronic interface, equation (3.1) is rearranged as,

$$P_{pv} = V_{pv} Ipv = \frac{V_{pv} I_{load}}{\eta(1-D)} \tag{3.2}$$

$$P_{pv}^{\star} = \frac{I_{load}}{\eta(1-D)} \tag{3.3}$$

$$P_{pv}^{\star} = f\left(D, \eta, I_{load}\right) \tag{3.4}$$

where, η is the efficiency of the DC-DC boost power converter, D is the duty cycle of the boost DC-DC converter switch, $P_{pv}^{\star}$ is the objective function to be maximized.

From equations (3.3) and (3.4), maximizing the load current I_{load} of constant load applications, by varying the duty cycle (D) results in the maximizing the power from PV source. Since, the proposed PV-Battery system (refer Fig.2.8) also maintains the constant DC link voltage, a single current sensor is used in this work to track the GMPP. Moreover, from equations (3.3) and (3.4) it is clear that, the DC link current vs. duty cycle characteristics of the power electronic interface replicates the $P-V$ characteristics of the PV array during PSC which is shown in Fig. 3.2. Therefore, the proposed GMPPT technique scans the I_{dc_link} $vs.$ D curve instead of $P-V$ curve to locate the GMPP neighborhood.

The complete flowchart of the proposed two-stage GMPPT technique is shown in Fig. 3.3. PSC routine in Fig. 3.3 shows the algorithm to identify the event of PSC. Considering that a PV array is operating at the MPP with an uniform insolation on whole PV array, due to passage of the clouds, PV modules receives non-uniform insolation. Consequently, the DC link current I_{dc_link} reduces. Therefore, the controller (block 3) measures the change in the current (i.e. ΔI_{dc_link}) in two successive perturbations. During PSC, the value of ΔI_{dc_link} will be more than predefined critical value and the controller initiates the global peak (GP) tracking routine (block 6), if the value of ΔI_{dc_link} is more than critical value in block 4. As reported in (Patel and Agarwal, 2008), that the maximum insolation variation on PV module in 1s time interval is less than $27W/m^2$. Therefore, a 5% change in the battery current is observed for more than $27W/m^2$ insolation change and this value is considered

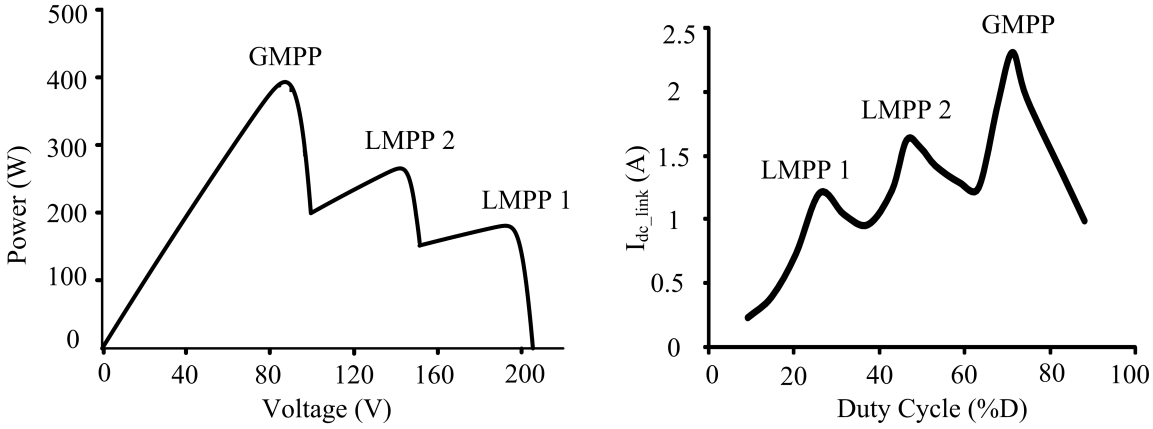

Figure 3.2: $P-V$ characteristics of PV array and its corresponding I_{dc_link}-D characteristics

as critical value (I_C) in block 8. During some non-uniform insolation conditions, due to fractional variation in insolation on PV modules, the change in I_{dc_link} is not sufficient to determine the occurrence of PSC. In such cases, GMPP tracking algorithm cannot track the actual GMPP. To avoid this problem, a 15mins delay timer (block 5) is incorporated to the controller. This initiates the scanning of I_{dc_link} $vs.$ D characteristics periodically.

GP routine in the flowchart scans the I_{dc_link} $vs.$ D characteristics of the boost converter at selective duty cycles to identify the shading pattern and to detect the GMPP neighborhood. Further, controller (block 8) calculates the duty cycle corresponding to 80% of V_{oc} of a single PV module from the leftmost peak in the I_{dc_link} $vs.$ D characteristics using the equation 3.5,

$$D(i) = \left(1 - \frac{0.8\,(N-i+1)\,V_{oc\_module}}{V_{dc\_link}}\right) \times 100\% \tag{3.5}$$

where, V_{oc_module} is an open circuit voltage of a single PV module, $i = 1, 2, N$ (N is number bypass diodes in series) and V_{dc_link} is the DC link voltage or output voltage of the power electronic interface.

For every duty cycle perturbation during the scanning of I_{dc_link} $vs.$ D curve, the DC link current (I_{dc_link}) will have the oscillations due to switching and converter non-idealities. The measurement of I_{dc_link} before it get settles to a steady state affects the GMPP tracking accuracy. To overcome this, a delay timer (block 9) with time period equal to a boost converter settling time is incorporated to the controller. If the

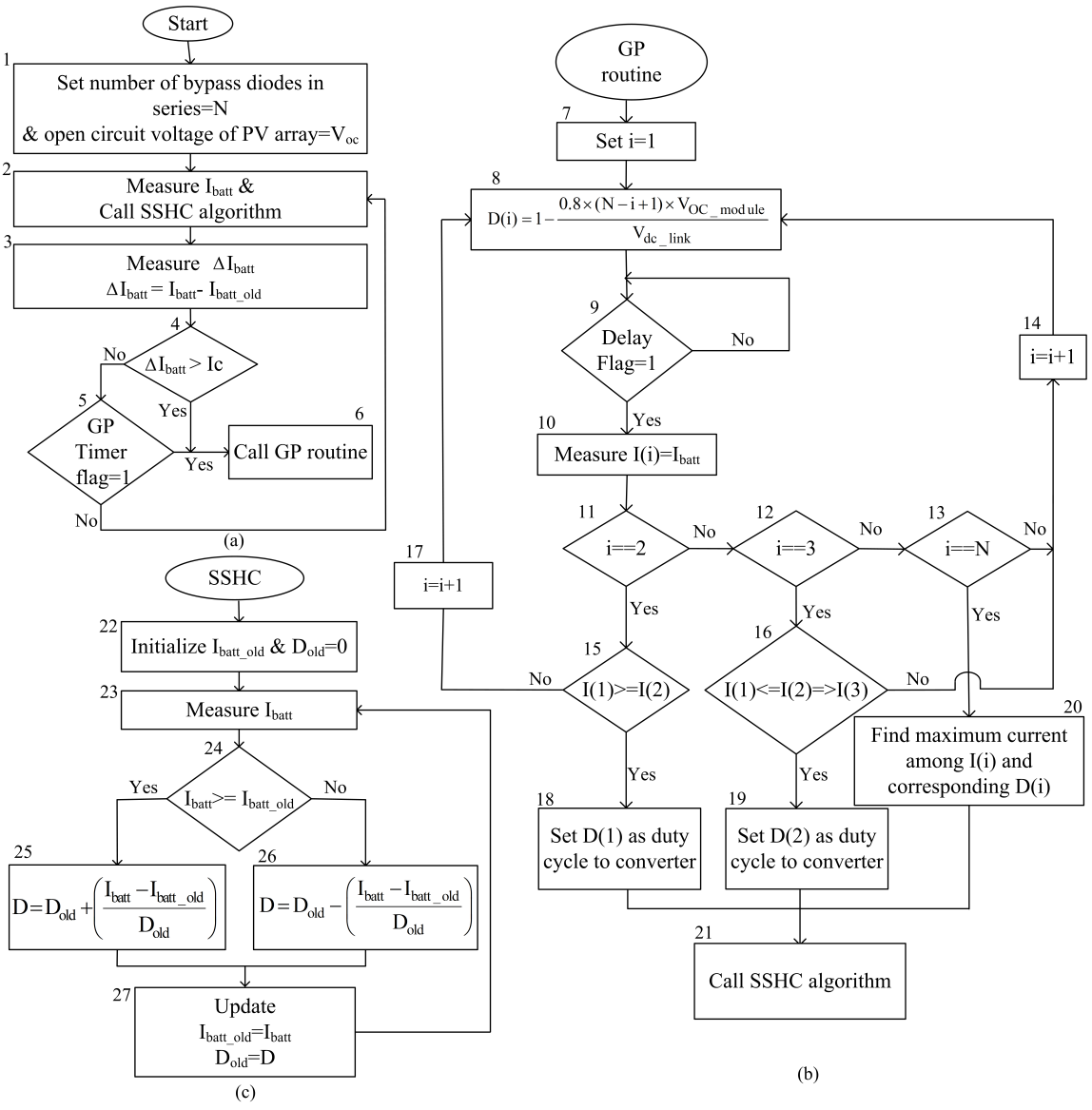

Figure 3.3: Flowchart of the proposed two-stage GMPPT technique

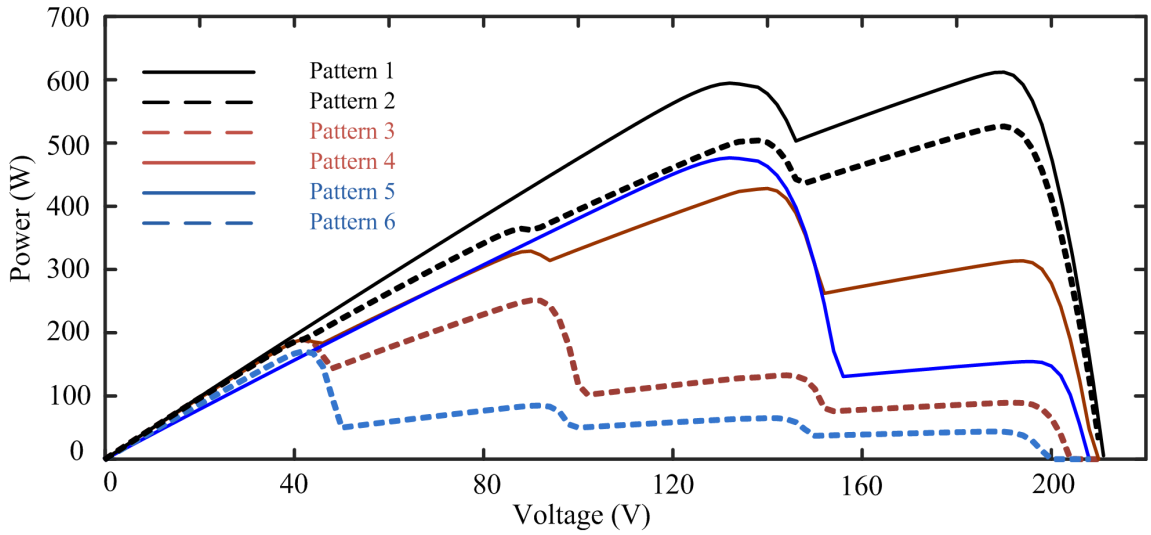

Figure 3.4: $P-V$ characteristics used for validating the proposed GMPPT technique

status of the delay timer is true, then the controller measures the I_{dc_link} and stores the measured current as $I(1)$ and its corresponding duty cycle as $D(1)$. Tracking of GMPP for the $P-V$ curves under different PSCs shown in Fig. 3.4 have been explained for three cases. In case 1, tracking of GMPP for shading pattern 1 & 2 (i.e. first peak of $P-V$ curve is GP) is explained. In case 2, tracking of GMPP for shading pattern 4 & 5 (i.e. second peak of $P-V$ curve is GP) is explained. In case 3, tracking of GMPP for shading patterns 3 and 6 (i.e. GP is not from first two peaks of $P-V$ curve) is explained.

Case 1:

The proposed algorithm checks for the number of iterations (i) in block 11, if the value of 'i' is less than two, the algorithm redirects to block 8 to calculate the next duty cycle $D(2)$. After applying $D(2)$ to the power electronic interface, the above explained process continues from block 8 to 10. Furthermore, the controller (block 15) compares the measured currents at the $D(1)$ and $D(2)$ to identify the type of shading pattern and to find the GMPP neighborhood. If the measured current $I(1)$ is greater than $I(2)$ then the first peak in the rightmost region of the $P-V$ curve will be the GP as shown in Fig. 3.4 (i.e. shading pattern 1 & 2). Hence, the duty cycle corresponds to $I(1)$ will be in the vicinity of GMPP. Therefore, controller stops the scanning procedure and initiates the single sensor hill climbing (SSHC) routine to track and retain GMPP.

SSHC algorithm works on the principle of maximizing the load current of constant voltage load applications (i.e. gradient ascent method). Therefore, SSHC routine compares the measured value of battery current in two successive steps ($I(k)$ & $I(k-1)$) in block 24. If the value of $I(k)$ is more than $I(k-1)$, controller increments the duty cycle to shift the operating point towards GMPP in block 25. However, controller decrements the duty cycle if $I(k)$ is less than $I(k-1)$ in block 26. In this case, the convergence speed of the algorithm is more since very less portion of I_{dc_link} *vs.* D curve is scanned.

Case 2:

If the measured currents $I(1)$ is less than $I(2)$ in block 15, the first peak of the $P-V$ curve cannot be the GMPP. Therefore, controller checks for the possibility of second peak of $P-V$ curve to be global peak, hence the controller increments the iteration count (block 18) and redirects to block 8 to calculate the next duty cycle $D(3)$. After applying the $D(3)$ to the boost converter, the process continues up to the measurement of $I(3)$. Subsequently, controller (block 16) compares the measured currents $I(1)$, $I(2)$ and $I(3)$ to analyze the type of $P-V$ curve shading pattern and to locate the GMPP neighborhood. If the value of $I(2)$ is greater than $I(1)$ and $I(3)$ the global peak exist between two local peaks similar to shading pattern 4 & 5 in Fig. 3.4. Therefore, duty cycle corresponds to $I(2)$ i.e. $D(2)$ will be in the vicinity of GMPP. Hence, the controller (block 19) sets the $D(2)$ as a duty cycle to the power electronic interface and stops the scanning procedure. Similar to the case 1, block 21 calls SSHC routine to track and retain the GMPP.

Case 3:

If the value of $I(2)$ is not greater than $I(1)$ and $I(3)$, then the global peak cannot exist in the first two peaks from the right side of $P-V$ curve, hence GMPP exist anywhere in the left side region of $P-V$ curve similar to shading patterns 3 & 6 shown in Fig. 3.4. Therefore, the controller needs to scan complete I_{dc_link} *vs.* D characteristics at every $0.8V_{oc\_module}$ to find the GMPP existing area. After scanning complete I_{dc_link} *vs.* D, the controller (block 20) sets the duty cycle corresponding to maximum current of $I(i)$ and block 21 calls the SSHC routine to track and retain the GMPP. During most of the practical non-uniform insolation conditions, the differences in insolation levels on PV modules are very less. As a result, GMPP exists in the rightmost corner of $P-V$ characteristics (Manickam et al., 2016). Therefore, measuring the I_{dc_link} at three places finds the GMPP neighborhood in most of the

practical cases.

In this study, a PV array composing of four PV modules connected in series is taken as example for simulation and experimentation. However, proposed algorithm in Fig. 3.3 is given for a generalized n number of PV modules in a PV array. The convergence speed of proposed algorithm reduces with increase in number of PV modules during shading patterns 3 and 6.

3.2.1 RESULTS AND DISCUSSION

A single diode model of a PV array (four series and one parallel (4s1p) configuration), the boost converter and the proposed GMPPT controller are modeled in MATLAB/Simulink platform. The parameters used for the PV array and boost converter model are given in Table 3.1. In this section, simulation and hardware results of the proposed algorithm are presented for $1000W_p$ PV system. For the better understanding of the proposed algorithm, the above explained three cases i.e. tracking of GMPP during three types of shading patterns are simulated and shown in Figs. 3.5-3.7.

For testing the proposed GMPPT technique, a battery is connected at the output terminal of the boost converter. This configuration works similar to the PV-Battery power supply system as shown in Fig. 2.8, since the battery voltage will have less than 10% variations, hence it is assumed to be constant as DC link voltage. Therefore, while testing the proposed GMPPT technique, battery charging current is termed as DC link current (i.e., I_{dc_link}) and battery voltage is termed as DC link voltage (i.e., V_{dc_link}).

Two shading patterns i.e., pattern 1 (i.e., $1000W/m^2$, $1000W/m^2$, $1000W/m^2$ and $800W/m^2$) and pattern 2 (i.e., $1000W/m^2$, $900W/m^2$, $800W/m^2$ and $700W/m^2$) have been applied to the PV array. The duration of pattern 1 on PV array is 1.5s and pattern 2 is 1s as shown in Fig. 3.5(a). Fig. 3.5(b) shows the PV power and I_{dc_link} characteristics during the tracking of GMPP for patterns 1 & 2. In Fig 3.5(b), the controller started the scanning of I_{dc_link} - D curve at 0.07s. Further, the controller measured the I_{dc_link} at two duty cycles. Since the value of I_{dc_link} at $D(1)$ is more than I_{dc_link} at $D(2)$, and from the analysis of $P-V$ characteristics (i.e., case 1), it is clear that GP exists in the rightmost corner of a $P-V$ curve. Hence, the controller stops the scanning and initiates the HC algorithm around the $D(1)$ to track and retain

the GMPP.

The tracking efficiency and tracking speed of the proposed algorithm for this case are found to be 98.16% and 0.14s respectively. Furthermore, after a 1.5s pattern of $P-V$ curve has been changed, consequently, I_{dc_link} has been varied more than 5%. Therefore, controller restarted the scanning of I_{dc_link} D curve and tracked the GMPP successfully.

Shading patterns 3 (i.e., $1000W/m^2$, $600W/m^2$, $200W/m^2$ and $100W/m^2$) and 4 (i.e., $1000W/m^2$, $900W/m^2$, $720W/m^2$ and $400W/m^2$) have been applied to PV array as shown in Fig. 3.6(a). PV power tracking characteristics for these patterns are shown in Fig. 3.6(b). Firstly, pattern 4 has been applied for the duration of 1.5s, during this period controller scanned the I_{dc_link} - D characteristics. The value of I_{dc_link} at $D(1)$ is found to be less than I_{dc_link} at $D(2)$, then the controller calculated the next duty cycle (i.e., $D(3)$). Since, the value of current at $D(2)$ is more than $D(1)$ and $D(3)$, then the second peak in the $P-V$ curve is the global peak (i.e. shading pattern 3). The proposed technique tracked the maximum power of 426W with the tracking efficiency of 97.93%. The tracking time for this case is 0.26s, which is slightly more compared to the previous case. Further, after 1.5s, the pattern 3 has been applied, the controller scanned the I_{dc_link} D curve at 4 duty cycles since the GP is not from the first two peaks of $P-V$ curve from rightmost region. In this case the proposed technique tracked the maximum power of 233.5W with the efficiency of 98.10% in the duration of 0.375s.

Table 3.1: Parameters Used for PV Array and Boost Converter Modeling

Parameter	**Value**
No. of bypass diodes	4
V_{oc} and I_{sc} of a PV module	50V & 4A
Inductor (L) and Capacitor (C) value in boost converter	560μH & 940μF
Switching frequency	40kH
Rated capacity and voltage of the battery	10Ah & 240V

Similar to the above two cases, pattern 2 & 6 have been applied as shown in Fig. 3.7(a). PV power tracking characteristics for these patterns are shown in Fig. 3.7(b).

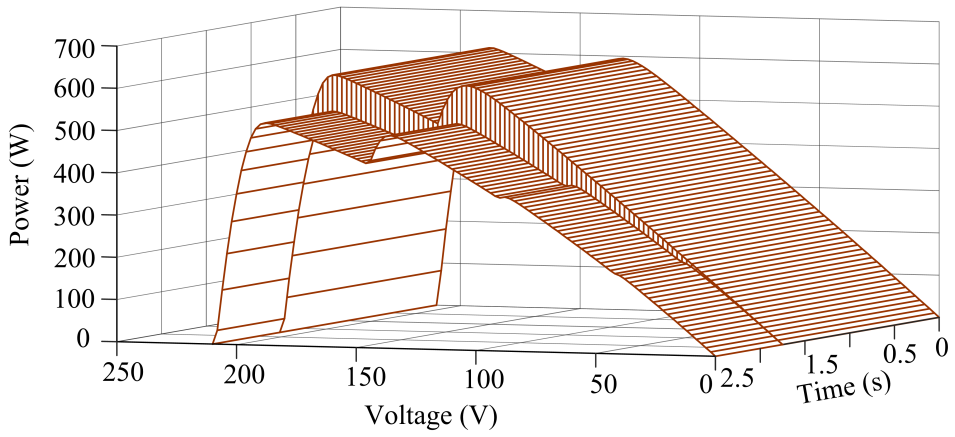

(a)

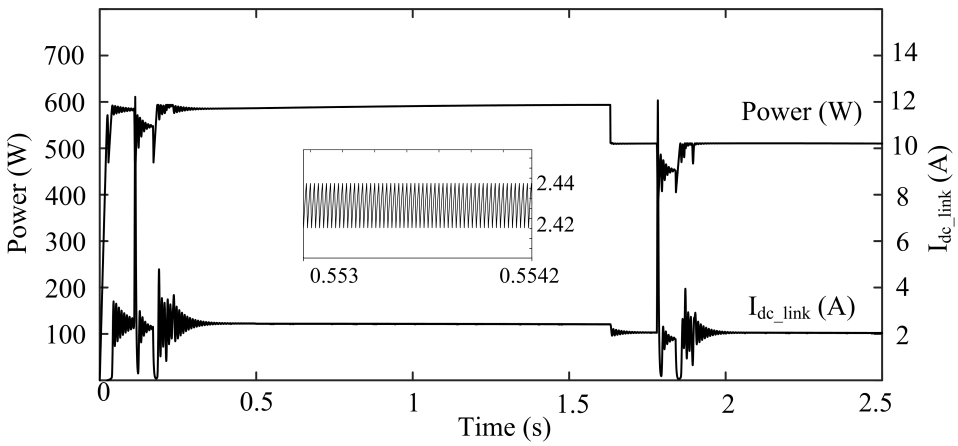

(b)

Figure 3.5: (a) $P - V$ characteristics (patterns 1 & 2) of PV array (b) GMPP tracking characteristics of PV power for the patterns 1 & 2

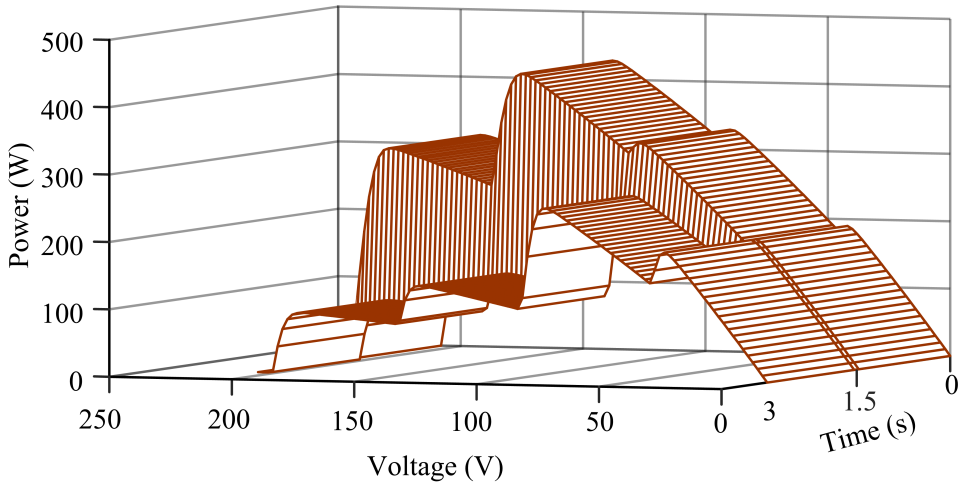

(a)

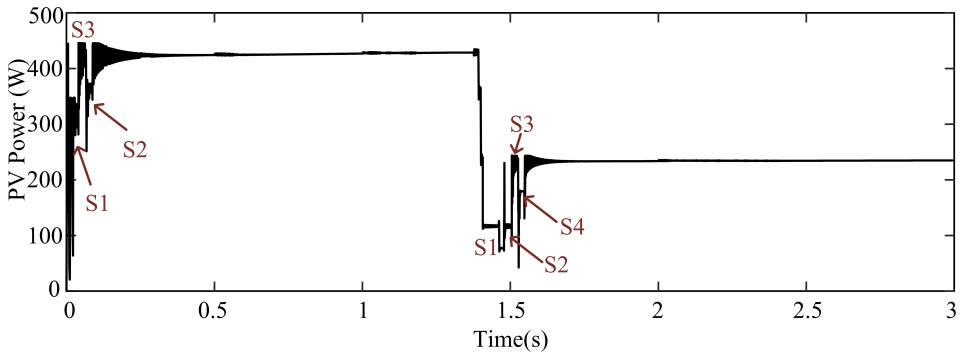

(b)

Figure 3.6: (a) $P-V$ characteristics (patterns 3 & 4) of PV array (b) GMPP tracking characteristics of PV power for the patterns 3 & 4

Firstly, pattern 2 has been applied for the duration of 1.5s, since the value of I_{dc_link} at $D(1)$ is greater than at $D(2)$, the controller instigated the SSHC routine around the $D(1)$. In this case the proposed technique successfully tracked the maximum power of 457W. Further, after 1.5s, the shading pattern is changed to pattern 6, in this case the value of I_{dc_link} at $D(3)$ is more than $D(1)$ and $D(2)$. Therefore, GMPP does not exist in the first two peaks from the right side of $P-V$ curve. Hence, the controller has to scan the entire I_{dc_link}-D curve to locate the GMPP existing area. After the completion of scanning procedure, the value of current at $D(4)$ is found to be maximum among all. Therefore, the controller operated the SSHC algorithm around $D(4)$. The tracking time in this case is more since, it requires complete scanning of I_{dc_link}-D characteristics. Further, if the number of PV modules is increased in PV array and global peak is not from the first two peaks of $P-V$ curves (i.e. shading patterns 3 & 6 in Fig. 3.4) then the controller has to completely scan the I_{dc_link}-D curve. Hence, the tracking speed of the proposed technique degrades. During the practical cases of PSC, global peak mostly exist in the rightmost region of $P-V$ characteristics. Therefore, in most of practical cases tracking speed of the proposed technique is very high.

The performance of the proposed method is validated using a experimental prototype; and the description of the prototype is explained in section 6.3. The experimental performance of the proposed algorithm is investigated for three different patterns and the results are shown in Figs. 3.8-3.11. Figs. 3.12 shows the steady state GMPP performance details for 3 different shading conditions on PV array.

In Fig. 3.8, initially shading pattern 1 with the insolation levels of $1000W/m^2$, $900W/m^2$, $800W/m^2$ and $800W/m^2$ has been applied to PV array. The proposed algorithm measures the I_{dc_link} at two different operating points (i.e. $D(1)$ & $D(2)$) with the time delay of 2s. The motive behind the measurement of I_{dc_link} after 2s is to ensure the power converter to reach the steady state for a large change in duty cycle while scanning the I_{dc_link}-D characteristics. Since, the maximum settling time of the converter for the step change of 0.3 (duty cycle) has been used in the present study. As the value of I_{dc_link} at first operating point (i.e. $D(1)$) is greater than second, the global peak exists in the neighborhood of $D(1)$ (i.e. first peak from the right side). Therefore, the controller initiates the SSHC algorithm with $D(1)$ as a initial operating point. During the SSHC execution a delay time of 20ms is used between two successive perturbations. Under this shading pattern the proposed

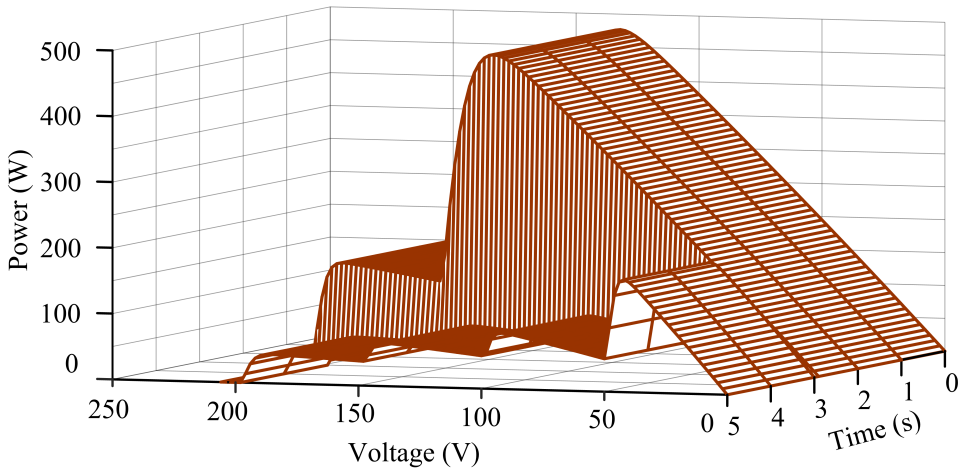

(a)

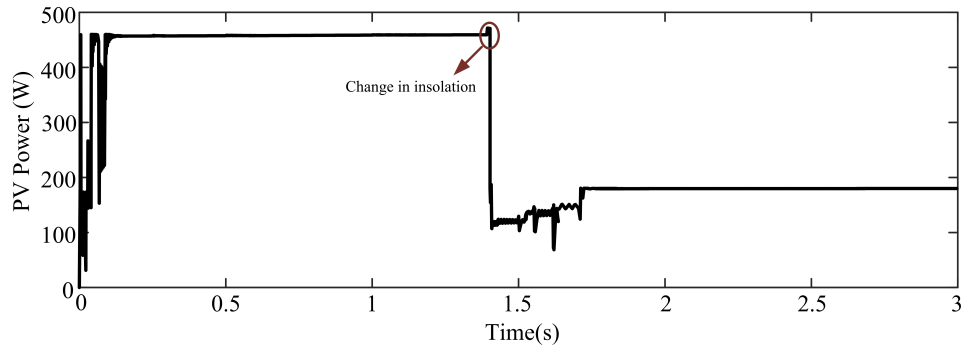

(b)

Figure 3.7: (a) $P-V$ characteristics (patterns 5 & 6) of PV array (b) GMPP tracking characteristics of PV power for the patterns 5 & 6

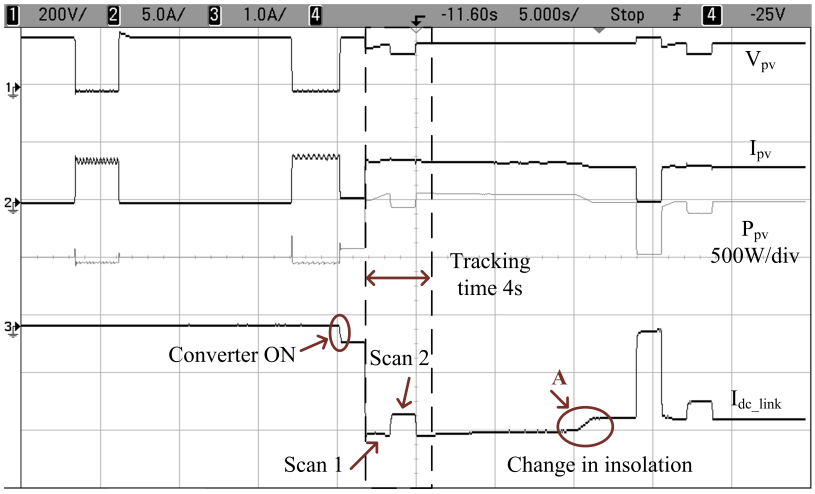

Figure 3.8: V_{pv},I_{pv} ,P_{pv} and I_{dc_link} characteristics while the tracking the GMPP for pattern 1 shown in Fig. 3.12(a)

algorithm extracted 622.2W of PV power in 4s with the efficiency of 99.89%. In Fig. 3.8, at point A, the insolation levels on modules has been changed to $900W/m^2$, $800W/m^2$, $700W/m^2$ and $600W/m^2$. The proposed GMPPT algorithm detects the change in I_{dc_link}, which is more than 5% and re-initiated the scanning procedure to track GMPP.

Fig. 3.9 shows V_{pv}, I_{pv}, P_{pv} and I_{dc_link} characteristics of proposed algorithm for the insolation levels of $1000W/m^2$, $900W/m^2$, $720W/m^2$ and $400W/m^2$ (i.e. shading pattern 4). In this case I_{dc_link} at $D(2)$ is more than at $D(1)$ and $D(3)$. Therefore, second peak of the $P-V$ curve from right side will be the global peak. Hence, the SSHC algorithms operates around $D(2)$ and tracks the maximum power of 505W with the efficiency of 99.58% in 4.5s. Further, after a delay of 15s, the insolation on PV modules has been changed to $1000W/m^2$, $900W/m^2$, $780W/m^2$ and $450W/m^2$. The proposed GMPPT algorithm has detected a change in insolation and re-initiated the scanning procedure to track GMPP.

In Fig. 3.10(a), insolation levels of $1000W/m^2$, $400W/m^2$, $200W/m^2$ and $100W/m^2$ has been applied to PV system and the controller scans the complete I_{dc_link}-D characteristics at 4 places as the GMPP is not found from first two peaks of the $P-V$ curve from right side. The proposed controller tracks the maximum power of 204W with the efficiency of 99.52% in 5.8s. The time required to track the GMPP in this case is more due to requirement of scanning at more number of places. Fig. 3.10(b) shows the DC link voltage, boost converter parameters such as inductor current, voltage

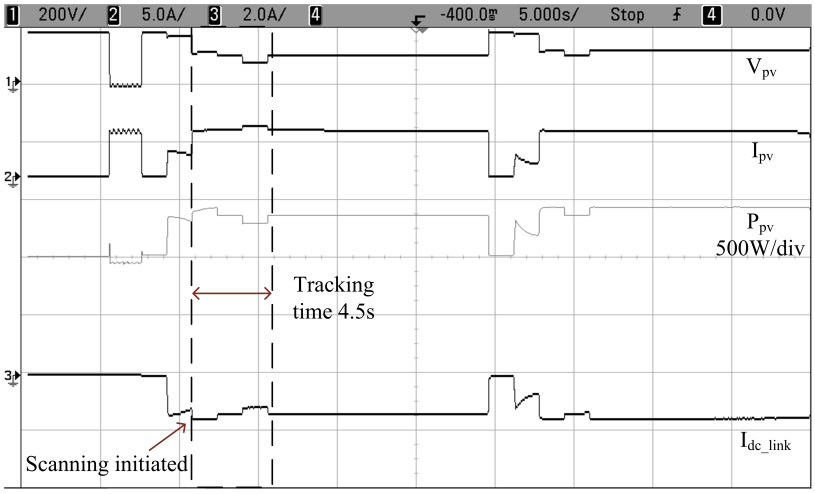

Figure 3.9: V_{pv},I_{pv} ,P_{pv} and I_{dc_link} characteristics while the tracking the GMPP for pattern 4 (i.e., pattern 2 shown in Fig. 3.12(b))

across the switch and duty cycle variation during the tracking of GMPP.

The proposed technique is also tested at reduced power levels (i.e., V_{oc}=100V and I_{sc}=3A), the GMPP tracking characteristics for the 3 different shading patterns are given in Fig. 3.11. From the simulation and experimental results it is observed that, the tracking speed varies with the $P-V$ curve pattern and number of series connected bypass diodes. However, tracking accuracy will be almost same in all PSCs.

3.3 SOFT COMPUTING AND HC ALGORITHM BASED HYBRID GMPPT TECHNIQUE

From the literature it is observed that, soft computing based GMPPT techniques accurately find the GMPP location during all PSCs but have a slow convergence speed and they have high implementation complexity. Therefore, to overcome these limitations, a hybrid GMPPT technique is proposed which combines the artificial bee colony (ABC) optimization technique and HC algorithm to improve the tracking speed and accuracy. The reason behind selecting the ABC optimization technique is, simple in computation when compared to other soft computing based techniques.

The complete flowchart of the proposed hybrid GMPPT technique is shown in Fig. 3.13. The main routine in Fig. 3.13 detects the event of PSC similar to the two-stage GMPPT technique presented in Section (3.2). Upon detecting the PSC, the proposed

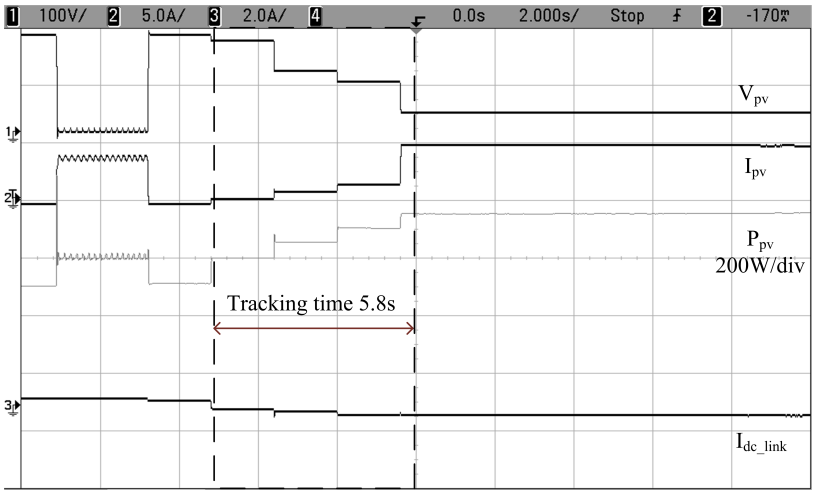

(a)

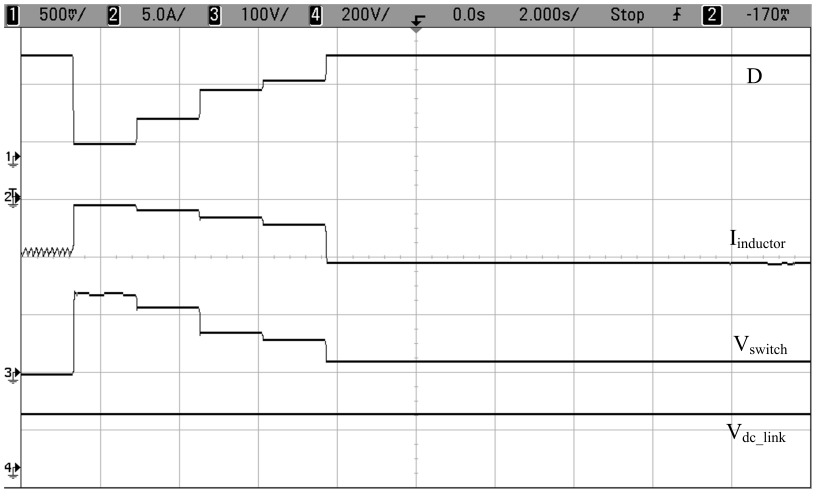

(b)

Figure 3.10: (a) GMPP tracking characteristics (b) DC link voltage and boost converter parameters of proposed algorithm for pattern 3 shown in Fig. 3.12(c)

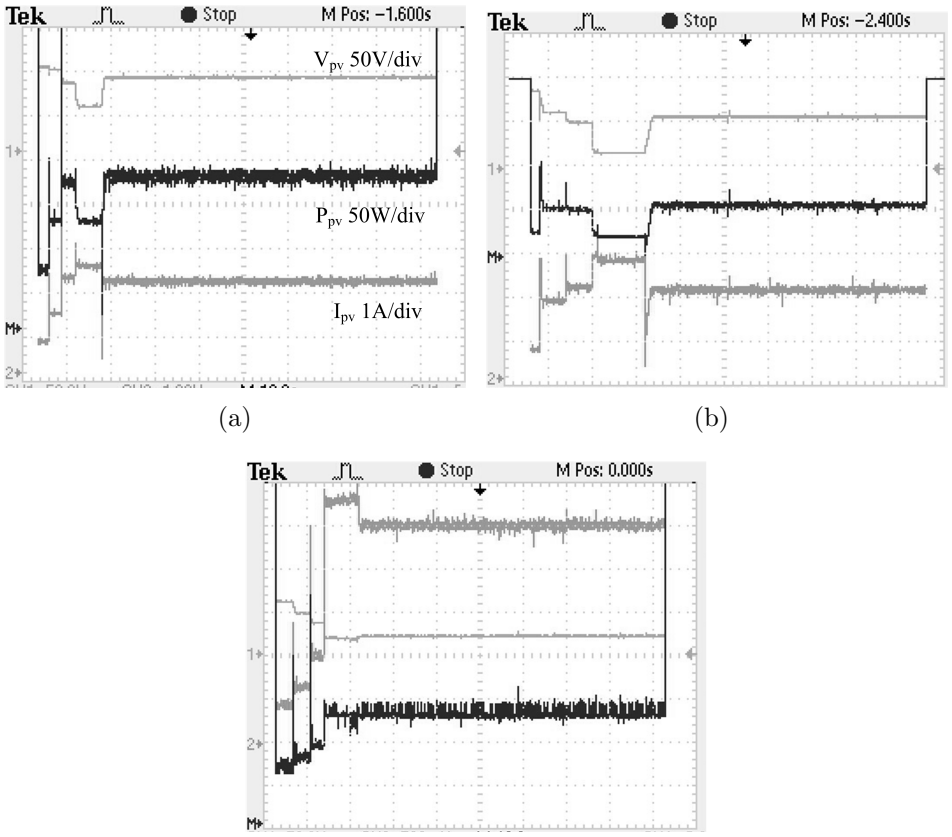

Figure 3.11: GMPP Tracking characteristics of $300W_p$ system (a) Pattern 1 (b) Pattern 2 (c) Pattern 3

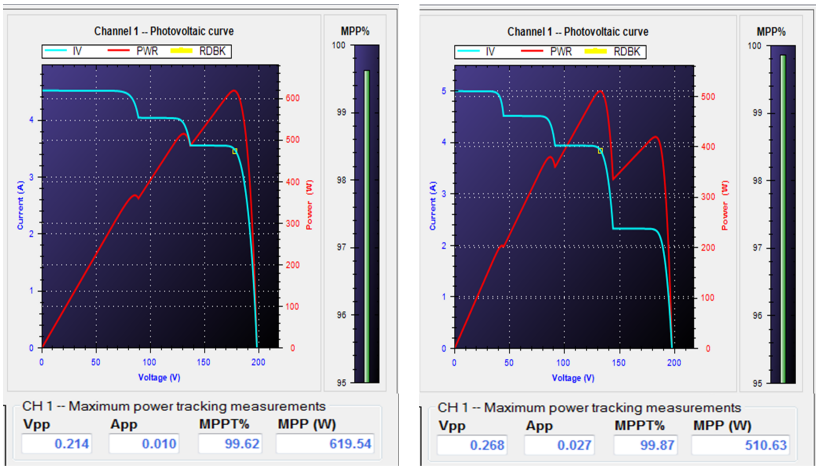

(a) (b)

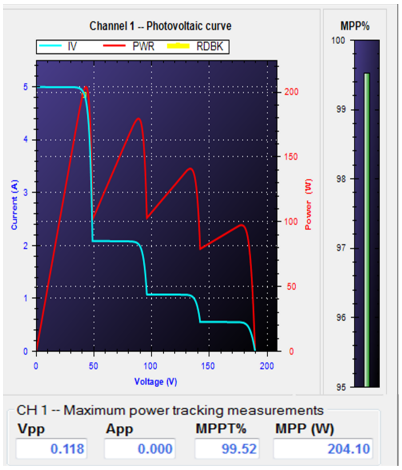

(c)

Figure 3.12: Steady sate GMPP Tracking characteristics of proposed technique for (a) Pattern 1 (b) Pattern 2 (c) Pattern 3

technique initiates the GP tracking routine. The GP tracking routine initially scans the I_{dc_link}-D characteristics using the equation (3.5). Due to the power electronic interface non-idealities, I_{dc_link} reaches to a steady state value by subsequent delay for respective duty cycle perturbation. Sampling the I_{dc_link} during this time affects the tracking accuracy. To overcome this, the controller is incorporated with a delay timer of time period equivalent to the boost converter settling time. If the status of the delay timer is true, then the controller measures the I_{dc_link} and stores it as $I(1)$, and the duty cycle corresponding to $I(1)$ is saved as $D(1)$.

In this hybrid GMPPT technique, the practical shading patterns shown in Fig. 3.4, have been categorized as case 1 and 2. In case 1, the rightmost peak of the $P-V$ curve is the GP (i.e., pattern 1 & 2). In case 2, the GMPP is not the rightmost peak of the $P-V$ curve (i.e., patterns 3, 4, 5, and 6). Tracking of GMPP using the proposed hybrid GMPPT technique is explained for the above two cases.

Case 1:

Similar to the two-stage GMPPT technique explained in the Section (3.2), the proposed hybrid GMPPT technique also scans the I_{dc_link}-D at two duty cycles (i.e., $D(1)$ and $D(2)$) and compares the measured currents $I(1)$ and $I(2)$ to recognize the type of shading pattern and thus to locate the GMPP neighborhood. From the $P-V$ characteristics analysis, if the measured current $I(1)$ is greater than $I(2)$, then the rightmost peak of the $P-V$ curve will be the GP as shown in Fig. 3.4 (i.e. shading pattern 1 & 2). Therefore, the duty cycle $D(1)$ will be in the neighborhood of the GMPP, thus the controller stops the scanning procedure and initiates the SSHC routine to track and retain the GMPP.

Case 2:

If the first peak in the rightmost region of $P-V$ curve is not the GP (i.e., $I(1)$ is less than $I(2)$), then the controller initiates the ABC algorithm to search for the GMPP. The ABC algorithm is a swarm based meta-heuristic algorithm developed by (Karaboga and Akay, 2009) based on the behavior of bee colonies searching for the food. The ABC algorithm uses artificial bees, categorized into three types; employed bees, onlooker bees, and scout bees. Wherein, there will be a single scout bee and the remaining bees are equally divided into employed and onlooker bees. The responsibilities of employed bees are to search for food sources and to pass the food information to the onlooker bees waiting at the hive. If the search process stagnates, a scout bee becomes employed bees and restarts the search process.

Employed bees go to the known nectar sources and search for new nectar sources in the neighborhood. If the new nectar is richer than the previous, the bee updates its position with the new nectar source. The onlooker bee selects the richest nectar found by the employed bees for further foraging. In the proposed algorithm, duty cycle D of the boost DC-DC power converter is termed as the position of the food source. Maximizing the I_{dc_link} results in extracting the maximum power from the PV source, therefore output current of boost converter (i.e., I_{dc_link}) is termed as amount of nectar and maximizing the I_{dc_link} current will be the objective function ($P^{\star}_{pv}$ in equation (3.4) The ABC routine starts by initializing the number of employed bees and their initial food position (i.e., initial duty cycles) in block 18, as follows (Sundareswaran et al., 2015):

$$D_x = D_{min} + \frac{(x-1)(D_{max} - D_{min})}{L-1} \tag{3.6}$$

where L is the number of employed bees, $x = 1, 2, 3...L$, and $(D_{max} - D_{min})$ constitutes the GMPP search space.

Since, the GP is not from the first peak, the search space for the ABC will be $D(2)$ to D_{max}. After finding the nectar amount at the initial positions, the employed bees update their position (block 21) within their surrounding area using the following equation:

$$D_x(k+1) = D_x(k) + \phi\,(D_x(k) - D_x(j)) \tag{3.7}$$

where k represents the iteration number, j is the random index $\in \{1, 2, ...L/2\}$, and ϕ is the random number [0-1] which directs the new position towards the GMPP.

The onlooker bees update their position (in block 20) to the neighborhood of the best nectar explored by the employed bees, as follows:

$$D_x(k+1) = D_{best}(k) + \phi\,(D_{max} - D_{min}) \tag{3.8}$$

where D_{best} is the position with richest nectar amount.

After reaching the predefined iteration count, and if there is no further increment in I_{dc_link}, the GMPP search terminates and the duty cycle corresponding to maximum I_{dc_link} will be applied to the power electronic interface. If the search process stagnates after the predefined iteration count, the algorithm restarts the search process by initializing employed bees and iteration count (i.e. scout bee phase).

In a practical scenario, during some PSCs the change in output current of power electronic interface (ΔI_{dc_link}) can be less than the decisive value, and thus the ABC algorithm cannot track the new MPP if the insolation on the PV modules changes. To overcome this, a 15min timer (block 6) is incorporated to the controller which runs the GP routine periodically; although the 15min timer is not incorporated in cases such as of shading pattern 1 & 2 or uniform insolation, as the SSHC algorithm can respond to the variations in insolation changes. In the proposed hybrid GMPPT technique, during scanning of the I_{dc_link}-D curve, the I_{dc_link} will have a smaller amount of variations for each duty cycle perturbation. Therefore, an accurate and sensitive current measurement unit is necessary for effective GMPP tracking.

3.3.1 RESULTS AND DISCUSSION

The same experimental setup and same shading patterns used for two-stage GMPPT technique in Section (3.2) is used for validating the hybrid GMPPT Technique. The tracking characteristics for pattern 1 & 2 using hybrid GMPPT technique is not shown here, since the hybrid GMPPT method works similar to the two-stage GMPPT technique.

Shading patterns 3 & 4 have been applied to the PV array as shown in Fig. 3.14(a). Firstly pattern 3 has been applied for the duration of 3s. Further, during the scanning of I_{dc_link}-D curve, the value of I_{dc_link} at $D(1)$ is found to be lesser than I_{dc_link} at $D(2)$. Hence, the controller instigates the ABC algorithm to track the GMPP. The search space for the ABC is defined as $D(2)$ to D_{max} (i.e. 0.9), and six employed bees are initiated using (3.6). After six iterations of ABC searching process, the controller measured I_{dc_link} value at around 25 duty cycles in the search space of D= 0.5 to 0.9. Scanning only 40% of I_{dc_link}-D curve at around 25 duty cycle can find the GMPP location efficiently. Hence, the termination criterion for the proposed method is set to 6 fixed iterations. Therefore, the proposed hybrid GMPPT controller has tracked the maximum power of 248W with the efficiency of 99.13% after 6 iterations and the tracking speed of the algorithm is found to be 1.35s. After 3s, the pattern of $P-V$ curve has been changed and the proposed GMPPT controller initiated the ABC algorithm since the GP is not from the rightmost region of the $P-V$ curve and the GMPP is tracked successfully with the tracking efficiency of 99%. The characteristics of PV power during the tracking of GMPP are shown in Fig. 3.14(b).

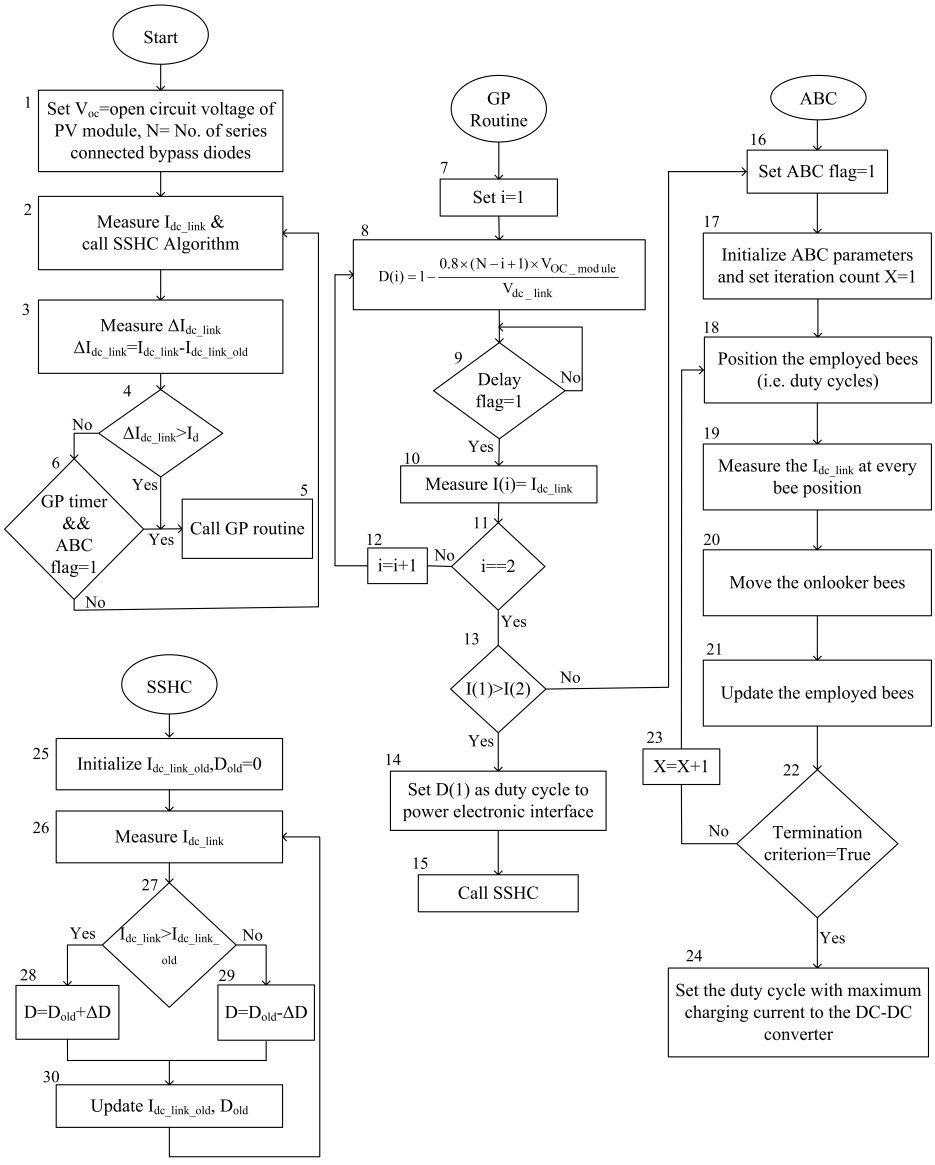

Figure 3.13: Flowchart of the proposed ABC and HC based Hybrid GMPPT Technique

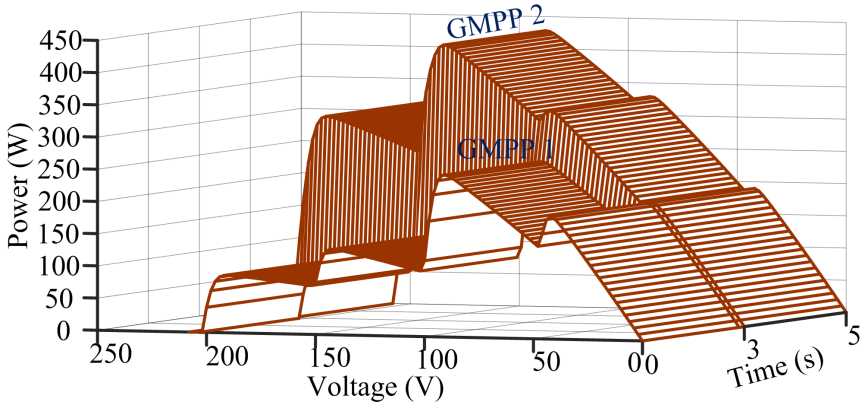

(a)

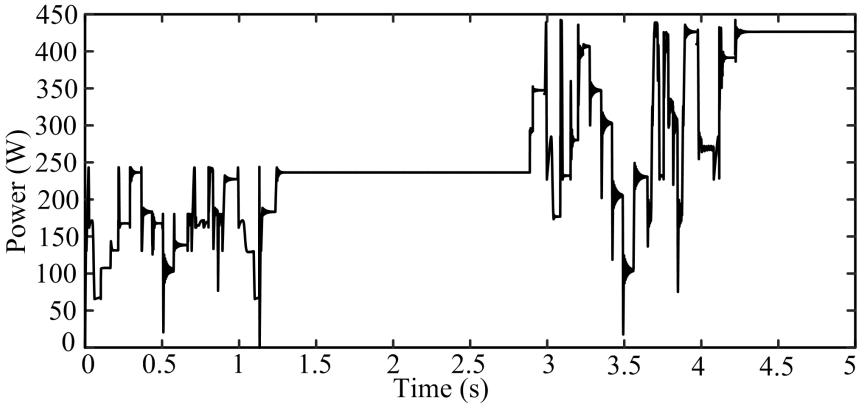

(b)

Figure 3.14: (a) $P-V$ characteristics (patterns 3& 4) of PV array (b) GMPP tracking characteristics of PV power for the patterns 3 & 4

Shading patterns 5 & 6 shown in Fig. 3.15(a) have been applied to the PV system and the proposed GMPPT controller instigated the ABC routine since the GP is not in the rightmost corner of the $P-V$ curve. The ABC routine has efficiently tracked the GMPP with 97.57% tracking accuracy. Similar to the previous case, the pattern of $P-V$ curve has been changed after 3s, and the proposed algorithm detected the change in I_{dc_link} and restarted the GP routine and successfully tracked the GMPP. The convergence speed of the proposed technique for patterns 3, 4, 5 & 6 is less when compared to patterns 1 & 2. The characteristics of PV power during the tracking of GMPP are shown in Fig. 3.15(b).

In case of most of the practical mismatch conditions on PV array, the difference in irradiation levels on modules in an array is very less. Consequently, GP occurs in the rightmost region of the $P-V$ curve. Therefore, the tracking speed of the proposed technique is very fast as less section of a $P-V$ curve is scanned in most cases. Moreover, the proposed method can efficiently track the GMPP in all mismatch insolation conditions.

Experimental results of tracking the GMPP for the insolation levels $1000W/m^2$, $400W/m^2$, $200W/m^2$ and $100W/m^2$ have been shown in Fig. 3.16. The proposed GMPPT controller has initiated the ABC algorithm as the GP is not in right most corner of $P-V$ curve. The maximum power of 204.1W was tracked in 14s with a tracking efficiency of 99.52%. A delay timer with 10s is incorporated to restart the GP routine. In Fig. 3.16, when the GP routine was initially restarted, the insolation on the PV modules had not changed; therefore, unwanted power loss occurred during the ABC searching process. When the GP routine restarted on the second occasion, the insolation level on module 2 had been increased to $450W/m^2$ and the proposed algorithm successfully tracked the GMPP. Fig. 3.17 shows the boost DC-DC converter duty cycle variation (D), PV current (I_{pv}), boost converter switch voltage (V_{sw}), and DC link voltage (V_{dc_link}) characteristics during the tracking of GMPP for the shading patterns 3 and 2 shown in Fig. 3.12. From Fig. 3.17 it is clear that the proposed hybrid GMPPT technique tracks the maximum power of 204.1W and 510.6W, with tracking efficiencies of 99.52% and 99.87% for shading patterns 3 and 2 respectively. Fig. 3.18 shows the performance characteristics of proposed GMPPT technique during the tracking of only shading pattern 2.

For the proposed hybrid GMPPT technique and I_{dc_link} vs. D curve scanning based two-stage GMPPT technique, effect of PV panel temperature on the tracking

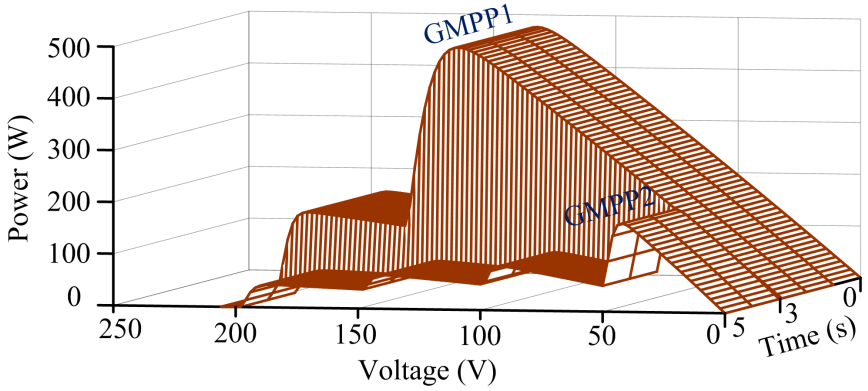

(a)

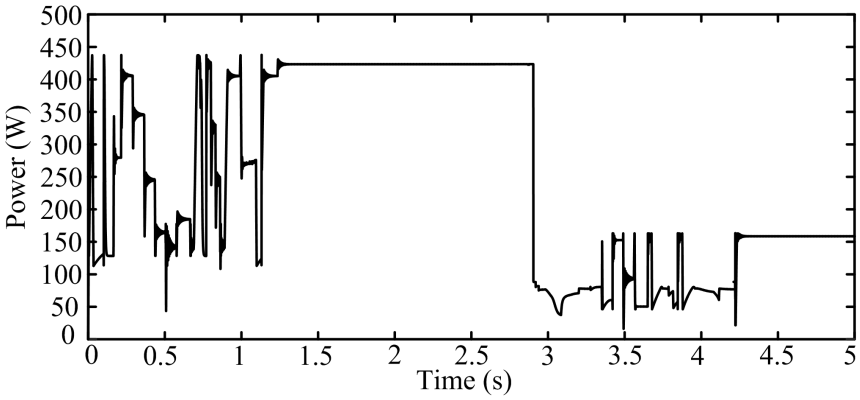

(b)

Figure 3.15: (a) $P-V$ characteristics (patterns 5 & 6) of PV array (b) GMPP tracking characteristics of PV power for the patterns 5 & 6

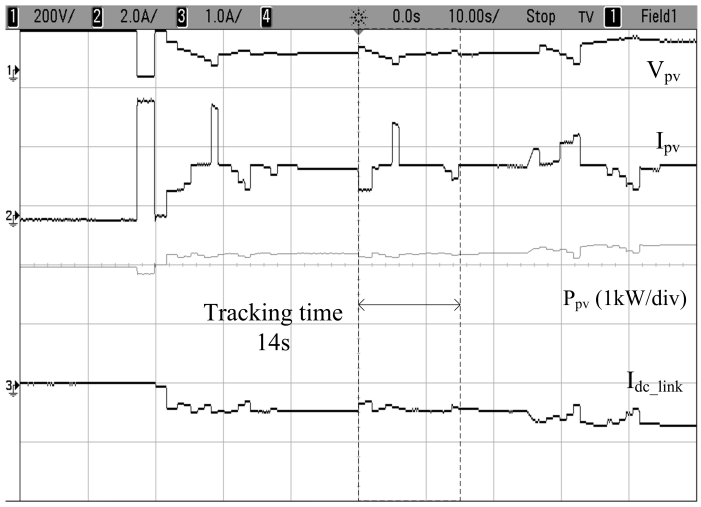

Figure 3.16: V_{pv}, I_{pv}, P_{pv}, and I_{dc_link} characteristics during the tracking of GMPP for pattern 3 shown in Fig. 3.12

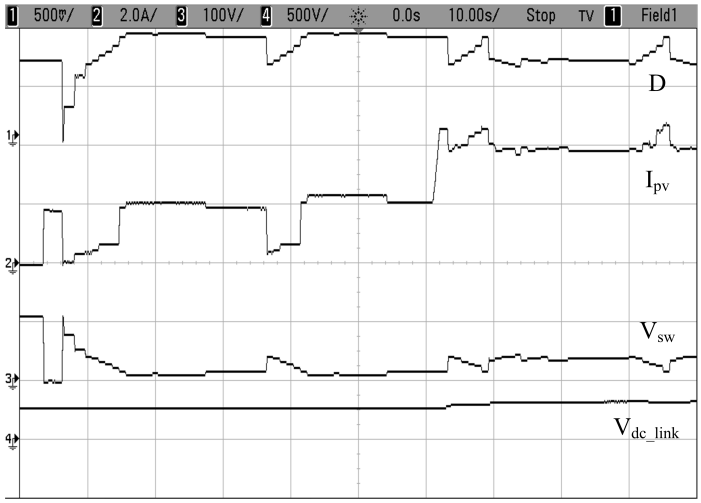

Figure 3.17: DC link voltage and boost converter parameters during the tracking of GMPP for shading patterns 2 and 3 shown in Fig. 3.12

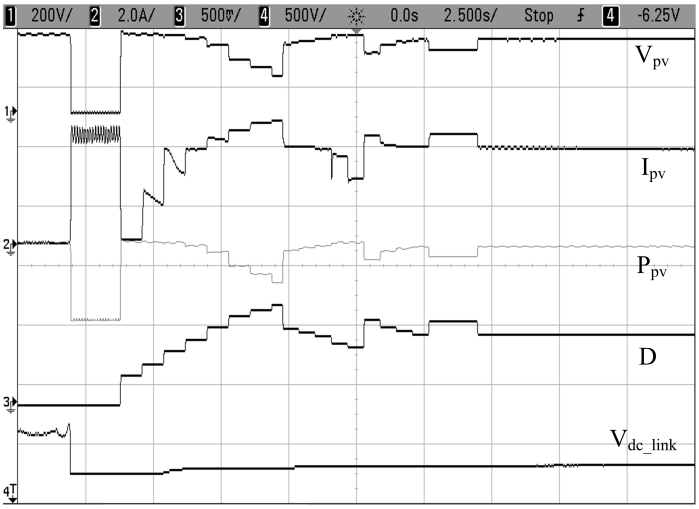

Figure 3.18: GMPP tracking characteristics for pattern 2 shown in Fig. 3.12

performance is not considered. Since, from the thermal analysis of PV panels in (Armstrong and Hurley, 2010), temperature of a PV module takes 10-15min to reach a steady state temperature for a large step change in insolation (i.e. $600W/m^2$). However, the tracking time of the proposed GMPP algorithm is within few seconds and during this time change in V_{oc_module} due to the effect of temperature is very less. The proposed hybrid GMPPT technique and two-stage GMPPT technique is compared with the other GMPPT techniques in literature, the comparison details are discussed in the next section.

3.4 COMPARISON OF PROPOSED GMPPT TECHNIQUES WITH OTHER GMPPT TECHNIQUES IN LITERATURE

The proposed hybrid GMPPT technique and two-stage GMPPT technique is compared with the HC based variable voltage controlled two-stage GMPPT technique proposed in (Wang et al., 2016) and the conventional ABC algorithm with large search space was introduced in (Sundareswaran et al., 2015). Fig. 3.19 shows the PV power characteristics during the tracking of GMPP for the three shading patterns (i.e., Patterns 1, 4 & 6) using the GMPPT technique proposed in (Wang et al., 2016). To scan the voltage range (from 30V to 180V), this GMPPT technique re-

quired around 0.36s. Moreover, the tracking time of this method further increases with the increase in the voltage range of the PV string.

Fig. 3.20 shows the PV power characteristics while tracking the GMPP for three shading patterns using the conventional ABC technique (Sundareswaran et al., 2015). The search space defined for conventional ABC algorithm is more (i.e., $D = 0.2$ to 0.9) and the number of employed bees used are eight, which is more than the proposed method. The tracking speed of this method is found to be 1.6s. Moreover, the methods in (Wang et al., 2016) & (Sundareswaran et al., 2015) require two measurements units to track the GMPP, which increases the cost of the system. Further, the comparison details of these methods in terms of tracking accuracy, tracking speed and the number of sensors used are tabulated in Table. 3.2.

From the comparison it is observed that, the proposed I_{dc_link} vs. D curve scanning based two-stage GMPPT technique performs superior to the HC based variable voltage controlled two-stage GMPPT technique in terms of tracking speed and tracking accuracy. In a similar way, proposed HC and ABC based hybrid GMPPT technique reduces the search space for the ABC algorithm and reduces the tracking time.

3.5 SUMMARY

To track the GMPP with acceptable tracking speed and accuracy, two GMPPT algorithms are developed in this work. The first GMPPT technique is from the scanning based two-stage GMPPT techniques, which efficiently scans the I_{dc_link} vs. D cycle characteristics of power electronic interface at selective duty cycles in stage 1 to locate the GMPP neighborhood area, in stage-2 hill climbing algorithm is implemented to track and retain the GMPP. Moreover, this technique identifies the type of shading pattern on PV array by measuring the I_{dc_link} at selective duty cycles to improve the convergence speed. The minimum tracking time of proposed algorithm for 4s1p PV array configuration is found to be 4s.

The second proposed GMPPT technique combines the ABC and HC techniques for the effective utilization of PV system under non-uniform insolation conditions.This technique uses the HC algorithm during uniform insolation conditions and to detect the occurrence of PSC. An effective and fast scanning of I_{dc_link} vs. D characteristics is carried out to identify the type of shading pattern of the $P-V$ curve, and thus operate the ABC or SSHC algorithm. The proposed hybrid GMPPT technique reduces the

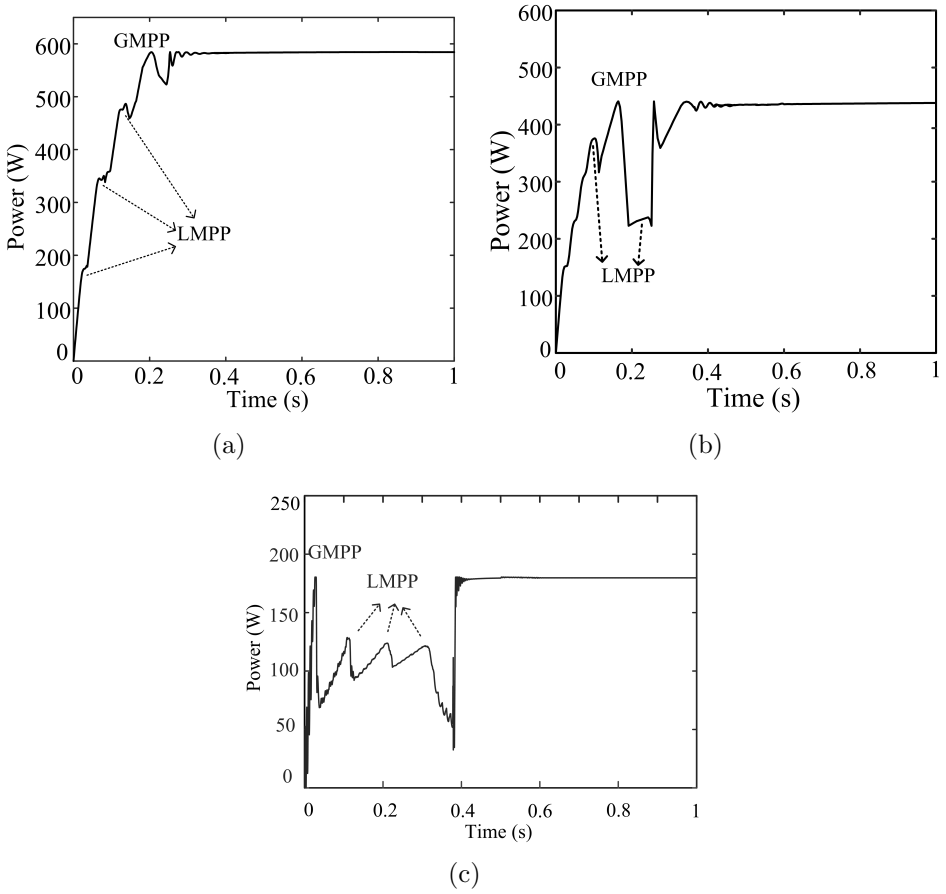

Figure 3.19: PV power characteristics using the method in (Wang et al., 2016) during non-uniform insolation (a) Pattern 1 (b) Pattern 4 (c) Pattern 6

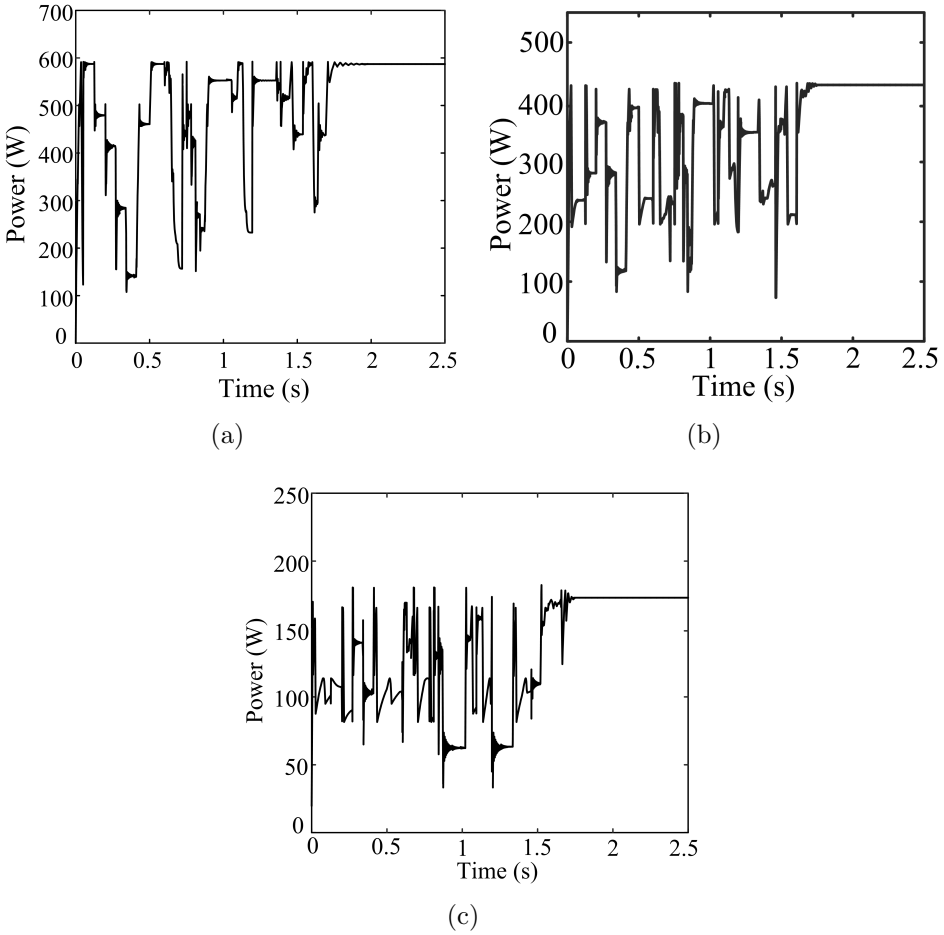

Figure 3.20: PV power characteristics using the method in (Sundareswaran et al., 2015) during non-uniform insolation (a) Pattern 1 (b) Pattern 4 (c) Pattern 6

Table 3.2: Comparison of Proposed GMPPT Techniques with the Other Methods in Literature

Method	**Tracking Time (s)**	**Tracked Power (W)**	**Max. Power (W)**	**Tracking Efficiency (%)**	**Shading Pattern**
Two-stage GMPPT	0.14	590		98.16	
Hybrid GMPPT	0.14	590		98.16	
(Wang et al., 2016)	0.36	588	601	97.84	Pattern 1
(Sundareswaran et al., 2015)	1.67	585.97		97.5	
Two-stage GMPPT	0.26	426		97.93	
Hybrid GMPPT	1.33	430		99	
(Wang et al., 2016)	0.38	428	435	98.55	Pattern 4
(Sundareswaran et al., 2015)	1.71	427		98.34	
Two-stage GMPPT	0.34	179		98.62	
Hybrid GMPPT	1.25	177		97.57	
(Wang et al., 2016)	0.4	176.2	181.5	97.05	Pattern 6
(Sundareswaran et al., 2015)	1.68	175.7		96.85	

search space for ABC and thus it improves the convergence speed when compared to conventional ABC technique. The proposed two GMPPT techniques uses only single current sensor, hence overall cost of the system reduces.

Chapter 4

DEVELOPMENT OF LI-ION BATTERY MANAGEMENT SYSTEM BY ESTIMATING STATE OF HEALTH

Contents

4.1 GENERAL

From the Chapter 1.3, it is observed that knowing the battery aging mechanism and estimating the state of health (SoH) reduces the failure rate of the battery and improves the reliability of overall PV-Battery power supply system. From the literature

study presented in Chapter 2, it is observed that most of the available SoH techniques are model dependent and off-line methods. Therefore, in this research work, two on-line SoH estimation techniques are proposed. In order to validate the proposed SoH techniques in practical way, it requires the exhaustive accelerated battery charging and discharging results till the battery reached to its end of life (EoL). To arrive at the battery behavior for multiple charge discharge cycles in a limited time, effect of aging factors on battery life has to be modeled and added to the equivalent circuit of single cell Li-Ion battery discussed in Chapter 1.3.1.

During the battery course of usage, there exists two type of capacity losses such as calendar loss and cycle loss. Typically, the calendar losses are minimal and can be ignored if the battery is cycle every day. From the cycle life test reports of lithium iron phosphate (LFP) cells in (Xu et al., 2018) & (Wang et al., 2011), it is observed that, large DoD of battery cycled at high charge/discharge rates and operating the battery at elevated temperatures degrades the battery usable capacity at faster rate. Therefore, the effect of operating temperature and DoD on battery capacity degradation has been added to the equivalent circuit of Li-Ion cell shown in Fig.1.10 in chapter 1.

The capacity degradation (i.e., change in C_{cap} in Fig.1.10) due to the effect of DoD (cycling at C/2 charge/discharge rate) is modeled as follows (Gholizadeh and Salmasi, 2014),

$$\Delta Q = 30330 exp\left(\frac{-31500}{8.314 \times T}\right)(N \times DoD \times 2)^{0.552} \tag{4.1}$$

where, ΔQ is the percentage change in usable capacity of the battery, T is the operating temperature (Kelvin), N is the number of elapsed charge/discharge cycles and DoD is the percentage depth of discharge.

The effect of operating temperature on battery capacity degradation has been modeled using following equation (Han et al., 2014).

$$\Delta Q = 0.1825 exp\left(\frac{-1324.65}{T}\right) N^{0.5878} \tag{4.2}$$

The equations (4.1) & (4.2) determines the capacity loss due to the effect of aging parameters of the battery. Therefore, the effective usable capacity is expressed as,

$$C_{cap} = C_{cap\_rated} - (\Delta Q_{DoD} + \Delta Q_{Temperature}) \tag{4.3}$$

where, C_{cap_rated} is the rated capacity of the battery specified by the manufacturer.

The effect of aforementioned aging parameters on battery run time over a period of time is shown in Figs. 4.1 & 4.2. From Fig. 4.1(b), battery capacity degrades at a faster rate when it is operating at elevated temperatures. Similarly, from Fig. 4.2(b) it is observed that, higher DoDs degrades the battery faster. Moreover, it is also observed that, effect of temperature on battery life cycle is higher than the effect of DoD.

With the knowledge of battery aging mechanism, two SoH estimation techniques are proposed in the following sections. The proposed two methods estimates the SoH without disturbing the ongoing charging/discharging process. The first method suitably modifies the coulomb counting (i.e. current integration) method to calculate the discharge capacity of the battery, when the discharge current of the battery is varying and DoD of the battery is not 100%. The second method method measures the DC resistance of the battery in every discharge cycle and thereby the SoH.

4.2 DEVELOPMENT OF COULOMB COUNTING BASED STATE OF HEALTH ESTIMATION TECHNIQUE

The conventional current integration (i.e. coulomb counting) based SoH estimation techniques require 100% DoD and constant discharge rate to estimate the life of the battery. However, in most of the practical applications discharge current and DoD level varies based on load variation. Therefore, in the proposed method, current integration technique is appropriately tailored to measure the discharge capacity and then to estimate the SoH, when the discharge current is varying and the DoD of the battery is not 100%.

The proposed technique is validated using a Bi-directional power electronic interface circuit as shown in Fig. 2.8. In Fig. 2.8 voltage and current sensors at the battery terminals are used to measure the SoC and discharge capacity of the battery. Fig. 4.3 shows the complete flowchart of the proposed modified current integration based SoH estimation technique. The proposed method measures the discharge capacity of the battery in every cycle and compares it with capacity of the battery when it was new as described in equation (2.11).

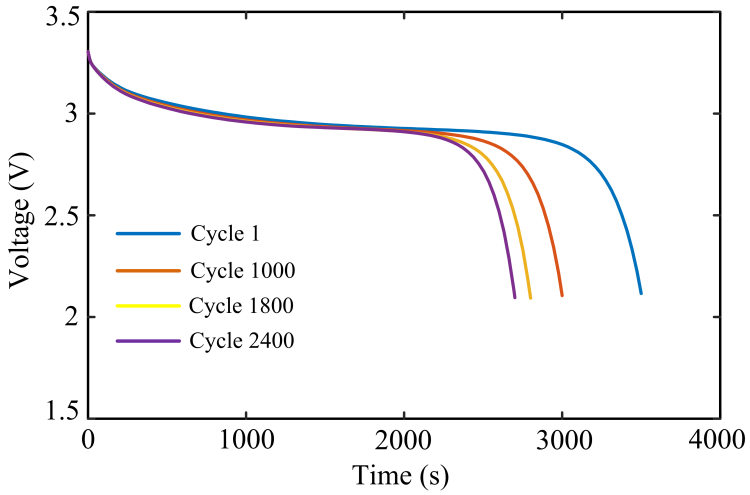

(a)

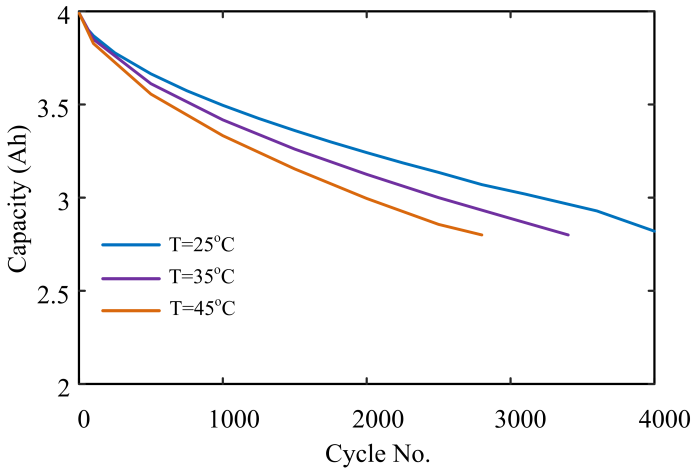

(b)

Figure 4.1: (a) Battery runtime characteristics at different cycle numbers and at operating at 35^oC (b) Capacity degradation of LFP battery at different cycle numbers and operating at different temperature conditions

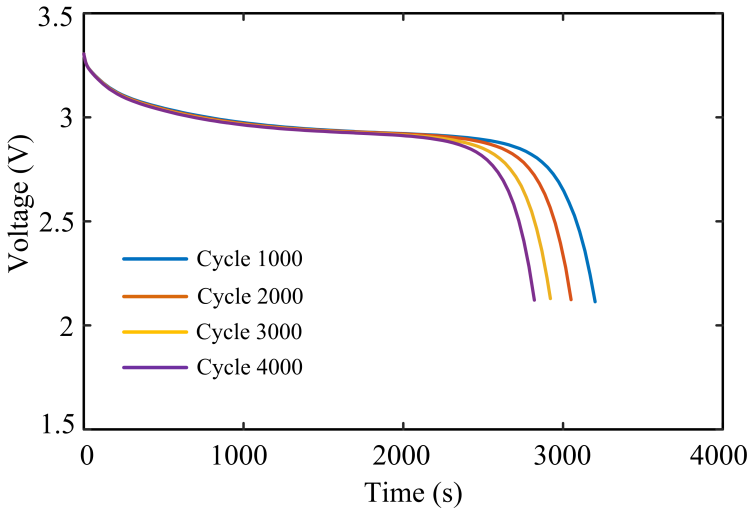

(a)

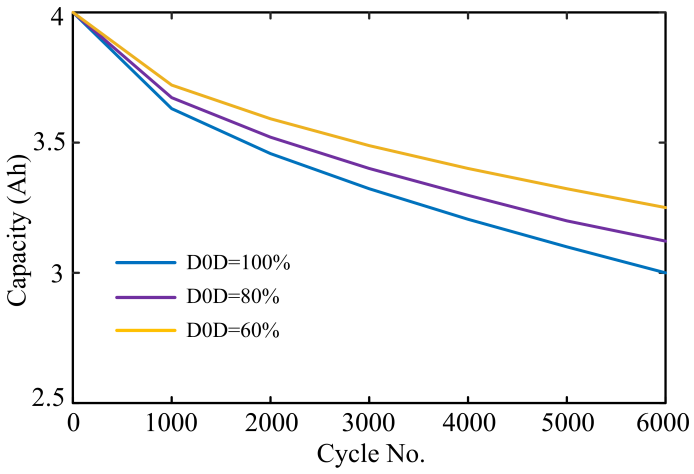

(b)

Figure 4.2: (a) Battery runtime characteristics at different cycle numbers and at operating at 100% DoD (b) Capacity degradation of LFP battery at different cycle numbers and operating at different DoD conditions

To measure the discharge capacity (Q_i), current integration technique is used, which continuously monitors the discharge current of the battery and integrates it with the discharge time as described in equation (4.4).

$$Q_i = \int_0^{\infty} I_{discharge} dt \tag{4.4}$$

where, $I_{discharge}$ is the discharge current of the battery, $t = 0$ is fully charged state (i.e. SoC = 100%) and t = end is the time taken to discharge the battery completely.

In conventional coulomb counting technique (Q_0) is set to a constant value equal to a rated capacity mentioned in the manufacturer specification and that is stored in the memory. Due to use of the constant rated capacity (Q_0), on number of occasions the SoH determined is inaccurate. For example, the SoH measured when the battery is fully discharged and when the battery is partly discharged shall be different. Thereby providing a different SoH when the battery has undergone a same number of charge/discharge cycles. To illustrate the disadvantage further, considering 200 cycles elapsed 4Ah rated capacity battery is charged to 100% SoC and then discharged to 0% SoC with the 1C discharge rate as shown in Fig. 4.4(a). From the discharge characteristics, the total discharge time of the battery is found to be around 3380s and by using the current integration technique, the discharge capacity of the battery may be determined as 3.78Ah. Therefore, the estimated SoH of the battery from equation (2.11) is 94.5%. However, for the same battery, if the discharge process terminates through midway at 2180s as shown in Fig. 4.4(b) , then the calculated discharge capacity through current integration technique would be 2.88Ah. The reduced discharge capacity is not due to the aging of the battery, but due to the battery being not discharged completely. Therefore, the estimated SoH value using equation (2.11) gives an incorrect result. Further, in various applications, full discharge of the battery is undesirable.

From the datasheet of LFP battery (MARQUE ACL9014) and from the discharge Ampere-hour throughput (Ah-V) characteristics of a 4Ah Li-Ion battery shown in Fig.4.5 it is evident that, rated capacity (Q_0) of the battery varies with the discharge rate. In most of the practical applications like BTS, load current varies with the signal traffic. As a result, discharge current varies in a single discharge process. Thus, by keeping the constant rated capacity (Q_0) in equation (2.11) yields an inaccurate SoH results.

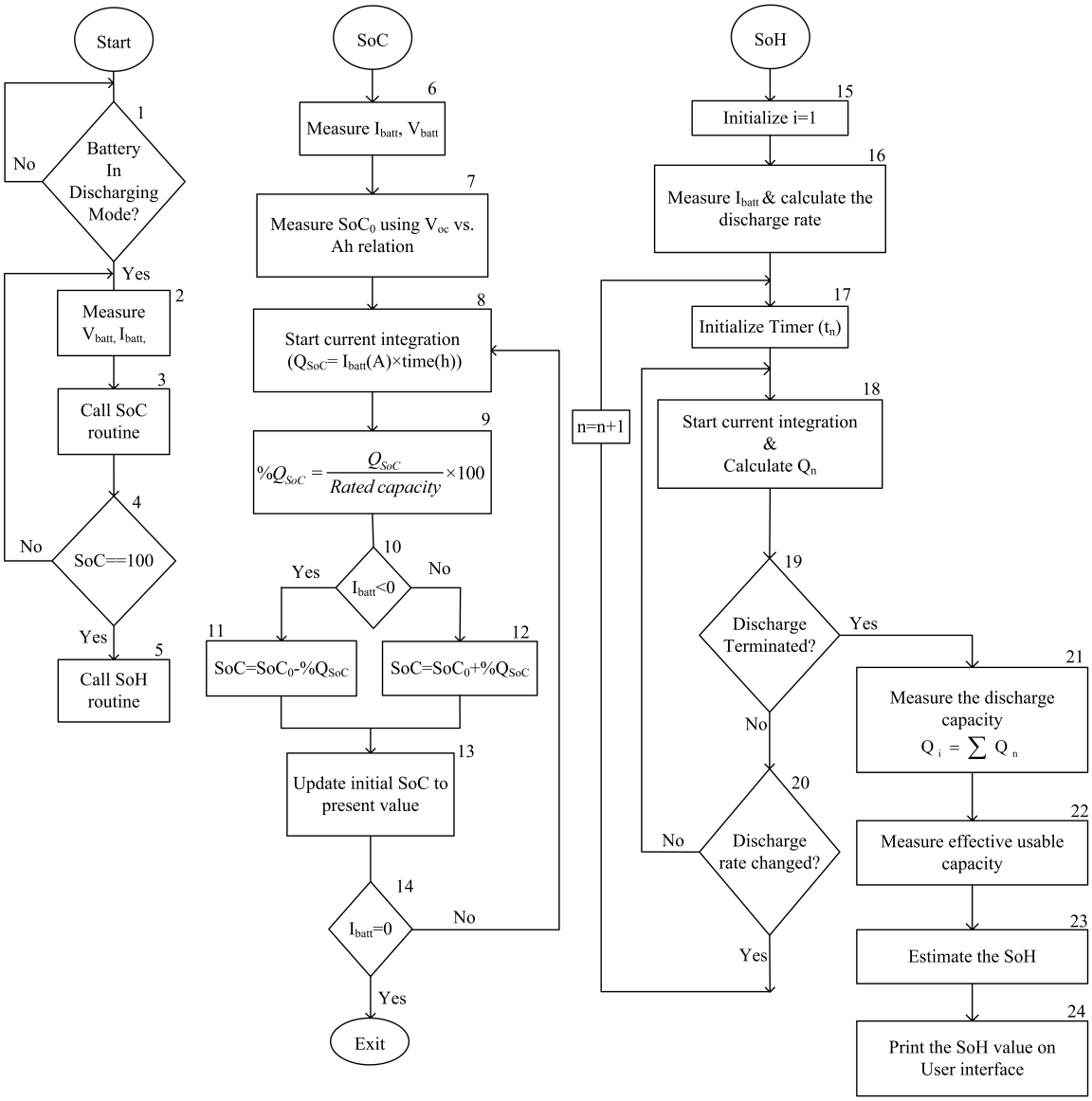

Figure 4.3: Flowchart of the proposed coulomb counting based SoH estimation technique for Li-Ion battery

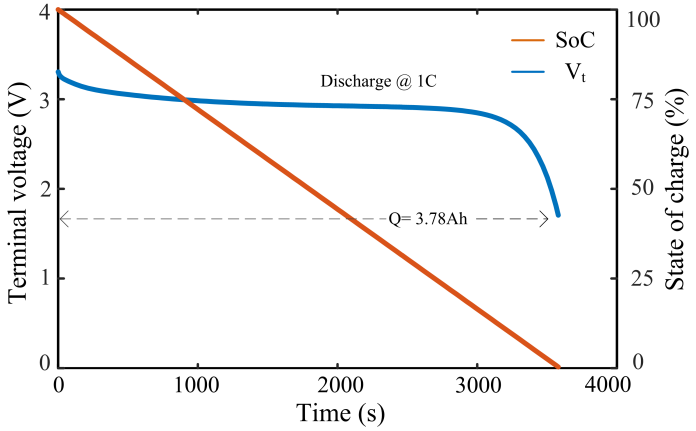

(a)

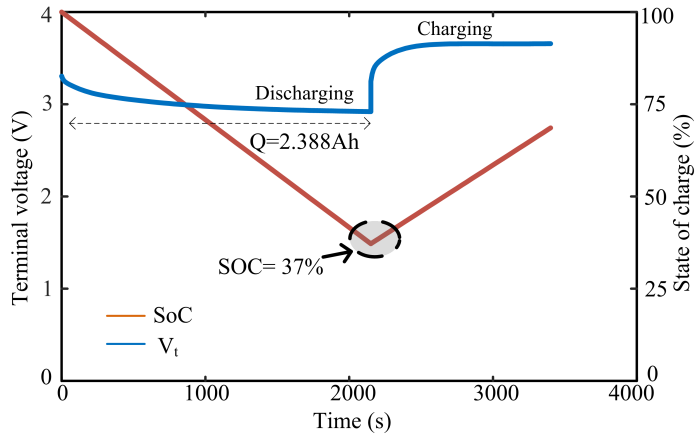

(b)

Figure 4.4: (a) Discharge characteristics of a completely discharged battery (b) Discharge characteristics of a battery with 63% DoD

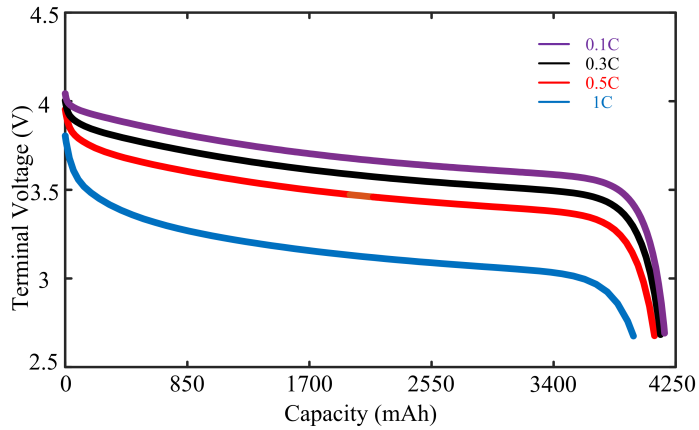

Figure 4.5: Ah-V characteristics of LFP battery at different discharge rates

In Fig. 4.4(b), discharge process is terminated when the battery terminal voltage is reached to 3V and the Q_i is calculated through current integration, whereas Q_0 is can be calculated from Fig. 4.5 (i.e. capacity at 3V). The effect of change in discharge rate in a single discharge process is addressed in the proposed method by calculating the effective Q_0 using a time weightage method (i.e. amount of time spent by battery at each discharge rate) as described in equation 4.5.

$$Q_0 = \frac{(Q_{o1} \times t_1) + (Q_{o1} \times t_1) + ... + (Q_{o1} \times t_1)}{t_1 + t_2 + ... + t_n} \times (1 - SoC_{termination}) \tag{4.5}$$

Where Q_{o1}, Q_{o2},. . . Q_{on} are usable capacities of battery for each discharge rate given in the manufacturer data sheet, t_1, t_2,. . . t_n are the time spent by battery in each corresponding discharge rate. $SoC_{termination}$ is the SoC of the battery at which discharge process was terminated.

In the equation 4.5, the term $(1-SoC_{termination})$ overcomes the problem of variable DoD and the other term $\frac{(Q_{01}\times t_1)+(Q_{02}\times t_2)+...+(Q_{0n}\times t_n)}{t_1+t_2+...+t_n}$ overcomes the problem of multiple discharge rates in a single discharge process. In the flowchart of the proposed method, block 1 checks if the battery is in discharging mode. Since, the proposed technique requires the battery to be charged to 100% and it has to be in discharging mode. Block 2 measures the battery terminal voltage and discharge current continuously to estimate the SoC. To measure the SoC of the Li-Ion battery, the controller calls the SoC routine (i.e. conventional coulomb counting method). The SoC of the battery is measured as follows,

$$SoC = SoC_0 + \left(\frac{\int I_{charge} dt}{RatedCapacity} - \frac{\int I_{discharge} dt}{RatedCapacity} \right) \times 100 \qquad [\%] \tag{4.6}$$

where, SoC_0 is the initial SoC of the battery measured based on V_{oc} vs Ah characteristics of the battery. $RatedCapacity$ will be specified in the manufacturer data sheet.

The controller (i.e. block 4) ensures battery is completely charged (i.e., 100% SoC) and calls the proposed SoH routine. Further, controller (blocks 16 & 17) identifies the discharge rate of the battery and initiates the timer to measure the amount of time spent by the battery in same discharge rate. Furthermore, controller initiates the

current integration technique. During the discharging process, if the discharge rate varies (i.e. in block 20), controller initiates the new timer and calculates the amount of charge delivered to the load with the new discharge rate. This process continuous till the battery gets completely drained or discharge process terminates in middle.

The controller (Block 21) calculates the total discharge capacity (Q_i) of the battery and the block 22 calculates the normalized usable capacity (i.e. Q_0) of the battery after the discharge process terminates. Further, the controller estimates the SoH of the battery using the equation (2.11). Hence, the proposed SoH estimation technique estimates the health of the battery accurately at the end of the every discharge cycle. Moreover, the proposed SoH technique considers the variable discharge rate and variable depth of discharge conditions for estimating SoH. The calculated SoH details can be displayed on a user interface through serial communication of the controller. Moreover, the proposed technique does not require any additional circuitry to estimate SoH.

4.2.1 RESULTS AND DISCUSSION

The proposed method has been evaluated using two test cases such as complete discharge test (i.e.,using the conventional coulomb counting technique) and the partial discharge test (i.e., using the proposed modified coulomb counting technique).

Case 1: Complete Discharge

A 4Ah LFP battery is cycled at $35°C$ with 100% DoD for 450 cycles, and then it is subjected for the SoH estimation using the proposed method. In this case, the battery is discharged with 1C rate and the controller initiated the 0.5ms timer for the current integration. The controller calculated the discharge capacity (Q_i) at the end of 100% DoD and the value of SoH found to be 90.875%. The battery discharge current, SoC and the current integration characteristics are shown in Fig. 4.6. From the Fig. 4.6, it is observed that battery is holding 3.635Ah capacity after 450 cyles of aging.

Fig. 4.7 shows the discharge current, SoC and the current integration characteristics of 1020 cycles aged battery. In this case, battery is subjected to stress factors of temperature $40°C$, 50% DoD and 0.5C discharge rate. The proposed SoH estimation method is implemented at the 1021^{st} discharge cycle. The proposed method calculated the discharge capacity ($Q_i = 3.366$) after the end of discharge and the estimated

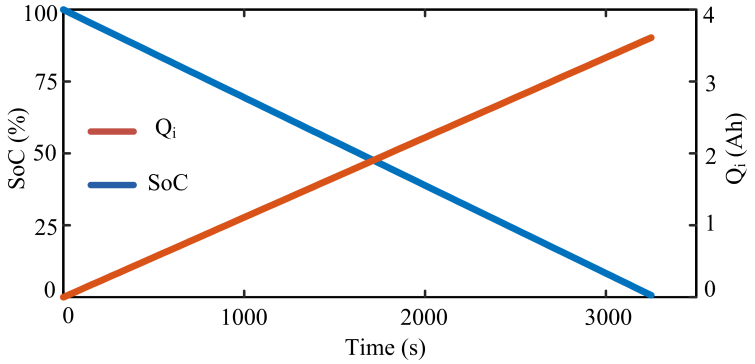

Figure 4.6: SoC and coulomb counting characteristics of a 450 cycles aged completely discharged battery

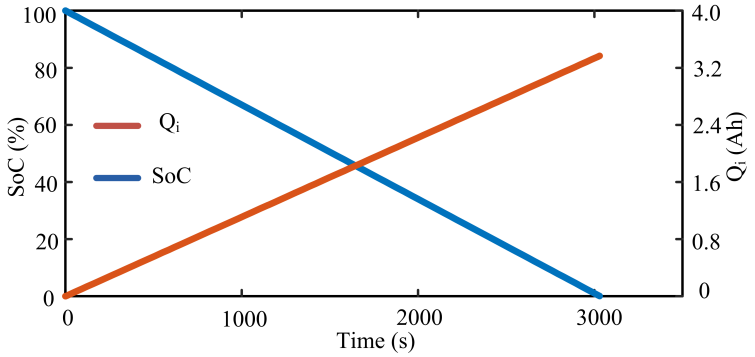

Figure 4.7: SoC and coulomb counting characteristics of a 1020 cycles aged completely discharged battery

SoH value is found to be 84.15%. In (Gholizadeh and Salmasi, 2014), it is reported that, if the value of SoH reaches to 60%, then the battery is approaching to its end of life (EoL). Therefore, 70% SoH alerts the user to plan for the replacement of the battery or to take the remedial action (i.e. operating the battery at safe operating conditions).

Case 2: Partial Discharge

To verify the effectiveness of the proposed technique for the partial discharge, the same stress factors as used in the case of complete discharge is applied in this case. A 450 cycles aged battery with stress conditions of $35°C$ and 1C discharge rate is subjected for the SoH estimation. The proposed controller initiated the SoH routine, battery discharge process is terminated after battery SoC reaches to 66.3%. The calculated discharge capacity for 33.7% DoD is found to be 1.22Ah. Fig. 4.8 shows the discharge characteristics. Further, the controller calculated the normalized

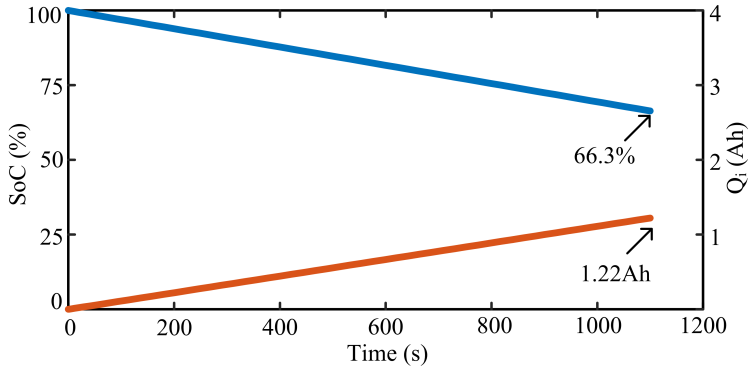

Figure 4.8: SoC and coulomb counting characteristics of a 450 cycles aged partially discharged battery

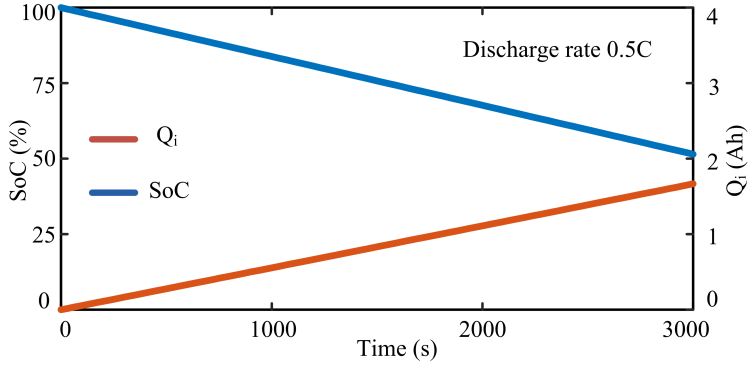

Figure 4.9: SoC and coulomb counting characteristics of a 1020 cycles aged partially discharged battery

usable capacity using equation 4.5 and estimated the SoH as 90.57%. Due to the bi directional converter used, the discharge current is having the ripple content of around 12%, but in the proposed technique average current is considered for the current integration process.

The test conditions of $40°C$, 0.5C & 50% DoD for a 1020 cycle elapsed battery as similar to the previous case is applied for the partial discharge test. The discharge characteristics of the battery for this test condition is shown in Fig. 4.9. From the Fig. 4.9, it is evident that the proposed SoH estimation controller has calculated the (Q_i) is 1.66Ah and the normalized usable capacity as 1.94Ah. Thus, the estimated SoH is 85.5%. For the same test conditions, the estimated SoH values for partial and complete discharge test conditions are almost same with the deviation of less than 1.5%.

SoH estimation during multiple discharge rates in a single discharge process is

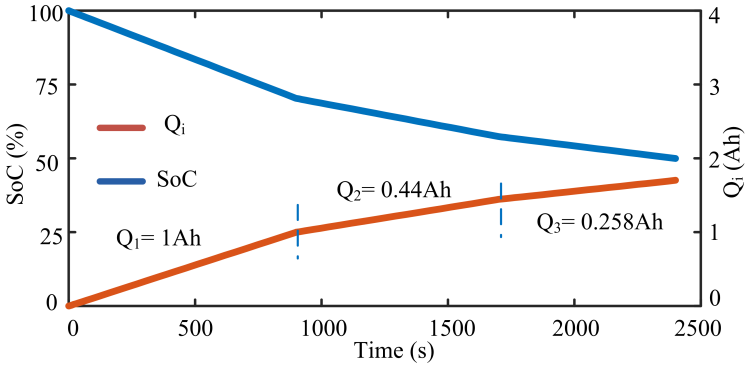

Figure 4.10: SoC and coulomb counting characteristics of a 1020 cycles aged battery discharged with multiple discharge rates with 50% DoD

tested with the 3 different discharge rates (i.e. 1C, 0.5C & 0.33C) for the test conditions of $40°C$, 0.5C & 50% DoD for the 1020 cycle elapsed battery. In this case, battery is first discharged with 1C discharge rate for 900 seconds, then the discharge rate is changed to 0.5C for the next 750 seconds and finally battery is discharged with 0.5C till the SoC reaches to 50% (i.e. DoD is 50%). In this case, the proposed controller initiated the timer for 3 times and calculated the discharge capacity in 3 discharge rate conditions (i.e. $Q_1 = 1Ah$, $Q_2 = 0.44Ah$ & $Q_3 = 0.25Ah$). Further, the normalized (Q_o) is calculated as 2.02Ah using battery data sheet and equation 4.5 and thus the SoH is found to be 84.05%, which is same as previous case. Therefore, from the results it is evident that the proposed technique estimates the SoH under variable DoD and variable discharge rate conditions effectively. Coulomb counting characteristics of multiple discharge rates is shown in Fig. 4.10.

The proposed modified coulomb counting based SoH estimation technique is experimentally validated using a prototype shown in Appendix C. The prototype consists of a half bridge bi-directional DC-DC converter, a LFP battery of 48V, 4.5Ah rating and digital signal processor (i.e. dSPACE 1104) is used. The experiment tests have been carried for two batteries of different ages. The experimental results of the proposed SoH estimation technique are shown in Figs. 4.11. Fig. 4.11(a) & (b) shows the coulomb counting and SoC characteristics of a battery is discharged with 1C & 0.5C discharge rate respectively for 200s duration. The proposed controller has calculated the SoH at end of discharge (i.e. at 100% DoD).However, in Fig. 4.11, only 200s characteristics are shown due to the oscilloscope constraints.

Fig. 4.11(c) shows the coulomb counting and SoC characteristics of a battery is

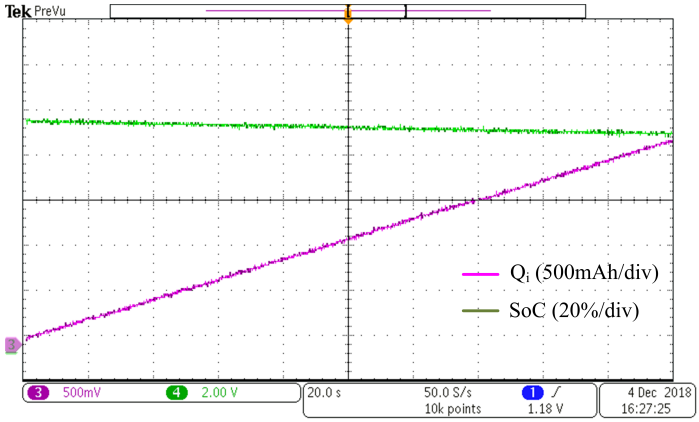

(a)

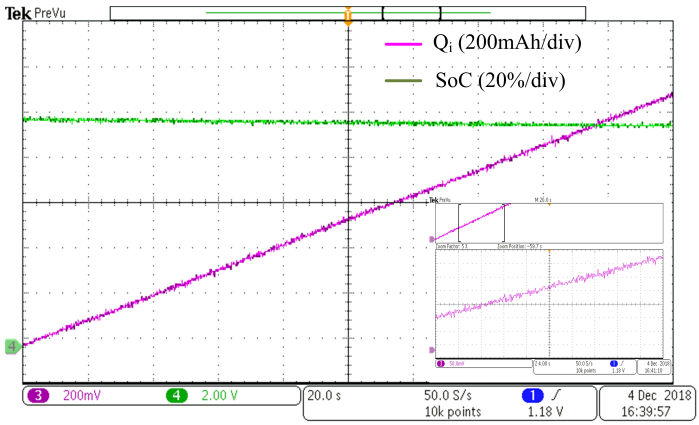

(b)

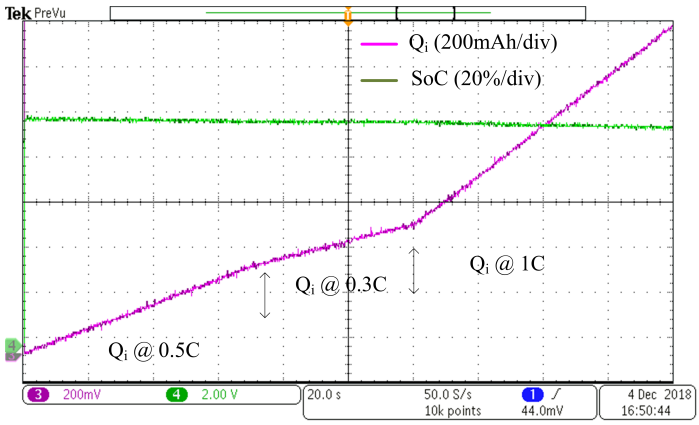

(c)

Figure 4.11: Experimental characteristics of SoC and coulomb counting technique for (a) Constant 1C discharge rate (b) Constant 0.5C discharge rate (c) multiple discharge rates in a single discharge process

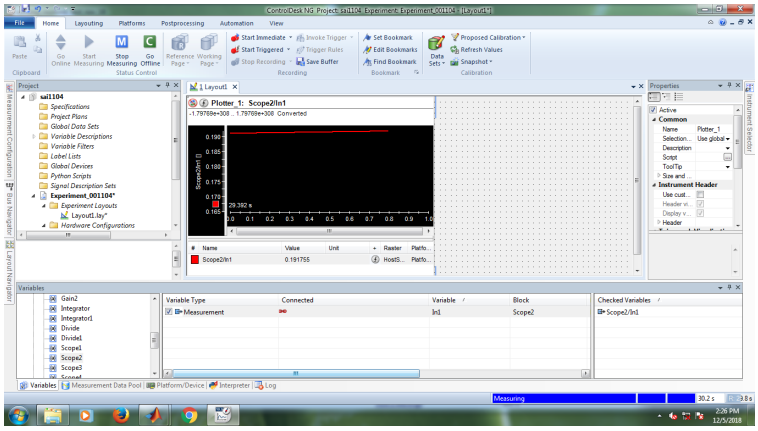

Figure 4.12: User interface system (i.e. dSPACE control desk) to display BMS parameters

discharged to 50% SoC with multiple discharge rates. The controller has calculated the (Q_i) in each discharge rate and calculated the normalized (Q_0) for SoH estimation. The estimated SoH is printed on user interface (i.e. dSPACE control desk) as shown in Fig. 4.12. From the simulation and experimental results it is clear that the proposed technique estimates the SoH of a LFP battery accurately even when the DoD and discharge rates are varying. Moreover, the proposed technique is an on-line technique and it is simple in implementation and requires less component count. The estimated SoH values at he end of every discharge cycle is printed on user interface (i.e., dSPACE control desk is used in this work) as shown in Fig. 4.12.

4.3 DEVELOPMENT OF DC RESISTANCE BASED STATE OF HEALTH ESTIMATION TECHNIQUE

As the battery ages, the DC resistance (i.e. R_{Ser} in Fig. 1.10) increases. The increase in the R_{Ser} has been modeled using the MATLAB curve fitting tool by considering the LFP cell cycle life test results presented in (Omar et al., 2014). The equation (4.7) describes the R_{Ser} evolution profile over the battery cycle number. The resistance growth model has been added to the electrical equivalent model of LFP cell shown in Fig. 1.10 in chapter 1.

$$R_{Ser} = -2.581 \times 10^{-12} \times N^3 + 8.998 \times 10^{-9} \times N^2 + 1.355 \times 10^{-6} \times N + 0.1007 \quad (4.7)$$

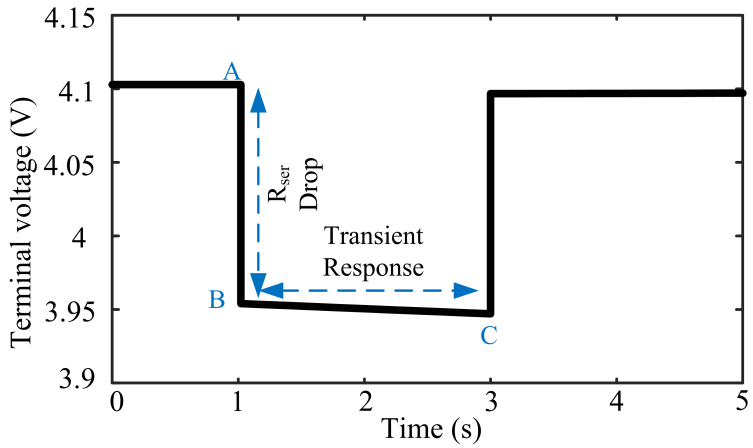

Figure 4.13: Terminal voltage characteristics of Li-Ion battery for short duration of pulse current

The DC resistance monitoring method is used to estimate the SoH of the battery at any cycle number without disturbing the ongoing charge/discharge process. This method applies a short duration current pulse to the battery as shown in Fig. 4.13. For this pulse current, terminal voltage (V_t) of the battery immediately drops from point A to B due to the DC resistance of the battery. Further, the battery terminal voltage drops from point B to C due to the transient impedance network (i.e., Z_S and Z_L in Fig. 1.10). The change in (V_t) increases as the battery gets age. Therefore, by observing the change in resistance in every charge/discharge cycle, SoH of the battery can be estimated using the equation (2.9).

Using equation (2.10) resistance of the battery at i^{th} cycle (i.e. R_i) can be calculated and R_{EoL} can be found from the resistance evolution model of the battery. Using equation (2.10) resistance of the battery at i^{th} cycle (i.e. R_i) can be calculated by applying the current pulse and R_{EoL} can be found from the resistance evolution model of the battery. In (Omar et al., 2014), authors have considered R_{EoL} as 80% of R_{New}.

Fig.4.14 shows the flowchart of the proposed DC resistance method, and this method has been implemented when the battery SoC is 100% and the battery is in discharging mode. The proposed SoH estimation technique is developed using MATLAB/Simulink for a 4Ah Li-Ion battery. In this study, 1C discharge pulse for the duration of 5s is used to evaluate the DC resistance. The controller measured the variation in terminal voltage before and after applying the pulse discharge. Further,

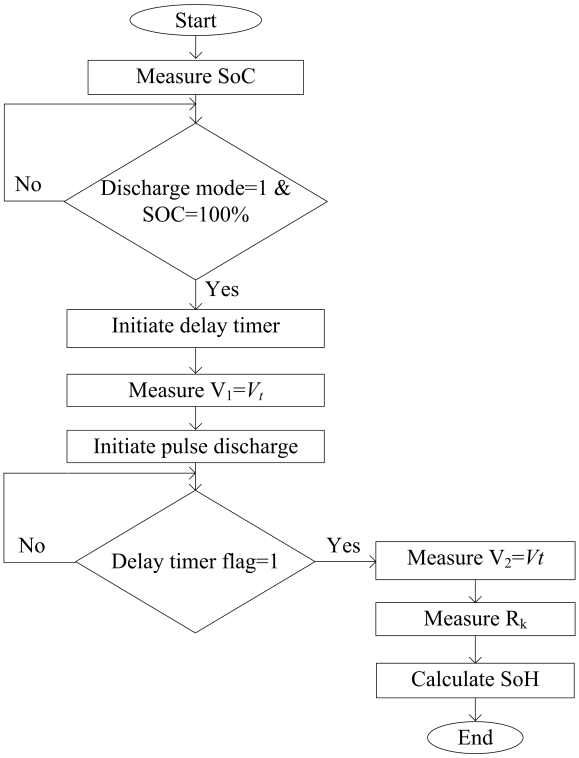

Figure 4.14: Flowchart for the SoH estimation using DC resistance method

the controller calculates the R_i of the battery using the equation 2.11, after measuring the resistance, SoH of the battery at i^{th} discharge cycle will be calculated using equation 2.10.

4.3.1 RESULTS AND DISCUSSION

The proposed technique is validated in MATLAB/Simulink environment by giving a 1C pulse current. When the battery SoC is 100% SoC and it is in discharging mode, switch SB1 in Fig. 2.8 is turned ON for 5seconds to measure the variation in terminal voltage. The variation in terminal voltage for short duration pulse discharge at different cycle number is shown in Fig.4.15. From Fig. 4.15 it is clear that as the battery ages, resistance of the battery increases, as a result the terminal voltage profile deforms. The calculated DC resistance and SoH using the proposed technique for the modeled battery at different cycle numbers is listed in Table. 4.1.

For validating the proposed SoH technique experimentally, the same experimental setup in previous section (4.2) is used. The test results of pulse discharge are shown

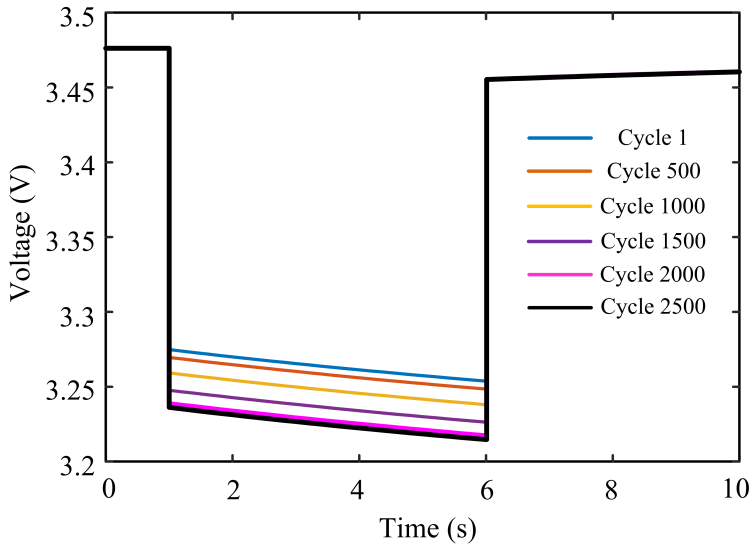

Figure 4.15: Voltage profile of Li-Ion battery for pulse discharge current when the battery is at different cycle numbers

Table 4.1: DC resistance and SoH of a LFP battery at different cycle numbers

Cycle No.	ΔV	$R_i(m\Omega)$	**SoH (%)**
1	0.2221	55.525	100
500	0.2273	56.825	97.07
1000	0.2381	59.525	90.99
1500	0.2499	62.475	84.35
2000	0.2589	64.725	79.28
2500	0.2615	65.375	77.82

in Fig. 4.16. The test results describes the terminal voltage variation of two Li-Ion batteries at different ages for the pulse discharge current. From the test results, it is clear that a fresh battery has 360mV (i.e., ref Fig. 4.16(a)) variation in V_t for the pulse discharge current, whereas, a few cycles aged battery has 420mV variation in V_t for the same pulse discharge current (ref Fig. 4.16(b)). Therefore, the proposed method accurately identifies the changes in the terminal voltage due to aging of the battery, and estimates the SoH. The implementation cost of the proposed SoH estimation technique is insignificant, since it does not require any additional circuitry and to implement the pulse discharge for estimating the R_i, the proposed technique uses the same bi-directional converter used for charge/discharge process. Therefore, a simple

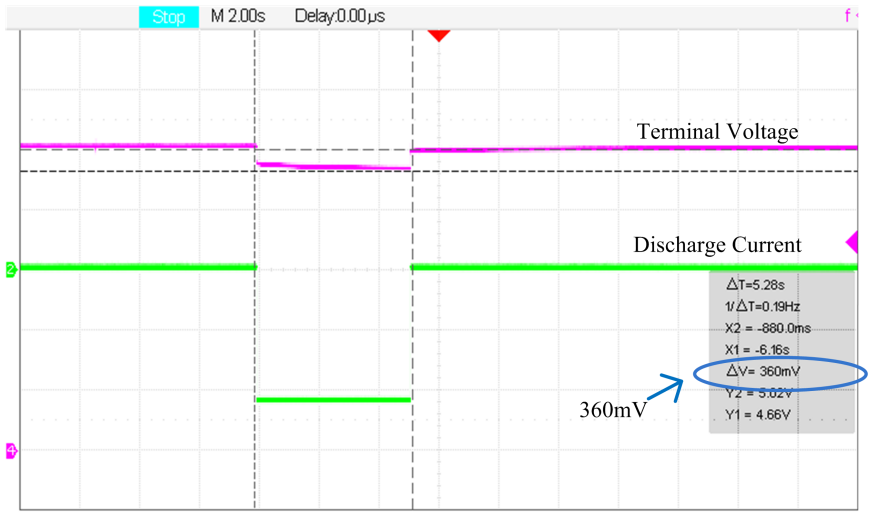

(a)

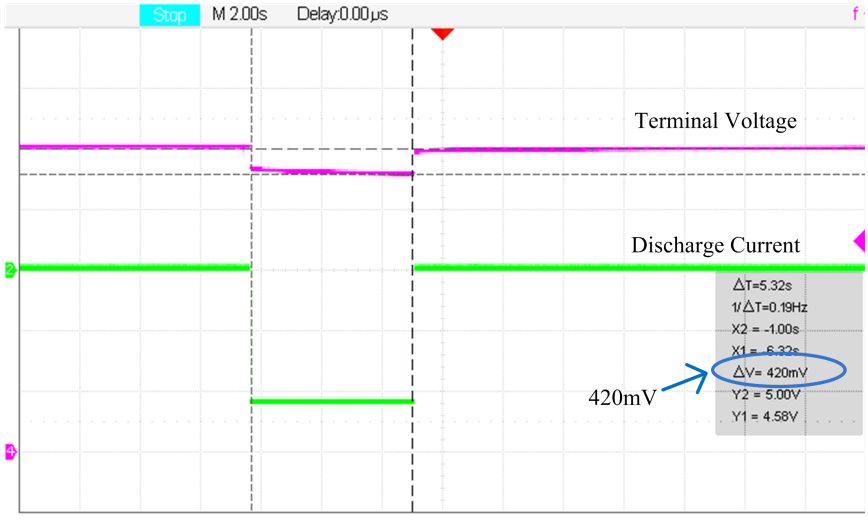

(b)

Figure 4.16: Terminal voltage variation of (a) fresh LFP batery (b) few cycles aged battery for pulse discharge current

and low cost micro controller is sufficient to implement the proposed method.

Comparison of the two proposed SoH estimation techniques (i.e., Coulomb counting based and DC Resistance based techniques) has not been done in this work, since the resistance growth data set used for developing the DC resistance based SoH technique, and the capacity degradation model data set used for developing coulomb counting technique are taken from two different LFP cells tested at different conditions.

4.4 SUMMARY

For enhancing the useful life of Li-Ion (i.e. LFP) battery, two on-line state of health estimation (SoH) techniques have been developed. The proposed techniques estimates the SoH of a battery without disturbing the ongoing charge/discharge process. The first SoH estimation technique modifies the coulomb counting method to calculate the discharge capacity of the battery and thereby estimates the SoH. This method requires the continuous monitoring of battery discharge current and state of charge (SoC) and it estimates the SoH at the end of any discharge process. The second proposed SoH technique estimates the SoH by measuring the battery DC resistance. This method applies short duration discharge current pulses to measure the battery DC resistance. Thus, by comparing the measured DC resistance at i^{th} cycle with the resistance of the battery when it was new gives the information of battery health index. The proposed SoH estimation methods have been simulated in MATLAB/Simulink environment and tested under various stress conditions of the battery. Moreover, the two proposed techniques have been validated experimentally using the two LFP batteries of different ages. From the simulation and experimental results, it is observed that the proposed techniques estimates the SoH of Li-Ion battery accurately.

Chapter 5

DEVELOPMENT OF VOLTAGE REGULATION TECHNIQUE FOR TELECOM LOAD

Contents

5.1 GENERAL

The DC loads of telecom station (i.e., transceivers) operates in pulsed power mode, and also the power consumption of these loads depends on signal traffic. (Liu et al., 2005) have modeled the transceivers in BTS station operates in a pulsed-power mode intermittently also the power BTS load profile based on the assumptions that the transceiver operates for 200s out of every 250s. During the on state condition, load draws the high amount of power for 10s and for the next 10s it draws low power as shown in Fig. 5.1. The DC loads in BTS stations requires the constant DC voltage (i.e., 48V or 24V) (Energy, 2012). However, due to pulsed power consumption of DC loads voltage will have fluctuations. Therefore, for safe operation voltage across DC

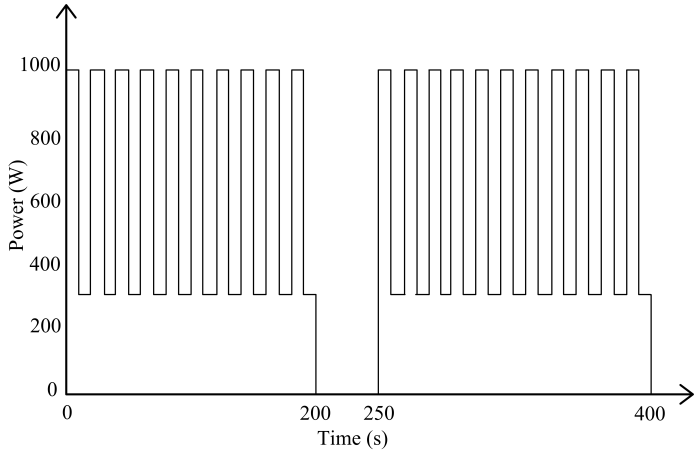

Figure 5.1: Load profile of Telecom Tower

loads has to be maintained constant. Therefore, in this chapter a Type II compensator is designed to regulate the voltage at the terminals of DC loads.

5.2 TYPE II COMPENSATOR DESIGN

Type II compensators are popularly being used in controlling the output voltage of switching power electronic converters. Type II compensator has two poles and one zero, which provides the required phase and gain to the total control loop of the switching converter. In this research work, to step down the voltage to 48V from DC link voltage of 220V, a buck converter is used (ref. Fig. 2.8 in Chapter 2). In general, it is significant to have adequate phase margin and gain margin to work the control loop properly in all conditions. The schematic of the Type II compensator is shown in Fig. 5.2.

To implement the Type II compensator to the buck converter, it is required to have the control to output voltage transfer function considering the parasitic elements of energy storage components of the buck converter. Equivalent series resistance (ESR) of the output capacitor in buck converter is a very critical parameter, since it introduces a zero in the converter transfer function. The buck converter control to output voltage transfer function is given in equation (5.1). From the control point of view, it is important to derive the transfer function of all the blocks shown in Fig. 5.3. The transfer function of Type II compensator is derived from the Fig. 5.2 and it is given in equation (5.2). The transfer function of PWM is generally described as

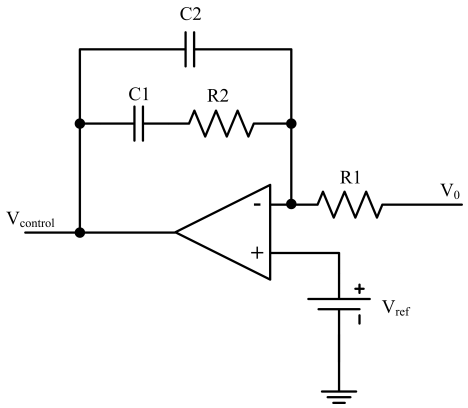

Figure 5.2: Schematic of the Type II compensator

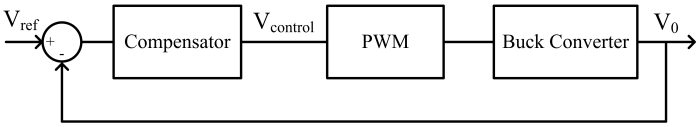

Figure 5.3: Complete control diagram of a buck converter with the Type II compensator

$\frac{1}{V_{PWM}}$, where V_{PWM} is the peak to peak voltage of the carrier wave used.

$$\frac{V_0}{d}(s) = \frac{V_{dc\_link} R_{load}(s(C_0 \times ESR) + 1)}{L_0 C_0 s^2 (R_{Load} + ESR) + s(L_0 + R_{Load} \times C_0 \times ESR) + R_{Load}} \tag{5.1}$$

$$\frac{V_{control}}{V_0}(s) = -\frac{s + \frac{1}{R_2 C_2}}{R_1 C_2 s(s + \frac{1}{R_2 C_2})} \tag{5.2}$$

$$\frac{V_0}{d}(s) = \frac{1056 + 0.0696s}{5.745 \times 10^{-7} s^2 + 8.768 \times 10^{-4} s + 4.8} \times \frac{1}{6.6} \tag{5.3}$$

To design the compensator with required loop characteristics, it is required to evaluate the Bode plot of the open loop system (i.e., Buck converter with PWM). Buck converter parameters considered for deriving the open loop transfer function is listed in Table. 5.1. The open loop transfer function of buck converter with PWM voltage is given in equation (5.3) and the bode plot for the same is shown in Fig. 5.4. The rest of the design steps are explained as follows,

Step 1:

Selecting the crossover frequency (F_0) plays an important role in any compensator design. For the desired loop characteristics, typically (F_0) is selected to be in the range of 10% to 20% of switching frequency (F_s). Moreover, selecting the higher (F_0) results

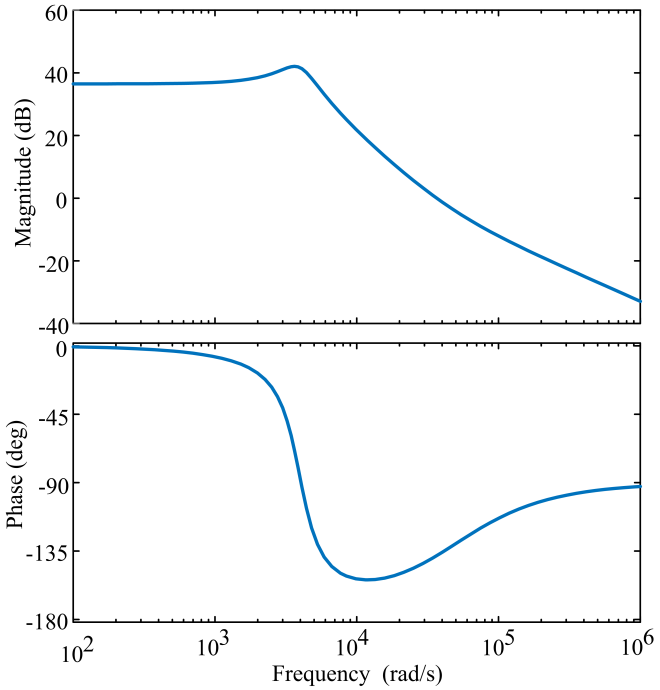

Figure 5.4: Bode diagram of open loop buck regulator

in the faster dynamic response during the load change. Therefore, in this study, (F_0) is selected as 7.2kHz.

Step 2:

Determine the phase and gain of the open loop transfer function at the selected crossover frequency using the bode plot shown in Fig. 5.4. The gain and phase values of open loop buck converter with PWM at (F_0) is found to be $-2.98dB$ and $-133°$.

Step 3:

Determining the ratio of R2/R1 of compensator (ref. Fig. (5.2)) using the calculated gain value in the previous step as follows (Hart, 2011),

$$\frac{R2}{R1} = 10^{\frac{Gain@F_0}{20}} \tag{5.4}$$

Step 4:

From the calculated phase at crossover frequency from bode plot of open loop transfer function, determine the required poles and zeros of compensator to provide required phase margin using the K factor technique as follows (Basso, 2008),

$$\theta_{compensator} = \theta_{phasemargin} - \theta_{@F_0} \tag{5.5}$$

where, $\theta_{phasemargin}$ is the required phase margin of the closed loop system, which is selected to be 45° and θ_{F_0} is found to be $-133°$.

From equation (5.5), K factor is calculated as follows,

$$K = tan\left(\frac{\theta_{compensator}}{2}\right) \tag{5.6}$$

The feedback capacitors of compensator is calculated using the K value as follows,

$$C1 = \frac{K}{2\pi F_0 R2} \tag{5.7}$$

$$C2 = \frac{1}{2\pi F_0 K R2} \tag{5.8}$$

From the design equations, the value of compensator elements are found to be R1=10kΩ, R2=7.09kΩ, C1=175nF and C2=53pF. From the calculated values, transfer function of compensator is expressed as follows,

$$G(s)_{compensator} = \frac{-(s + 805.28)}{5.3 \times 10^{-7}s^2 + 1.409s} \tag{5.9}$$

From the equations (5.3) & (5.9), loop transfer function is calculated and the bode characteristics of loop transfer function is plotted and shown in Fig. 5.5. From the loop characteristics, it is clear that the phase of the loop is around 45.5° at the crossover frequency. Moreover, gain of the loop is crossing the 0dB at the low frequency (i.e., less than F_s). Therefore, this ensures the stability of the overall closed loop system. Voltage regulation for the variation in DC link voltage and load is discussed in the following section.

Table 5.1: Parameters Used for Type II Compensator Design

Parameter	**Value**
PWM oscillator peak voltage	6.6V
Buck regulator filter capacitor ESR	0.5Ω
Inductor (L) and Capacitor (C) value of buck regulator	100μH & 100μF

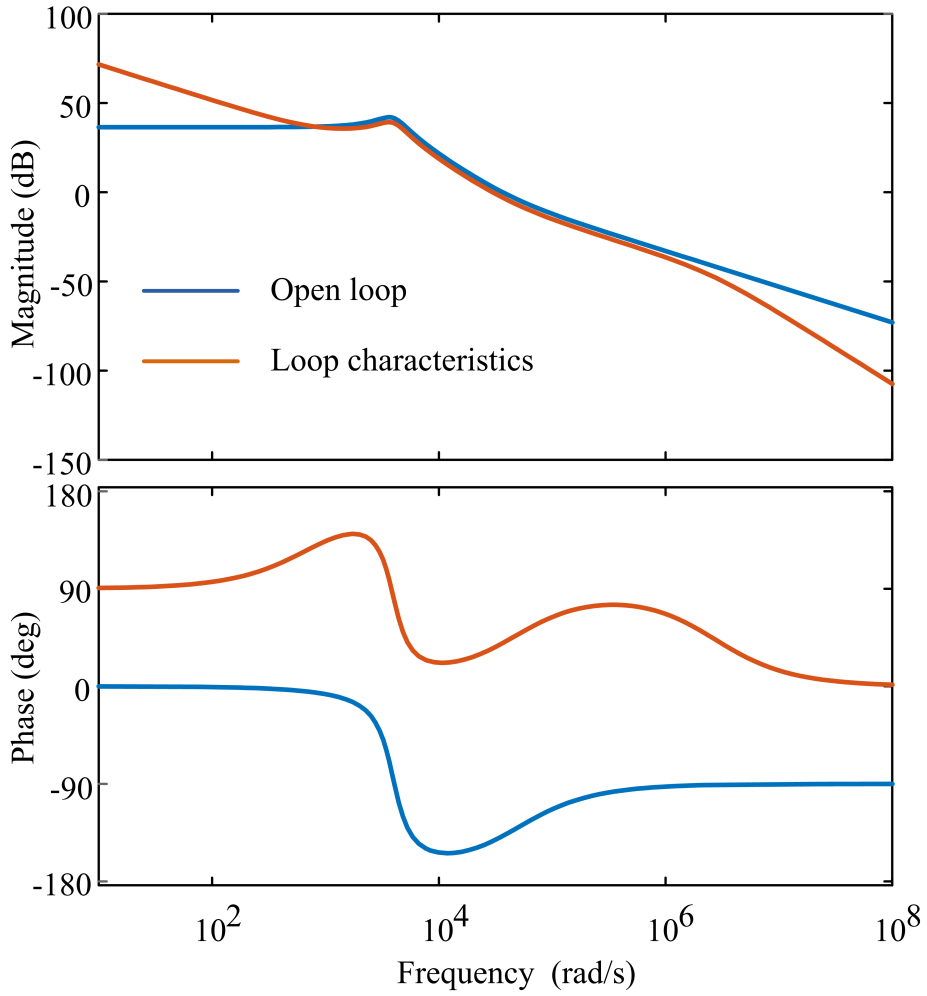

Figure 5.5: Bode diagram of loop characteristics and open loop characteristics of buck regulator

5.2.1 RESULTS AND DISCUSSION

The developed Type II compensator for buck regulator at the DC loads of BTS is tested for 50% load change condition i.e., BTS draws the load current of 20A for the duration of 3s and for the next 3s it draws 10A. Load current and load voltage characteristics for this case is shown in Fig. 5.6. From the load regulation characteristics, it is evident that, response time of the compensator is very fast and it has a settling time of less than 5ms which is shown in Fig. 5.6(b). Therefore, for the pulsed power operation of BTS, the designed compensator regulates the load voltage effectively.

The designed compensator is tested for the input voltage (i.e., DC link voltage) variation. The voltage regulation characteristics using the designed compensator is shown in the Fig. 5.7. In Fig. 5.7, at two instants DC link voltage is varied manually for the testing purpose. Initially, the DC link voltage was 220V, after 3s (i.e., at instant 1), the voltage is dropped to 200V and after 6s (i.e., at instant 2), the voltage again dropped to 180V. At both the instants the developed compensator maintained the output voltage constant at 48V. Generally, the DC link voltage does not vary, however, for testing the designed compensator change in DC link voltage is considered. From the test results shown, it is clear that closed loop system is always stable for load and input voltage variations and response time of compensator is very fast.

5.3 SUMMARY

In this chapter, a type II compensator is designed and developed to regulate the voltage at the DC loads of BTS. To design the compensator with required loop characteristics, buck converter transfer function is derived and frequency response is plotted. To design the compensator parameters, K factor method is used. Moreover, for the fast response time, higher F_0 is selected to design the compensator. The designed closed loop system is tested for the 50% load variation and 10% dc link voltage variation. From the results, it is clear that the system is always stable and the response time is around 5ms, which is less than the typical BTS load variation time. The designed compensator is tested in MATLAB/Simulink platform.

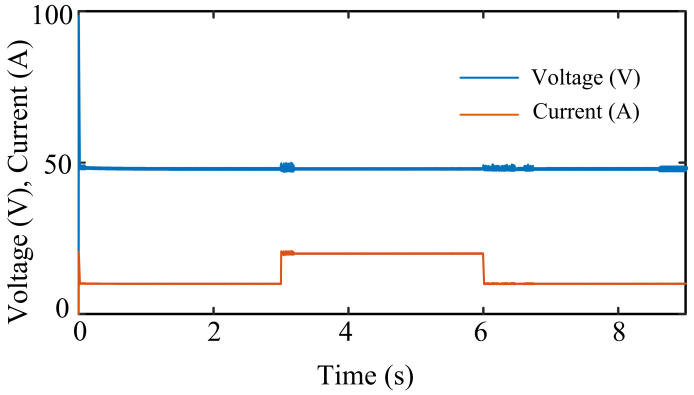

(a)

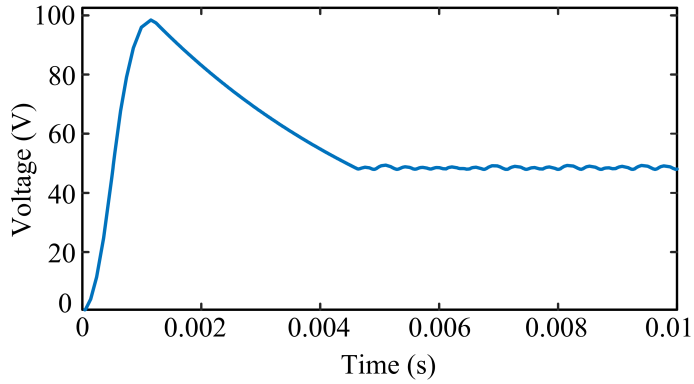

(b)

Figure 5.6: (a) Load voltage characteristics during change in load current (b) Initial response and settling time characteristics of designed compensator

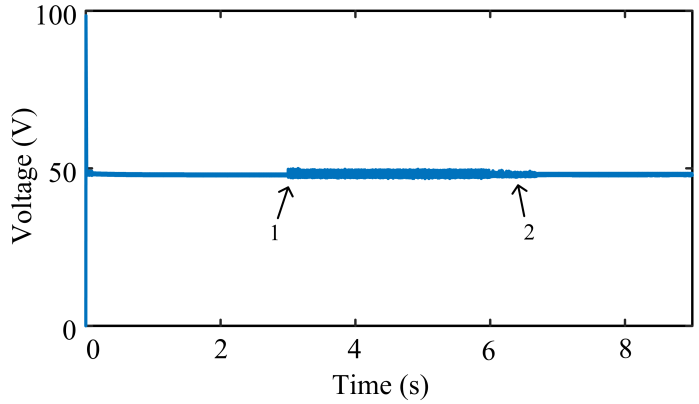

Figure 5.7: Load voltage regulation characteristics for change in DC link voltage

Chapter 6

MAIN CONCLUSIONS AND FUTURE SCOPE

For the effective utilization of PV and Battery sources in PV-battery based hybrid power supply system, two different global maximum power point tracking techniques are developed to increase the efficiency of PV system during non-uniform insolation conditions. Furthermore, in this thesis, battery aging mechanism is discussed and two different on-line SoH estimation techniques are developed. The contributions, main conclusive remarks and the future works of this thesis are presented below.

6.1 CONTRIBUTIONS

6.1.1 MAJOR CONTRIBUTIONS

- Proposed a single current sensor based two stage scanning based GMPPT technique to track the GMPP with the minimum tracking time.

- Proposed a single current sensor based hybrid GMPPT algorithm to track the GMPP in all non-uniform insolation conditions.

- Modified coulomb counting based SoH estimation technique of Li-Ion battery is proposed to estimate SoH during variable depth of discharge and discharge rate conditions.

6.1.2 MINOR CONTRIBUTIONS

- Proposed a DC resistance based SoH estimation technique of Li-Ion battery.
- Designed a Type II compensator with fast response time characteristics to regulate DC loads of BTS.

6.2 MAIN CONCLUSIONS

In this thesis several conclusions has been made. Main conclusions of the thesis are summarized as follows,

- During non-uniform insolation conditions, $P\ Vs.\ V$ curve paterns has been classified into three categories based on scanning the $I_{dc\_link}\ vs.\ D$ curve at selective places.
- Scanning the $I_{dc\_link}\ vs.\ D$ curve results in scanning the $P\ Vs.\ V$ curve of a PV array. Moreover, scanning $I_{dc\_link}\ vs.\ D$ curve reduces the number of measurement units required for GMPP tracking.
- The first proposed GMPPT technique operates in two stages. In stage one, it scans $I_{dc\_link}\ vs.\ D$ curve at selective places to locate the vicinity of GMPP. In stage two, hill climbing algorithm is implemented to track the GMPP. This technique has been tested for 4 series connected PV modules and minimum tracking time is found to be 4s. The GMPP tracking time of this method increases with increase in number of series connected modules.
- The second proposed GMPPT technique combines ABC optimization technique with hill climbing algorithm. In this technique, based on the type of shading pattern either ABC or HC algorithm is used to track he GMPP. Tracking time of this technique is more than two stage scanning based technique. however, its tracking time does not vary with increase in series connected PV modules.
- As the battery ages, usable capacity of the battery deteriorates, impedance and DC resistance of the battery increases. Therefore, by monitoring the change in this parameters results in SoH estimation.

- In the first SoH estimation technique, conventional coulomb counting technique is suitably tailored to estimate SoH during variable DoD and discharge rate conditions. This technique estimates SoH accurately at the end of any discharge level.

- In the second SoH estimation technique, a short duration 1C discharge pulse has been given to the battery to monitor the change in terminal voltage, thereby to calculate the DC resistance. Both the SoH estimation techniques are validated using the experimental prototype and the results are found satisfactory.

- To design the Type II compensator K factor method is used. Moreover, for the faster response of the closed loop, higher F_o is selected to design compensator. The developed compensator is tested in MATLAB/Simulink platform for different load and input voltage variation conditions and the results show that the system is always stable and having a fast response time.

6.3 FUTURE SCOPE

Based on the research carried out in this thesis, the recommendations for future research are presented.

1. The proposed GMPPT techniques uses single current sensor for the GMPP tracking. However, cost of current sensor is higher than voltage sensor. Therefore, the research can be extend in the direction of using single voltage sensor for GMPP tracking.

2. In the present study ABC colony optimization technique is explored for tracking the GMPP tracking, however, other optimization technique such as Tabu search, multi-swarm optimization, social cognitive optimization, etc... can be tested for improved tracking performance.

3. The research on SoH estimation can be extended using state observer methods and it can be compared with the benchmark EIS test results. Moreover, for the SoC estimation coulomb counting method is used in the thesis, however, other techniques such as EKF and SVM can be tested for better accuracy.

4. For the DC voltage regulation, Type II compensator is developed and tested in MATLAB/Simulink, however, it can be implemented experimentally to make the complete product (i.e. GMPPT stage, Battery stage and DC regulation stage). Moreover, other voltage controlled techniques such as sliding mode control, H-infinite control, etc... can be tested for voltage regulation.

Appendix A

For the seamless power supply to the BTS load, it is necessary to size the PV and battery optimally. Therefore, in this section, detailed sizing of PV and Battery are discussed. For designing the capacity of PV modules, monthly average equivalent hours of full sun (EHFS) data of Bangalore city is considered and which is listed in Table 1. The capacity of the PV panel is calculated as follows,

$$PV_{capacity} = \frac{P_L \times N}{\eta_{batt} \times \eta_{converter} \times (1 - f_{dust}) \times (1 - f_{temp}) \times EHFS} \tag{1}$$

where, P_L is the peak load on PV (i.e., Battery and telecom load), N is the average hours of solar availability, f_{temp} & f_{dust} is the loss due to temperature and dust on PV modules respectively, η_{batt} is the efficiency of the battery and $\eta_{converter}$ is the product of efficiencies of power electronic converters in complete system.

Table 1: Monthly average solar insolaion of Bangalore city

Month	**EHFS**	**Month**	**EHFS**
Jan	5.36	Jul	4.50
Feb	6.06	Aug	4.47
Mar	6.56	Sep	5.03
Apr	6.38	Oct	4.63
May	6.03	Nov	4.50
Jun	4.84	Dec	4.74
	Avg. EHFS		5.25

Generally, for calculating the PV panel capacity, average minimum insolation of the month in a year i.e., $4.47kW - hr/m^2$ or minimum EHFS of a month recorded

in last 20 years i.e., $3.5kW - hr/m^2$ are considered. However, in this configuration, there are no other power sources, hence PV has to be rated for the lower insolation levels. Therefore, minimum insolation day of a year i.e., $2.0kW - hr/m^2$ is considered for the PV sizing.

For sizing the battery average DoD is considered as 80% and to maintain the required capacity even after the end of battery life, K_{EoL} factor (i.e., 80%) is considered. Since the capacity of PV panel is sized for minimum insolation level in a day, autonomy days for battery design is not considered. The equation to calculate the size of the battery is expressed in equation (2).

$$Battery_{capacity} = \frac{P_{L\_batt} \times T}{\eta_{batt} \times DoD \times V_{batt} \times K_{EoL}} \tag{2}$$

where, V_{batt} is the nominal voltage of the battery, T is the number of backup hours, K_{EoL} is the factor related to end of life and P_L_batt is the load on battery (i.e., only telecom load).

Table 2: Size of PV panel required for different solar insolations

Solar Insolation	**PV Panel Size**
2.0 kW-hr/m^2	10.5 kW_p
4.47 kW-hr/m^2	5.74 kW_p
$3.5kW - hr/m^2$	4.5 kW_p

Both conventional and optimally sized systems are compared in terms of excess energy produced. To calculate the excess energy produced by the PV and Battery system, average insolation levels given in Table. 1 is used and the expression to calculate the excess energy is given in equation 3.

$$ExcessEnergy = E_{PV} - E_{Load} - E_{Battery_charging} \tag{3}$$

Expression to calculate the energy produced by PV in a month is given in equation 4.

$$E_{PV} = \frac{PV_{capacity} \times EHFS \times (1 - f_{temp}) \times (1 - f_{dust}) \times 30}{1000} \tag{4}$$

For calculating the excess energy produced by PV, average energy required by the

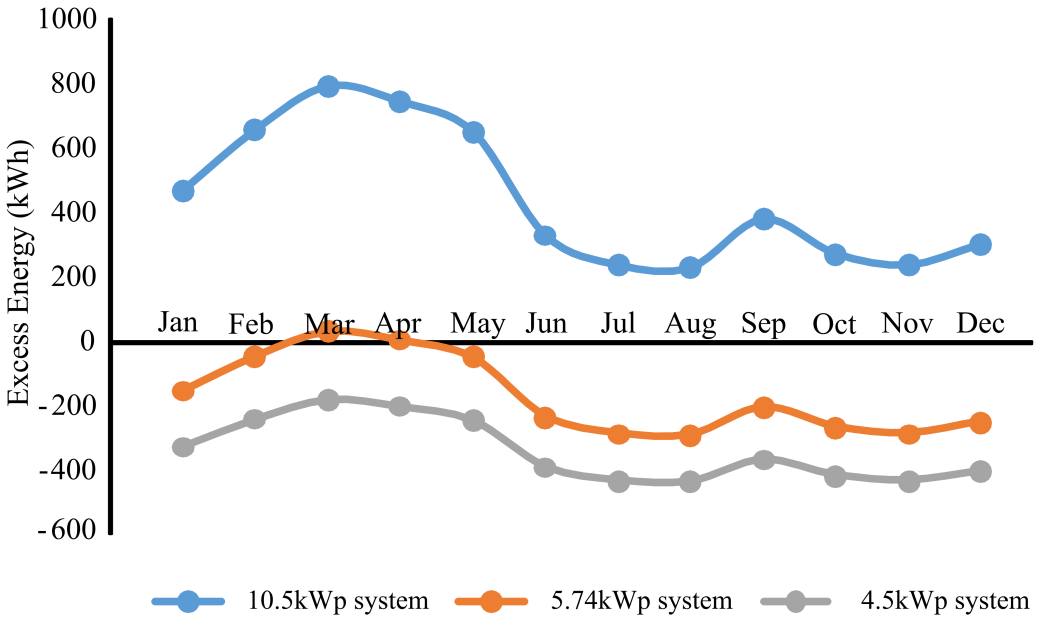

Figure 1: Excess Energy produced by different PV systems

telecom load during sunshine hours and also, energy consumed by the battery during charging from PV is considered. Monthly excess energy produced by all the three systems are shown in Fig. 1. from the Fig 1. , it is observed that, $10.5kW_p$ system can produce adequate energy even during cloudy months. Therefore, this ensures the continuous power supply to the load.

Appendix B

In this section description of experimental setup used for validating the proposed GMPPT technique is presented. The experimental prototype formed by a DC-DC boost converter, a battery bank of 7.5Ah 240V (Assumed to be constant DC link voltage), dSPACE MicroLab Box 1202 and a PV array simulator. The specifications of the DSP used is listed in Table 3. Since the V_{mpp} varies widely under PSC, the converter is developed for large PV voltage variations. Moreover, it works in continuous conduction mode (CCM) with the switching frequency of 10kHz. For measuring the I_{dc_link}, an accurate Hall Effect based sensor (LA-25P) is used. An opto-coupler (6N136) is used to provide isolation between the DSP and switch gate driver. The value of inductor and capacitor is used for boost converter is 1mH and 940μF. A 4s1p configured PV array (V_{oc_module} = 50V and I_{sc_module} = 5A) is emulated using PV array simulator. Fig. 2 shows the experimental prototype used for validating the proposed GMPPT techniques.

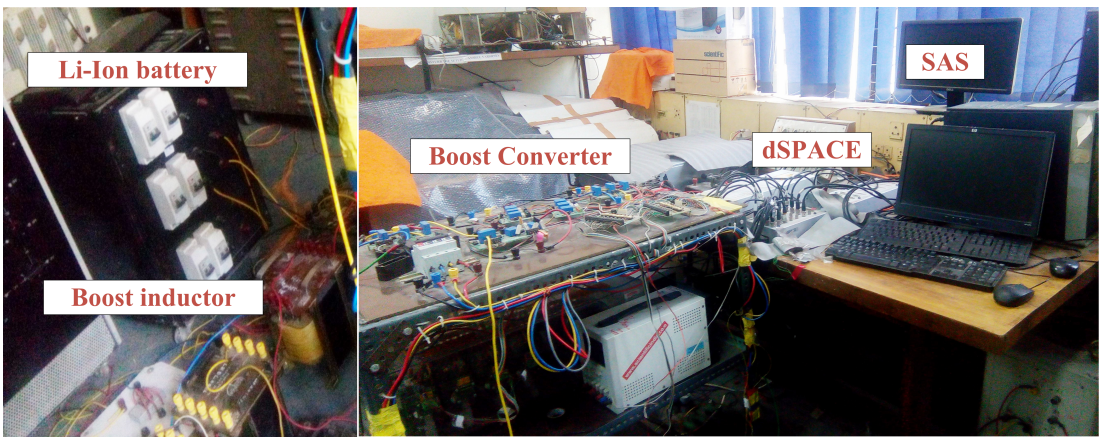

Figure 2: Experimental Setup Used for Validating the Proposed GMPPT Techniques

Table 3: Specifications of the dSPACE MicroLab Box 1202

Parameter	**Value**
Analog input	8 14bit and 24 16 bit channels
Analog input sampling rate	10Msps
Analog output	16 16bit channels
Digial I/O	48 channels
PWM Resolution	10ns
Input voltage range	-10 to 10V
Communication channels	USB 2.0, 2 CAN & 2 UART channels
Memory	128MB Flash

Appendix C

In this section description of experimental setup used for validating the proposed GMPPT technique is presented. A 1kW rating half bridge bi-directional converter is developed to charge and discharge the battery. Moreover, the converter is developed to operate in CCM mode for all the variations in battery voltage (i.e., from full charge to complete discharge). Two LFP batteries (48V and 4.5Ah) of different ages has been used to validate the estimated SoH. To implement the proposed SoH algorithms, a digital signal processor (i.e. dSPACE MicroLab Box 1202) is used. For measuring the battery charge and discharge currents, Hall Effect based sensor (LA-25P) configured to work for 5A is used. For measuring the voltage of the battery, voltage divider network is used. An opto-coupler (6N136) is used to provide isolation between the DSP and switch gate driver. The value of inductor and capacitor is used for bi-directional converter is 560μH and 940μF.

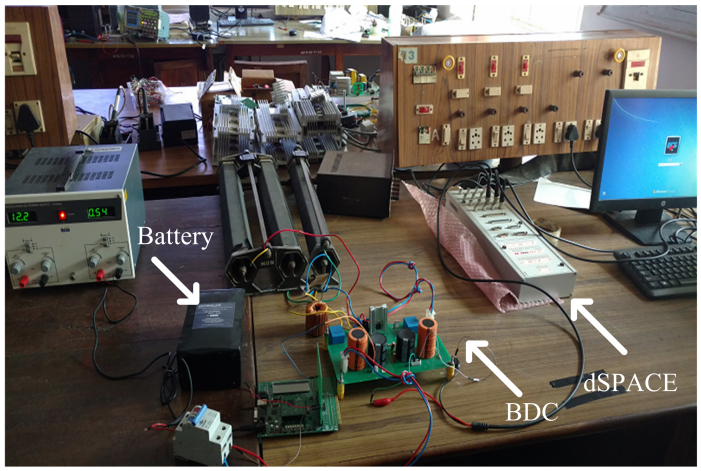

Figure 3: Experimental Setup Used for Validating the Proposed SoH Estimation Techniques

Bibliography

Abraham, D., Knuth, J., Dees, D., Bloom, I., and Christophersen, J. (2007). Performance degradation of high-power lithium-ion cellselectrochemistry of harvested electrodes. *Journal of Power Sources*, 170(2):465–475.

Ahmed, N. A. and Miyatake, M. (2008). A novel maximum power point tracking for photovoltaic applications under partially shaded insolation conditions. *Electric Power Systems Research*, 78(5):777–784.

Ajan, C. W., Ahmed, S. S., Ahmad, H. B., Taha, F., and Zin, A. A. B. M. (2003). On the policy of photovoltaic and diesel generation mix for an off-grid site: East malaysian perspectives. *Solar Energy*, 74(6):453–467.

Andre, D., Nuhic, A., Soczka-Guth, T., and Sauer, D. U. (2013). Comparative study of a structured neural network and an extended kalman filter for state of health determination of lithium-ion batteries in hybrid electricvehicles. *Engineering Applications of Artificial Intelligence*, 26(3):951–961.

Armstrong, S. and Hurley, W. (2010). A thermal model for photovoltaic panels under varying atmospheric conditions. *Applied Thermal Engineering*, 30(11-12):1488–1495.

Basso, C. (2008). *Switch-mode power supplies spice simulations and practical designs*. McGraw-Hill, Inc.

Berecibar, M., Gandiaga, I., Villarreal, I., Omar, N., Van Mierlo, J., and Van den Bossche, P. (2016a). Critical review of state of health estimation methods of li-ion batteries for real applications. *Renewable and Sustainable Energy Reviews*, 56:572–587.

Berecibar, M., Garmendia, M., Gandiaga, I., Crego, J., and Villarreal, I. (2016b). State of health estimation algorithm of lifepo4 battery packs based on differential voltage curves for battery management system application. *Energy*, 103:784–796.

Bifaretti, S., Iacovone, V., Cinà, L., and Buffone, E. (2012). Global mppt method for partially shaded photovoltaic modules. In *Energy Conversion Congress and Exposition (ECCE), 2012 IEEE*, pages 4768–4775. IEEE.

Bohlen, O. (2008). *Impedance-based battery monitoring*. Shaker.

Bounechba, H., Bouzid, A., Nabti, K., and Benalla, H. (2014). Comparison of perturb & observe and fuzzy logic in maximum power point tracker for pv systems. *Energy Procedia*, 50:677–684.

Boztepe, M., Guinjoan, F., Velasco-Quesada, G., Silvestre, S., Chouder, A., and Karatepe, E. (2014). Global mppt scheme for photovoltaic string inverters based on restricted voltage window search algorithm. *IEEE Transactions on Industrial Electronics*, 61(7):3302–3312.

Bueschel, P., Troeltzsch, U., and Kanoun, O. (2011). Use of stochastic methods for robust parameter extraction from impedance spectra. *Electrochimica Acta*, 56(23):8069–8077.

Chen, K., Tian, S., Cheng, Y., and Bai, L. (2014). An improved mppt controller for photovoltaic system under partial shading condition. *IEEE transactions on sustainable energy*, 5(3):978–985.

Chen, Z., Mi, C. C., Fu, Y., Xu, J., and Gong, X. (2013). Online battery state of health estimation based on genetic algorithm for electric and hybrid vehicle applications. *Journal of Power Sources*, 240:184–192.

Christophersen, J. P., Glenn, D. F., Motloch, C. G., Wright, R. B., Ho, C. D., and Battaglia, V. S. (2002). Electrochemical impedance spectroscopy testing on the advanced technology development program lithium-ion cells. In *Vehicular Technology Conference, 2002. Proceedings. VTC 2002-Fall. 2002 IEEE 56th*, volume 3, pages 1851–1855. IEEE.

de Vries, H., Nguyen, T. T., and het Veld, B. O. (2015). Increasing the cycle life of lithium ion cells by partial state of charge cycling. *Microelectronics Reliability*, 55(11):2247–2253.

El-Helw, H. M., Magdy, A., and Marei, M. I. (2017). A hybrid maximum power point tracking technique for partially shaded photovoltaic arrays. *IEEE access*, 5:11900–11908.

Energy, I. (2012). The true cost of providing energy to telecom towers in india. *White Paper*.

Enrique, J., Andújar, J., and Bohorquez, M. (2010). A reliable, fast and low cost maximum power point tracker for photovoltaic applications. *Solar Energy*, 84(1):79–89.

Escobar, G., Ho, C., and Pettersson, S. (2012). Maximum power point searching method for partial shaded pv strings. In *IECON 2012-38th Annual Conference on IEEE Industrial Electronics Society*, pages 5726–5731. IEEE.

Fathy, A. (2015). Reliable and efficient approach for mitigating the shading effect on photovoltaic module based on modified artificial bee colony algorithm. *Renewable Energy*, 81:78–88.

Feng, X., Li, J., Ouyang, M., Lu, L., Li, J., and He, X. (2013). Using probability density function to evaluate the state of health of lithium-ion batteries. *Journal of Power Sources*, 232:209–218.

Furtado, A. M., Bradaschia, F., Cavalcanti, M. C., and Limongi, L. R. (2018). A reduced voltage range global maximum power point tracking algorithm for photovoltaic systems under partial shading conditions. *IEEE Transactions on Industrial Electronics*, 65(4):3252–3262.

Ghasemi, M. A., Foroushani, H. M., and Parniani, M. (2016). Partial shading detection and smooth maximum power point tracking of pv arrays under psc. *IEEE Transactions on Power Electronics*, 31(9):6281–6292.

Gholizadeh, M. and Salmasi, F. R. (2014). Estimation of state of charge, unknown nonlinearities, and state of health of a lithium-ion battery based on a com-

prehensive unobservable model. *IEEE Transactions on Industrial Electronics*, 61(3):1335–1344.

Goebel, K., Saha, B., Saxena, A., Celaya, J. R., and Christophersen, J. P. (2008). Prognostics in battery health management. *IEEE instrumentation & measurement magazine*, 11(4).

Han, X., Ouyang, M., Lu, L., and Li, J. (2014). A comparative study of commercial lithium ion battery cycle life in electric vehicle: Capacity loss estimation. *Journal of Power Sources*, 268:658–669.

Hart, D. W. (2011). *Power electronics*. Tata McGraw-Hill Education.

Hu, C., Youn, B. D., and Chung, J. (2012). A multiscale framework with extended kalman filter for lithium-ion battery soc and capacity estimation. *Applied Energy*, 92:694–704.

Ishaque, K. and Salam, Z. (2013). A deterministic particle swarm optimization maximum power point tracker for photovoltaic system under partial shading condition. *IEEE Trans. Industrial Electronics*, 60(8):3195–3206.

Ishaque, K., Salam, Z., Taheri, H., and Shamsudin, A. (2011). Maximum power point tracking for pv system under partial shading condition via particle swarm optimization. In *Applied Power Electronics Colloquium (IAPEC), 2011 IEEE*, pages 5–9. IEEE.

Ji, Y.-H., Jung, D.-Y., Kim, J.-G., Kim, J.-H., Lee, T.-W., and Won, C.-Y. (2011). A real maximum power point tracking method for mismatching compensation in pv array under partially shaded conditions. *IEEE Transactions on power electronics*, 26(4):1001–1009.

Jiang, L. L., Maskell, D. L., and Patra, J. C. (2013). A novel ant colony optimization-based maximum power point tracking for photovoltaic systems under partially shaded conditions. *Energy and Buildings*, 58:227–236.

Kaldellis, J. (2010). Optimum hybrid photovoltaic-based solution for remote telecommunication stations. *Renewable Energy*, 35(10):2307–2315.

Kaldellis, J., Ninou, I., and Zafirakis, D. (2011). Minimum long-term cost solution for remote telecommunication stations on the basis of photovoltaic-based hybrid power systems. *Energy policy*, 39(5):2512–2527.

Karaboga, D. and Akay, B. (2009). A comparative study of artificial bee colony algorithm. *Applied mathematics and computation*, 214(1):108–132.

Karatepe, E., Hiyama, T., et al. (2009). Artificial neural network-polar coordinated fuzzy controller based maximum power point tracking control under partially shaded conditions. *IET Renewable Power Generation*, 3(2):239–253.

Killi, M. and Samanta, S. (2015). Modified perturb and observe mppt algorithm for drift avoidance in photovoltaic systems. *IEEE Transactions on Industrial Electronics*, 62(9):5549–5559.

Kim, I.-S. (2010). A technique for estimating the state of health of lithium batteries through a dual-sliding-mode observer. *IEEE Transactions on Power Electronics*, 25(4):1013–1022.

Kim, K. A., Xu, C., Jin, L., and Krein, P. T. (2013). A dynamic photovoltaic model incorporating capacitive and reverse-bias characteristics. *IEEE Journal of Photovoltaics*, 3(4):1334–1341.

Kobayashi, K., Takano, I., and Sawada, Y. (2003). A study on a two stage maximum power point tracking control of a photovoltaic system under partially shaded insolation conditions. In *Power Engineering Society General Meeting, 2003, IEEE*, volume 4, pages 2612–2617. IEEE.

Kobayashi, K., Takano, I., and Sawada, Y. (2005). A study of a two-stage maximum power point tracking control of a photovoltaic system under partially shaded insolation conditions. *Electrical Engineering in Japan*, 153(4):39–49.

Koutroulis, E. and Blaabjerg, F. (2012). A new technique for tracking the global maximum power point of pv arrays operating under partial-shading conditions. *IEEE Journal of Photovoltaics*, 2(2):184–190.

Kozlowski, J. D. (2003). Electrochemical cell prognostics using online impedance measurements and model-based data fusion techniques. In *Aerospace Conference, 2003. Proceedings. 2003 IEEE*, volume 7, pages 3257–3270. IEEE.

Kumar, N., Hussain, I., Singh, B., and Panigrahi, B. K. (2017a). Maximum power peak detection of partially shaded pv panel by using intelligent monkey king evolution algorithm. *IEEE Transactions on Industry Applications*, 53(6):5734–5743.

Kumar, N., Hussain, I., Singh, B., and Panigrahi, B. K. (2017b). Rapid mppt for uniformly and partial shaded pv system by using jayade algorithm in highly fluctuating atmospheric conditions. *IEEE Transactions on Industrial Informatics*, 13(5):2406–2416.

Kumar, N., Hussain, I., Singh, B., and Panigrahi, B. K. (2017c). Single sensor based mppt for partially shaded solar photovoltaic by using human psychology optimisation algorithm. *IET Generation, Transmission & Distribution*, 11(10):2562–2574.

Kuo, Y.-C., Liang, T.-J., and Chen, J.-F. (2001). Novel maximum-power-point-tracking controller for photovoltaic energy conversion system. *IEEE transactions on industrial electronics*, 48(3):594–601.

La Manna, D., Vigni, V. L., Sanseverino, E. R., Di Dio, V., and Romano, P. (2014). Reconfigurable electrical interconnection strategies for photovoltaic arrays: A review. *Renewable and Sustainable Energy Reviews*, 33:412–426.

Lagorse, J., Paire, D., and Miraoui, A. (2009). Sizing optimization of a stand-alone street lighting system powered by a hybrid system using fuel cell, pv and battery. *Renewable Energy*, 34(3):683–691.

Lam, L. and Bauer, P. (2013). Practical capacity fading model for li-ion battery cells in electric vehicles. *IEEE transactions on power electronics*, 28(12):5910–5918.

Lam, L., Bauer, P., and Kelder, E. (2011). A practical circuit-based model for li-ion battery cells in electric vehicle applications. In *Telecommunications Energy Conference (INTELEC), 2011 IEEE 33rd International*, pages 1–9. IEEE.

Lei, M., Yaojie, S., Yandan, L., Zhifeng, B., Liqin, T., and Jieqiong, S. (2011). A high performance mppt control method. In *Materials for Renewable Energy & Environment (ICMREE), 2011 International Conference on*, volume 1, pages 195–199. IEEE.

Li, H., Yang, D., Su, W., Lü, J., and Yu, X. (2019). An overall distribution particle swarm optimization mppt algorithm for photovoltaic system under partial shading. *IEEE Transactions on Industrial Electronics*, 66(1):265–275.

Liu, M., Liu, L., Wu, X., Teng, L., Cao, J., and Qin, S. (2013). A research on the telecommunication base station power consumption investment analysis and optimized configuration method for hybrid energy power. In *Telecommunications Energy Conference'Smart Power and Efficiency'(INTELEC), Proceedings of 2013 35th International*, pages 1–6. VDE.

Liu, S., Dougal, R., and Solodovnik, E. (2005). Design of autonomous photovoltaic power plant for telecommunication relay station. *IEE Proceedings-Generation, Transmission and Distribution*, 152(6):745–754.

Liu, Y.-H., Huang, S.-C., Huang, J.-W., and Liang, W.-C. (2012). A particle swarm optimization-based maximum power point tracking algorithm for pv systems operating under partially shaded conditions. *IEEE Transactions on Energy Conversion*, 27(4):1027–1035.

Maher, K. and Yazami, R. (2014). A study of lithium ion batteries cycle aging by thermodynamics techniques. *Journal of Power Sources*, 247:527–533.

Manickam, C., Raman, G. R., Raman, G. P., Ganesan, S. I., and Nagamani, C. (2016). A hybrid algorithm for tracking of gmpp based on p&o and pso with reduced power oscillation in string inverters. *IEEE Trans. Industrial Electronics*, 63(10):6097–6106.

Markervich, E., Salitra, G., Levi, M., and Aurbach, D. (2005). Capacity fading of lithiated graphite electrodes studied by a combination of electroanalytical methods, raman spectroscopy and sem. *Journal of power sources*, 146(1-2):146–150.

Masoum, M. A., Dehbonei, H., and Fuchs, E. F. (2002). Theoretical and experimental analyses of photovoltaic systems with voltageand current-based maximum power-point tracking. *IEEE Transactions on energy conversion*, 17(4):514–522.

Meng, Z. and Pan, J.-S. (2016). Monkey king evolution: a new memetic evolutionary algorithm and its application in vehicle fuel consumption optimization. *Knowledge-Based Systems*, 97:144–157.

Miyatake, M., Toriumi, F., Endo, T., and Fujii, N. (2007). A novel maximum power point tracker controlling several converters connected to photovoltaic arrays with particle swarm optimization technique. In *power electronics and applications, 2007 European conference on*, pages 1–10. IEEE.

Mohanty, S., Subudhi, B., and Ray, P. K. (2016). A new mppt design using grey wolf optimization technique for photovoltaic system under partial shading conditions. *IEEE Transactions on Sustainable Energy*, 7(1):181–188.

Ng, K. S., Moo, C.-S., Chen, Y.-P., and Hsieh, Y.-C. (2009). Enhanced coulomb counting method for estimating state-of-charge and state-of-health of lithium-ion batteries. *Applied energy*, 86(9):1506–1511.

Nguyen, T. L. and Low, K.-S. (2010). A global maximum power point tracking scheme employing direct search algorithm for photovoltaic systems. *IEEE transactions on Industrial Electronics*, 57(10):3456–3467.

Noguchi, T., Togashi, S., and Nakamoto, R. (2002). Short-current pulse-based maximum-power-point tracking method for multiple photovoltaic-and-converter module system. *IEEE Transactions on Industrial Electronics*, 49(1):217–223.

North, R. J. (2007). *Assessment of real-world pollutant emissions from a light-duty diesel vehicle*. PhD thesis, Department of Civil and Environmetnal Engineering, Imperial College London.

Omar, N., Monem, M. A., Firouz, Y., Salminen, J., Smekens, J., Hegazy, O., Gaulous, H., Mulder, G., Van den Bossche, P., Coosemans, T., et al. (2014). Lithium iron phosphate based battery–assessment of the aging parameters and development of cycle life model. *Applied Energy*, 113:1575–1585.

Patel, H. and Agarwal, V. (2008). Maximum power point tracking scheme for pv systems operating under partially shaded conditions. *IEEE transactions on industrial electronics*, 55(4):1689–1698.

Pilawa-Podgurski, R. C. and Perreault, D. J. (2013). Submodule integrated distributed maximum power point tracking for solar photovoltaic applications. *IEEE Transactions on Power Electronics*, 28(6):2957–2967.

Plett, G. L. (2004). Extended kalman filtering for battery management systems of lipb-based hev battery packs: Part 3. state and parameter estimation. *Journal of Power sources*, 134(2):277–292.

Prema, V., Rao, K. U., and Closepet, A. S. (2014). A novel predictive dsm strategy to match power outage pattern for optimal cost with solar and diesel power. In *Innovative Smart Grid Technologies-Asia (ISGT Asia), 2014 IEEE*, pages 377–382. IEEE.

Ram, J. P. and Rajasekar, N. (2017). A novel flower pollination based global maximum power point method for solar maximum power point tracking. *IEEE Transactions on Power Electronics*, 32(11):8486–8499.

Ramyar, A., Iman-Eini, H., and Farhangi, S. (2017). Global maximum power point tracking method for photovoltaic arrays under partial shading conditions. *IEEE Transactions on Industrial Electronics*, 64(4):2855–2864.

Remmlinger, J., Buchholz, M., Meiler, M., Bernreuter, P., and Dietmayer, K. (2011). State-of-health monitoring of lithium-ion batteries in electric vehicles by on-board internal resistance estimation. *Journal of Power Sources*, 196(12):5357–5363.

Remmlinger, J., Buchholz, M., Soczka-Guth, T., and Dietmayer, K. (2013). On-board state-of-health monitoring of lithium-ion batteries using linear parameter-varying models. *Journal of Power Sources*, 239:689–695.

Saha, B., Goebel, K., Poll, S., and Christophersen, J. (2009). Prognostics methods for battery health monitoring using a bayesian framework. *IEEE Transactions on instrumentation and measurement*, 58(2):291–296.

Saha, B., Poll, S., Goebel, K., and Christophersen, J. (2007). An integrated approach to battery health monitoring using bayesian regression and state estimation. In *autotestcon, 2007 IEEE*, pages 646–653. Citeseer.

Sarikurt, T., Ceylan, M., and Balikci, A. (2014). An analytical battery state of health estimation method. In *Industrial Electronics (ISIE), 2014 IEEE 23rd International Symposium on*, pages 1605–1609. IEEE.

Schoeman, J. and Wyk, J. v. (1982). A simplified maximal power controller for terrestrial photovoltaic panel arrays. In *Power Electronics Specialists conference, 1982 IEEE*, pages 361–367. IEEE.

Schwunk, S., Armbruster, N., Straub, S., Kehl, J., and Vetter, M. (2013). Particle filter for state of charge and state of health estimation for lithium–iron phosphate batteries. *Journal of Power Sources*, 239:705–710.

Seyedmahmoudian, M., Rahmani, R., Mekhilef, S., Oo, A. M. T., Stojcevski, A., Soon, T. K., and Ghandhari, A. S. (2015). Simulation and hardware implementation of new maximum power point tracking technique for partially shaded pv system using hybrid depso method. *IEEE transactions on sustainable energy*, 6(3):850–862.

Shi, J., Zhang, W., Zhang, Y., Xue, F., and Yang, T. (2015). Mppt for pv systems based on a dormant pso algorithm. *Electric Power Systems Research*, 123:100–107.

soufyane Benyoucef, A., Chouder, A., Kara, K., Silvestre, S., et al. (2015). Artificial bee colony based algorithm for maximum power point tracking (mppt) for pv systems operating under partial shaded conditions. *Applied Soft Computing*, 32:38–48.

Sundareswaran, K., Peddapati, S., and Palani, S. (2014a). Application of random search method for maximum power point tracking in partially shaded photovoltaic systems. *IET Renewable Power Generation*, 8(6):670–678.

Sundareswaran, K., Peddapati, S., and Palani, S. (2014b). Mppt of pv systems under partial shaded conditions through a colony of flashing fireflies. *IEEE Transactions on Energy Conversion*, 29(2):463–472.

Sundareswaran, K., Sankar, P., Nayak, P., Simon, S. P., and Palani, S. (2015). Enhanced energy output from a pv system under partial shaded conditions through artificial bee colony. *IEEE transactions on sustainable energy*, 6(1):198–209.

Tarek, B., Said, D., and Benbouzid, M. (2013). Maximum power point tracking control for photovoltaic system using adaptive neuro-fuzzy anfis. In *Ecological Vehicles and Renewable Energies (EVER), 2013 8th International Conference and Exhibition on*, pages 1–7. IEEE.

Teshome, D., Lee, C., Lin, Y., and Lian, K. (2017). A modified firefly algorithm for photovoltaic maximum power point tracking control under partial shading. *IEEE journal of emerging and selected topics in power electronics*, 5(2):661–671.

Tey, K. S., Mekhilef, S., Seyedmahmoudian, M., Horan, B., Oo, A. M. T., and Stojcevski, A. (2018). Improved differential evolution-based mppt algorithm using sepic for pv systems under partial shading conditions and load variation. *IEEE Transactions on Industrial Informatics*.

Veerachary, M., Senjyu, T., and Uezato, K. (2001). Maximum power point tracking control of idb converter supplied pv system. *IEE Proceedings-Electric Power Applications*, 148(6):494–502.

Vetter, J., Novák, P., Wagner, M. R., Veit, C., Möller, K.-C., Besenhard, J., Winter, M., Wohlfahrt-Mehrens, M., Vogler, C., and Hammouche, A. (2005). Ageing mechanisms in lithium-ion batteries. *Journal of power sources*, 147(1-2):269–281.

Villalva, M. G., Gazoli, J. R., and Ruppert Filho, E. (2009). Comprehensive approach to modeling and simulation of photovoltaic arrays. *IEEE Transactions on power electronics*, 24(5):1198–1208.

Wang, J., Liu, P., Hicks-Garner, J., Sherman, E., Soukiazian, S., Verbrugge, M., Tataria, H., Musser, J., and Finamore, P. (2011). Cycle-life model for graphite-lifepo4 cells. *Journal of Power Sources*, 196(8):3942–3948.

Wang, Y., Li, Y., and Ruan, X. (2016). High-accuracy and fast-speed mppt methods for pv string under partially shaded conditions. *IEEE Transactions on Industrial Electronics*, 63(1):235–245.

Wei, X., Zhu, B., and Xu, W. (2009). Internal resistance identification in vehicle power lithium-ion battery and application in lifetime evaluation. In *Measuring Technol-*

ogy and Mechatronics Automation, 2009. ICMTMA'09. International Conference on, volume 3, pages 388–392. IEEE.

Xu, B., Oudalov, A., Ulbig, A., Andersson, G., and Kirschen, D. S. (2018). Modeling of lithium-ion battery degradation for cell life assessment. *IEEE Transactions on Smart Grid*, 9(2):1131–1140.

Yamegueu, D., Azoumah, Y., Py, X., and Zongo, N. (2011). Experimental study of electricity generation by solar pv/diesel hybrid systems without battery storage for off-grid areas. *Renewable energy*, 36(6):1780–1787.

Yang, X.-S. and He, X. (2013). Firefly algorithm: recent advances and applications. *arXiv preprint arXiv:1308.3898*.

Zhang, C., Liu, J., and Sharkh, S. (1970). Identification of dynamic model parameters for lithium-ion batteries used in hybrid electric vehicles.

Zhang, F., Liu, G., and Fang, L. (2009). Battery state estimation using unscented kalman filter. In *Robotics and Automation, 2009. ICRA'09. IEEE International Conference on*, pages 1863–1868. IEEE.

Zhou, W. and Wang, Z. L. (2007). *Scanning microscopy for nanotechnology: techniques and applications*. Springer science & business media.

PUBLICATIONS BASED ON THE THESIS

Patents

1. Indian patent filed on A Method and System for Maximum Power Point Tracking of a PV-Array during Non-Uniform Insolation Conditions," May, 2017. (Application No: 201741017347).

2. Indian patent filed on Method and Device for Life Estimation of Li-Ion battery, December, 2018. (Application No: 201841047090).

Papers in refereed journals

1. **J Saikrishna Goud**, R Kalpana, Bhim singh and Shailendra Kumar., "A Global Maximum Power Point Tracking Technique of Partially Shaded Photovoltaic Systems for Constant Voltage Applications.", *IEEE Transactions on Sustainable Energy*, doi: 10.1109/TSTE.2018.2876756.

2. **J Saikrishna Goud**, R Kalpana and Bhim singh, "A Hybrid Global Maximum Power Point Tracking Technique With Fast Convergence Speed for Partially Shaded PV Systems" , *IEEE Transactions on Industry Applications*, vol. 54, no.5, pp. 5367-5376, Oct 2018.

3. **J Saikrishna Goud**, R Kalpana and Bhim singh, "Maximum Power Point Tracking Technique Using Artificial Bee Colony and Hill Climbing Algorithms During Mismatch Insolation Conditions on PV Array " , *IET Renewable Power Generation*, vol. 12, no.16, pp. 1915-1922, 2018.

4. **J Saikrishna Goud**, R Kalpana and Bhim singh, "An Accurate Online Estimation of State of Health of a Li-Ion Battery " , *IEEE Transactions on Energy Conversion*, (Communicated).

5. **J Saikrishna Goud** , R Kalpana and Bhim singh, "Modeling and Estimation of Remaining Useful Life of LFP Cell " , *IEEE Transactions on Industry Applications*, (Communicated (PEDES 2018 Extended)).

Papers published in referred conference proceedings

1. **J Saikrishna Goud** and R Kalpana, "Optimal sizing of hybrid power supply system for telecommunication BTS load to ensure reliable power at lower cost" , *2017 International Conference on Technological Advancements in Power and Energy (TAP Energy) IEEE*, 2017.

2. **J Saikrishna Goud**, R Kalpana and Bhim singh, "Modeling and Estimation of Remaining Useful Life of Single cell Li-Ion battery" , *IEEE Power Electronics, Drives and Energy Systems Conference (PEDES)*, 2018.

Achievements

Received IETE Best Research award-2018 for the paper "A Hybrid Global Maximum Power Point Tracking Technique With Fast Convergence Speed for Partially Shaded PV Systems".

Bio-data

Name : J Saikrishna Goud
Date of birth: 30-12-1991
E-mail: jskrishna307@gmail.com
Mobile: +91-9611135503

Education

- **M.Tech**, Power Electronic Systems and Control, Manipal Institute of Technology, Manipal, Karnataka, 2015.
- **B.Tech.**, Electrical & Electronics Engineering, Vidya Jyothi Institute of Technology, Hyderabad, Telangana, 2012.

Experience

- **Project Engineer** in Philips India Pvt. Ltd. Bangalore from June 2014 to December 2015.

Address

H.No:2-2-87/9A, Saipur, Sainagar Colony
Near New Nalanda High School, Tandur
Telangana -501141, India.